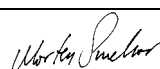


NGU Rapport 2006.076

Geological and geophysical investigations for  
the ROGFAST project.

Rapport nr.: 2006.076		ISSN 0800-3416	Gradering: Åpen
Tittel: Geological and geophysical investigations for the ROGFAST project.			
Forfatter: Rønning, J.S., Dalsegg, E., Dehls, J.F., Haase, C., Nordgulen, Ø., Olesen, O., Saintot, A. & Solli, A.		Oppdragsgiver: Statens vegvesen Region vest	
Fylke: Rogaland		Kommune: Bokn, Finnøy, Haugesund, Karmøy, Kvitsøy, Randaberg, Strand	
Kartblad (M=1:250.000) Haugesund		Kartbladnr. og -navn (M=1:50.000) 1113 II Skudeneshavn, 1213 III Rennesøy	
Forekomstens navn og koordinater: Kvitsøy 294500 - 6552600		Sidetall: 91 Kartbilag: 1	Pris: 500,-
Feltarbeid utført: 05 - 09.2006	Rapportdato: 15.11.2006	Prosjektnr.: 314300	Ansvarlig: 
<p><b>Sammendrag:</b> In cooperation with "Statens vegvesen Region vest" and "Statens vegvesen Vegdirektoratet", the Geological survey of Norway (NGU) has performed research where new methods in tunnel planning were tested in the ROGFAST project.</p> <p>Analysis of the new airborne magnetic data, petrophysical data, digital topography/ bathymetry and geological follow up work have revealed new information about the bedrock geology in the Boknafjord area. Results from digital structural analysis have already been used in the planning of seismic follow up studies. Magnetic dislocations coincide with lineaments from bathymetric studies, and seem to give information on the most pronounced faults in the area. The depth extent of magnetic bodies at the seabottom between Randaberg and Kvitsøy are calculated from aeromagnetic data.</p> <p>Geological follow up studies discovered outcropping rock of the Karmøy ophiolite complex at the islands between Randaberg and Kvitsøy. North of Kvitsøy lack of exposures and magnetic signature made it difficult to reveal new information. A new geological map with profiles is produced introducing a thrust plane at a few hundred metre depth between Randaberg and Kvitsøy. A major NE-SW trending fault zone is proposed just north of Kvitsøy. To avoid unexpected problems during the construction work, a vertical drillhole from the island Alstein, and a long drillhole along the tunnel trace from an island north of Kvitsøy are highly recommended.</p> <p>The Boknafjord area is located outside the Cretaceous etch surface as identified by Lidmar-Bergström et al. (1999) and consequently, there are some uncertainties about the applicability of the Amager method. The obtained results indicate that deep weathering may indeed occur in the area. Due to low magnetic susceptibility in the bedrock, it is not possible to calculate the depth extent of the possible weathering.</p> <p>The study by Olesen et al. (in press) in the greater Oslo region shows, however, that there may also be other causes of coincident topography and magnetic lows than deep weathering. It is important therefore, that the interpretations are checked by ground truth (ground geophysics or drilling) before being introduced in the planning of the tunnel construction. It is also important to study the geomorphology to estimate the glacial erosion of the area. If the erosion is deeper than 300 metres the chances of encountering deep weathered clay zones are significantly reduced.</p> <p>This project was proposed to evaluate modern geological mapping tools for tunnel planning. So far, interesting results are acquired, but these results has to be checked against other data as refraction seismics, drilling and of course the tunnel construction, to get a fully evaluation of the methods.</p>			
Emneord: Geophysics Geofysikk		Magnetometry Magnetometri	Bathymetry Batymetri
Structural geology Strukturgeologi		Bedrock geology Bergrunnsgeologi	Engineering geology Ingeniørgeologi
			Scientific report Fagrapport

## CONTENT

1	INTRODUCTION.....	4
2	GEOLOGICAL SETTING .....	5
2.1	Main units.....	5
2.1.1	Precambrian autochthonous basement and Cambro-Silurian cover.....	5
2.1.2	Caledonian allochthonous units .....	6
2.2	Karmsundet basin.....	7
2.3	Major faults .....	7
2.3.1	Large steep lineaments .....	7
2.4	Geological models based on the available geological map sheet Haugesund.....	8
2.4.1	Geological model along Randaberg-Kvitsøy profile .....	8
2.4.2	Geological model along Kvitsøy-Bokn profile .....	9
3	PETROPHYSICAL ANALYSIS.....	11
3.1	Sample collection and Laboratory measurements.....	11
3.2	In situ measurements .....	11
4	MAGNETIC ANALYSIS.....	12
4.1	Data acquisition and processing.....	12
4.2	Interpretation of deep weathering and magnetic dislocations.....	14
4.2.1	Scientific background.....	14
4.2.2	Deep weathering.....	16
4.2.3	Magnetic dislocations.....	18
4.3	Modelling of magnetic data.....	20
4.3.1	Modelling software and input parameters.....	20
4.3.2	Results of magnetic modelling .....	21
4.4	Discussion of magnetic interpretation.....	23
4.4.1	Deep weathering.....	23
4.4.2	Magnetic modelling.....	24
5	DIGITAL TOPOGRAPHY AND BATYMETRY .....	25
5.1	Data sets and acquisition.....	25
5.2	Data processing .....	25
5.3	Lineament analysis.....	26
6	STRUCTURAL AND GEOLOGICAL STUDIES.....	30
6.1	General description .....	30
6.1.1	Visited sites.....	30
6.1.2	Keys to read stereoplots in the following sections.....	31
6.2	Structural field studies.....	33
6.2.1	Field studies at Randaberg.....	33
6.2.2	Field studies at Kvitsøy.....	36
6.2.3	Field studies at Vestre Bokn.....	41
6.2.4	Field studies at Bru-Sokn-Mosterøy-Rennesøy .....	47
6.2.5	Conclusion on structural field analyses.....	53
6.3	Geological mapping .....	53
7	SYNTHESIS OF DATA AND NEW GEOLOGICAL MODEL .....	54
7.1	Tectonic map.....	54
7.2	Profile Randaberg to Kvitsøy.....	56
7.3	Profile Kvitsøy to Vestre Bokn.....	57
7.4	Conclusion on new geological model.....	59
8	CONCLUSIONS AND RECOMENDATIONS .....	59
9	REFERENCES.....	60

**Appendix A:** Petrophysical data from laboratory analysis.      **Appendix B:** Structural observations.

**MAP (in scale 1:50 000):**

2006.076-01: Topographic and magnetic lineaments with possible deep weathering zones.

## 1 INTRODUCTION

The Geological Survey of Norway (NGU) has performed geophysical and geological investigation in an area in Rogaland surrounding the ROGFAST tunnel project. Previous investigations in the Oslo area have proven that interpretation of airborne magnetic data can delineate possible deep weathering (Olesen 2004a, 2004b, Olesen et al. 2006). An investigation by Lidmar-Bergstrøm (1999) indicates that the same kind of weathering may occur in the outer coastal area of Rogaland. Analysis of digital topography and bathymetry has proven to be a powerful tool for structural analysis in both land and marine environments (Nordgulen & Dehls 2003, Ganerød & al 2006). During discussions between the NGU, "Statens vegvesen Vegdirektoretet" and "Statens vegvesen Region vest" (Rogfast project), it was decided to establish a research project to evaluate these techniques in the Boknafjord area where, in addition to the Rogfast tunnel, four other tunnel projects have been established or are under planning. As a part of the project, detailed bathymetric analysis was included as well as structural analysis in the field.

During the discussions, it was proposed that high-resolution magnetic data could give information about the general bedrock geology, geological lineaments (faults, fractures, geological boundaries etc.) and characterization of fractured zones through possible deep weathering. High-resolution airborne magnetic data did not exist, and as a part of the project, data acquisition was acquired using the Swedish Geological Survey (SGU) as a subcontractor. To do the deep weathering analysis, it is necessary to have detailed topographic/bathymetric data. On land, topographic data were taken from "Statens Kartverk". Detailed bathymetric data were provided by the Rogfast project.

To solve the mission, NGU organized a project group of experts with the following responsibilities:

Einar Dalsegg:	Magnetic modelling
John Dehls:	Digital structural analysis, map production
Claudia Haase:	Magnetic modelling
Øystein Nordgulen:	Bedrock and structural geology
Odleiv Olesen:	Interpretation of magnetic data
Jan S. Rønning:	Project leader
Aline Saintot:	Bedrock and structural geology
Arne Solli:	Bedrock geology.

The project was established April 1<sup>st</sup> 2006. High-resolution magnetic data were collected in the beginning of May. The first results were presented at a project meeting June 14<sup>th</sup>, and the first interpretations at a project meeting September 4<sup>th</sup>.

This aim of this report is to document the results obtained so far. A final evaluation of the project will be performed when data from tunnel work is available.

## 2 GEOLOGICAL SETTING

The following geological description is based upon geological material in existence prior to this project. An upgraded geological model based upon present work will be presented in section 7.

### 2.1 Main units

The bedrock in this area, as it is defined on the two available geological map sheets Stavanger and Haugesund scale 1:250 000, (Jorde et al. 1995, Ragnhildstveit et al. 1998) consists of a Precambrian autochthonous basement with a stack of Caledonian Nappes above. The allochthonous units seem to cover all the tunnel area, but the autochthonous basement cannot be very deep. Figure 2.1 gives a simplified overview of the bedrock mainly based on the two map sheets.

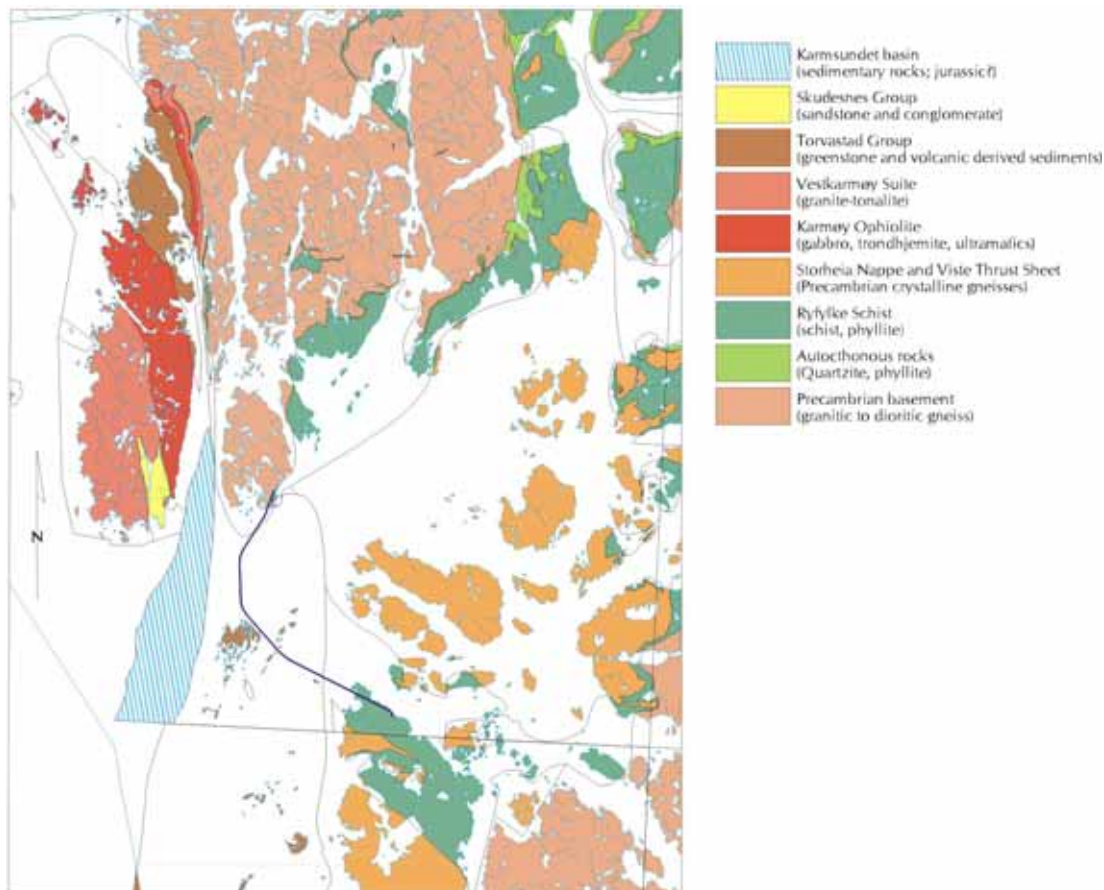


*Fig. 2.1. Map showing the main rock units in the Boknafjord area based on the map sheets Haugesund and Stavanger 1:250 000.*

#### 2.1.1 Precambrian autochthonous basement and Cambro-Silurian cover

The basement is widely exposed southeast of Stavanger and from Vestre Bokn northwards to the Tysver and Haugalandet regions. It consists of a wide variety of gneisses varying in composition from granite to diorite with some bodies of gabbro. The age is mainly Mesoproterozoic with some younger granites of Neoproterozoic age. In some areas to the

east and north in Rogaland, there is a thin cover of autochthonous sediments deposited on the Precambrian gneisses. It commonly starts with a thin unit of quartzite but its main constituent is phyllite. In the east and north, this unit can have a thickness of several hundred metres, but in the Randaberg and Bokn areas it seems to have been totally cut off by the overlying nappes. The age is thought to be Cambrian.

### 2.1.2 Caledonian allochthonous units

Nappe 1: The lowest nappe is called the Viste Thrust Sheet (Visteflaket). Its main constituent is the Ryfylke Schist consisting of quartz-rich schist/phyllite, which is thought to be Cambrian to Ordovician age. The boundary with the underlying autochthonous phyllite is often difficult to locate because the rock types are very similar. It is rather likely that everything originally was deposited as one sequence, but during the emplacement of the Caledonian nappes the upper part was thrust together with the overlying nappes. In the upper part of the Ryfylke Schist, thin wedges of the overlying Storheia Nappe can be found within the schists. The Ryfylke Schist has a thickness of several hundred metres in the eastern and northern part of Rogaland but is much thinner to the west. In the area between Randaberg and Stavanger it also seems thick.

Nappe 2 and 3: The Storheia Nappe and Boknafjorden Nappe consist mainly of granitic gneisses of Proterozoic age with some lenses of marble and mica schist. They have a wide distribution and a considerable thickness on the islands in Boknafjorden (Mosterøy, Rennesøy, Ombo), but it is uncertain if they occur along the planned tunnel. On the published map (Ragnhildstveit et al. 1998) these nappes are cut by a fault south of the tunnel trace but they can occur as a thin layer under the Hardangerfjord Nappe.

Nappe 4: The uppermost nappe in the tectonostratigraphy is the Hardangerfjord Nappe. On map sheet Haugesund 1:250 000 (Ragnhildstveit et al. 1998) this unit has been subdivided into about 20 different units. The main tectonic unit, however, is the Karmøy Ophiolite consisting of gabbroic rocks, a dyke complex and a sequence of volcanic rocks such as pillow lavas, tuffs and volcanic derived sediments. The age of the plutonic rocks in the ophiolite is c. 493 Ma. They are later intruded by a suite of granitic to trondhjemitic rocks (the Vest-Karmøy Suite), which is dated to c. 480-470 Ma. The supracrustal rocks belonging to the ophiolite are called the Torvastad Group and are of Middle to Late Ordovician age (470-440 Ma). The Karmøy Ophiolite and intrusive of the Vest-Karmøy Suite are reworked as pebbles in an unconformable sedimentary cover of Late Ordovician to Silurian in age (the Skudesnes Group) in Karmøy region.

According to Ragnhildstveit et al. (1998), only the supracrustals (tuffs, lavas and sediments) of Torvastad Group should occur along the planned tunnel, especially in the Kvitsøy area. Reconnaissance fieldwork during this project indicates, however, that mafic and ultramafic rocks of the Karmøy Ophiolite are also found in Boknafjorden between Randaberg and Kvitsøy. This item will be further developed (see section 6.3).

## 2.2 Karmsundet basin

The Karmsundet basin is a N-S trending fault-bounded graben, some 5 to 10 km wide laying just west of Kvitsøy, probably Mesozoic in age but possibly Permo-Triassic (see Bøe et al. 1992).

## 2.3 Major faults

The Caledonian pile of nappes and sheets are built following flat (or shallow dipping) thrusts. Such a flat contact can be well observed on Bru Island between the overlying Boknafjord nappe and the Ryfylke Schist (figure 2.2).



*Figure 2.2. View of the southern part of Bru-øya from Randaberg. The thrust between the Boknafjorddekket (hanging wall) and the Ryfylke schist (foot wall) is clearly displayed.*

### 2.3.1 Large steep lineaments

Gabrielsen et al. (2002) described four populations of nearly vertical lineaments in western and south western Norway trending 035°; 063°-066°; 122°-135° and 175°-176° based on a regional-scale study of lineaments extracted from satellite images. Gabrielsen et al. (2002 and references therein) gave some characterisation of these populations as follow:

The ENE-WSW population, and to some extent the NE-SW population, are typical of the Precambrian basement and are very well displayed south of the area studied here, where the basement crops out.

The NNW-SSE population are post-Caledonian structures and belong to the N-S to NNW-SSE Permo-Triassic fault system and associated dykes, which are well documented in the Sunnhordland region (as the Bergen zone of lineaments in Gabrielsen et al. 2002; Valle et al.

2002). As discussed in previous sections, the N-S normal faults associated to the Karmsundet rift basin may belong to the same system of Permo-Triassic faults or may be as young as Jurassic in age. Jurassic reactivations of the Bergen zone are also likely. Finally, seismic activity concentrates on this zone of nearly N-S faults. For example, historic seismic activity has been reported by Anundsen (1989) along the N-S Skjoldafjord fault (located between Hervikfjorden and Skjoldafjorden) with a downward displacement of the western compartment.

Characterisation of the NW-SE trend is poor in the investigated region. According to Gabrielsen et al. (2002), such trend in other parts of Norway and Scandinavia may be an old Archean to Precambrian structural grain. However, this population is the origin of the topographic lows between the groups of Islands from Rennesøy to Bru (as displayed of the geological map sheet Haugesund scale 1:250 000).

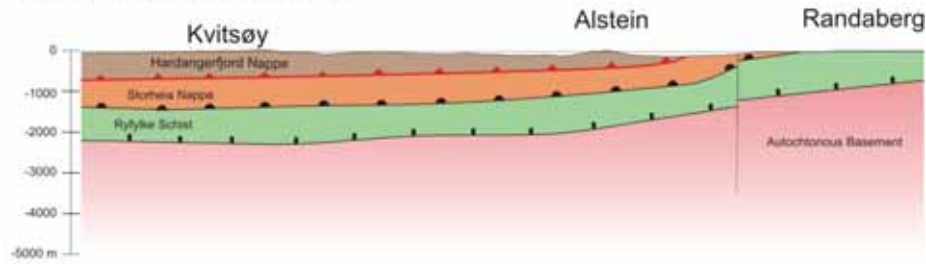
## **2.4 Geological models based on the available geological map sheet Haugesund**

### **2.4.1 Geological model along Randaberg-Kvitsøy profile**

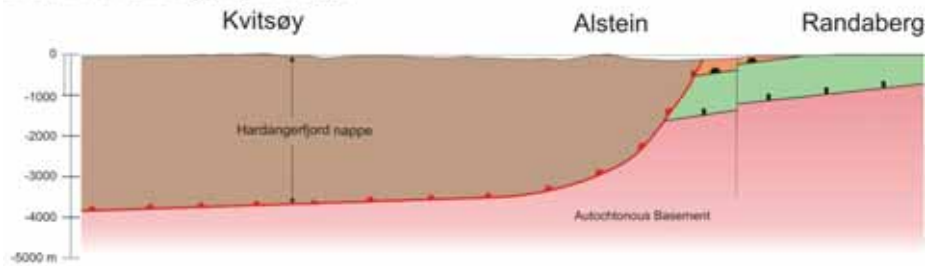
Figure 2.3 displays four possible cross-sections from Randaberg to Kvitsøy based on the available geological map sheet Haugesund. The first model (figure 2.3A) takes into account the only outcropping units in Randaberg and Kvitsøy. The Hardangerfjord nappe is reduced in thickness. It lays unconformably on the Storheia Nappe and Ryfylke Schist that crop out at Randaberg. The second model (figure 2.3B) displays a thick Hardangerfjord nappe (8 units) without the Storheia nappe and Ryfylke Schist underneath, whereas the third model (figure 2.3C) includes them. Between models A, B and C, the thickness of the Hardangerfjord nappe may vary depending on the numbers of units present (to a maximum of 8 units). According to the geological map, it is reduced to the Torvastad and Visne Groups. As previously mentioned, the Karmøy Ophiolite has been identified in the field and we favour a thicker Hardangerfjord Nappe than presented on model A. Also the Storheia nappe and Ryfylke Schist should be drawn if the Hardangerfjord nappe is thin (model A) to geometrically fit with what we can observe in the Randaberg area (considering that the thrust planes are generally flat lying in such geological frame). In turn if the Hardangerfjord is thicker, the Storheia nappe and Ryfylke Schist may or may not be present (Models B or C). However, the regional background strongly suggests that they are present beneath the Hardangerfjord nappe. The model that we feel is most probable, is a thick Hardangerfjord nappe overthrusting the Storheia nappe and Ryfylke Schist, cut by a large normal fault (model D). Such geometry is reported further north across Kamsundet basin (cf. cross-section A on the Haugesund geological map, scale 1/250000). These different profiles have been tested in the present study.



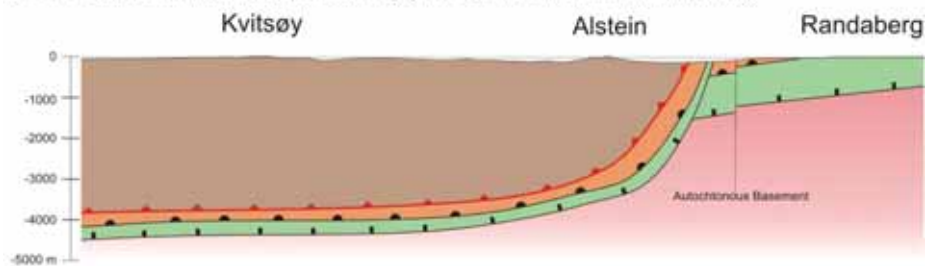
A: a thin Hardangerfjord Nappe



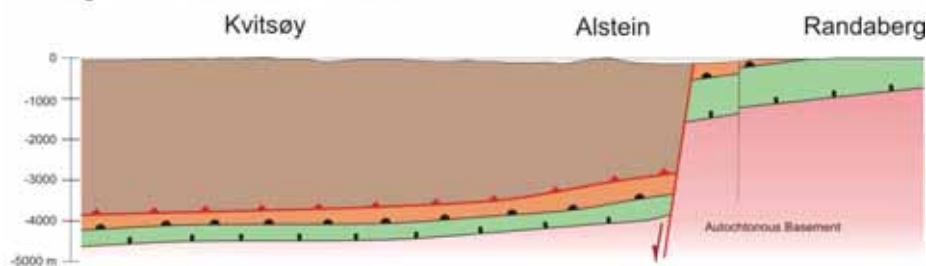
B: a thick Hardangerfjord Nappe



C: As B with Storheia Nappe and Ryfylke Schist involved in thrusting



D: A large normal fault across model C



Note: the internal deformation of sheets is not drawn/ the thicknesses of units are not constrained

Figure 2.3. Four geological models along Kvitsøy-Randaberg profile.

#### 2.4.2 Geological model along Kvitsøy-Bokn profile

The same uncertainty exists regarding the profile from Kvitsøy to Bokn (Figure 2.4). The different models follow the same hypotheses used to draw the Kvitsøy-Randaberg profile above. A large fault zone probably exists along the Boknafjord axis. Its exact location and extent, both vertical and horizontal, are unknown.

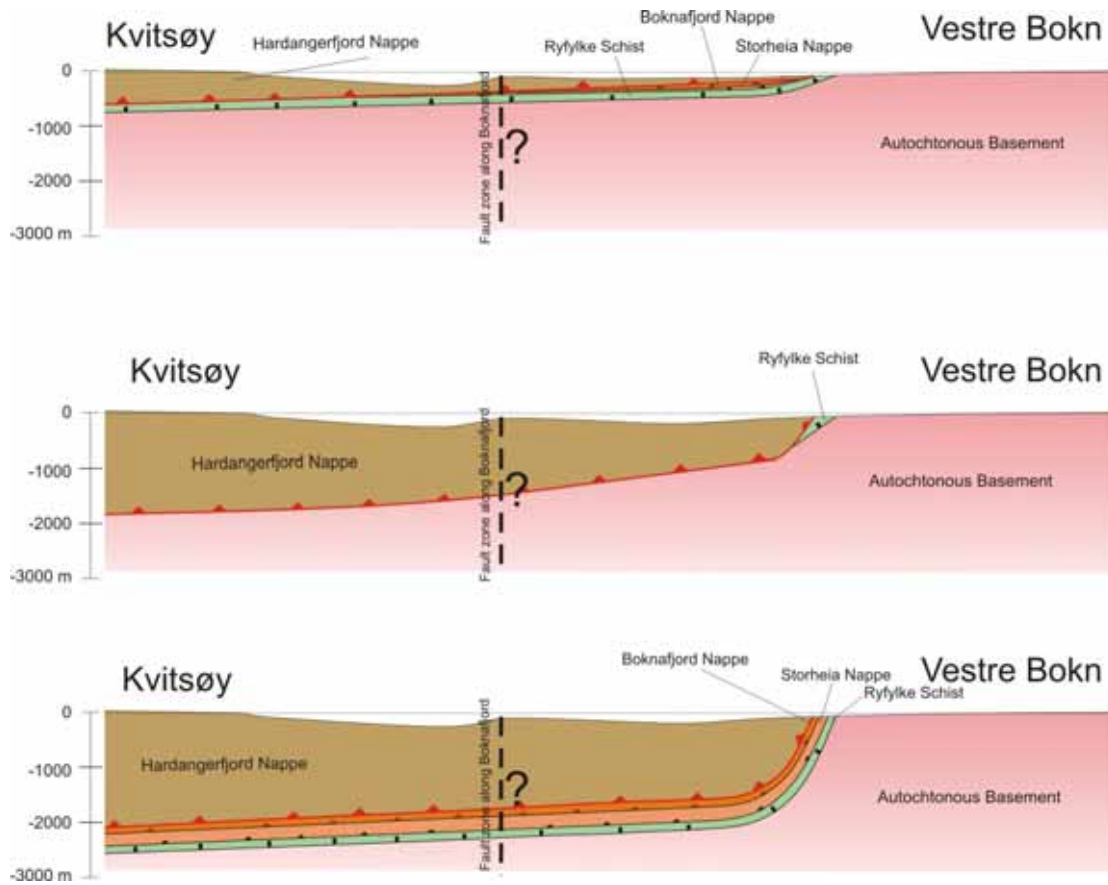


Figure 2.4. Three geological models along Kvitsøy-Bokn profile.

### **3 PETROPHYSICAL ANALYSIS**

In order to understand the origin of magnetic anomalies, it is important to know the magnetic properties of the bedrocks involved in the study.

#### **3.1 Sample collection and Laboratory measurements**

Samples for petrophysical analysis were collected during several campaigns. First, Rune Stumo from "Statens vegvesen Region vest" collected 68 samples along road cuttings at different locations in the vicinity of the proposed "Rogfast tunnel". Later in June, Aline Saintot and Øystein Nordgulen from NGU collected 16 rock samples while they were doing structural geological studies in the area. The last 8 samples were collected during follow up studies on the islands between Randaberg and Kvitsøy in September by Arne Solli.

Density, magnetic susceptibility and remanent magnetisation were analysed at NGU's Petrophysical laboratory. Procedures are described by Torsvik & Olesen (1988). The results are presented in Appendices A1 and A2.

In general, most of the samples show up a low magnetic susceptibility (less than  $1 \times 10^{-3}$  SI units). Exceptions are a granodiorite at Karmøy (sample 1 and 2, Appendix A1), a metasandstone/andesite at Karmøy (sample 13, Appendix A1), a micagneiss at Fosen (sample 18, Appendix A1) and phyllites at Randaberg (sample 65 and 67, Appendix A1). A granodiorite at Vestre Bokn and especially an amphibolite from Rennesøy show up a high susceptibility values (sample 10 and 11, Appendix A2). Highest magnetic susceptibilities are measured on ultramafic and gabbro samples from the islands Nordre Svartaskjær and Kråka between Randaberg and Kvitsøy (samples ASO-2 and ASO-4, Appendix A2).

#### **3.2 In situ measurements**

At Svartaskjær (UTM 299492 6544546), where an ultramafic rock type is exposed, magnetic susceptibility was measured in situ with a handheld instrument (Geofysika Kappameter). Altogether 12 readings gave an average value of  $1.01 \times 10^{-1}$  (SI units), which is very high. This value agrees with laboratory measurements on a rock sample from the same island (sample ASO-2, Appendix A2).

## 4 MAGNETIC ANALYSIS

In order to see if magnetic data could delineate possible fractured and/or deep weathered zones, which could cause problems during the tunnelling work, airborne magnetic data was acquired.

### 4.1 Data acquisition and processing

Magnetic data covering the Rogfast tunnel area and four other tunnel projects (Rennfast, Finnfast, Ryfast and T-forbindelsen) were collected by the Geological Survey of Sweden (SGU) at the beginning of May 2006. Line spacing was 250 metres, sensor height nominally 60 metres, and profile direction 90 – 270 °. Over national parks, densely populated areas and fox farms, sensor height was increased to 100 metres. The measured area is limited to the following coordinates (easting – northing, UTM WGS 84, zone 32):

285000 - 6552000, 285000 - 6592000, 306000 - 6592000  
306400 - 6574250, 313000 - 6568000, 325000 - 6556000  
325000 - 6539250, 302000 - 6539000

The data were processed by the SGU using standard procedures using Geosoft OASIS Montaj software. Data delivery to NGU was in Geosoft xyz-format and as grid files. More details about data quality insurance, data acquisition, data quality control and data processing are described in a technical report from SGU (Bystrøm 2006).

Data quality is characterized as very good. There are some gaps in the data coverage caused by limited access over industrial plants (at Karmøy and Kårstø), radio transmitters (Kvitsøy) and some natural park restricted areas. An illustration of the magnetic data is shown in figure 4.1. A map of the total magnetic field in scale 1: 50.000 (not included as a part of the report) can be ordered from NGU.

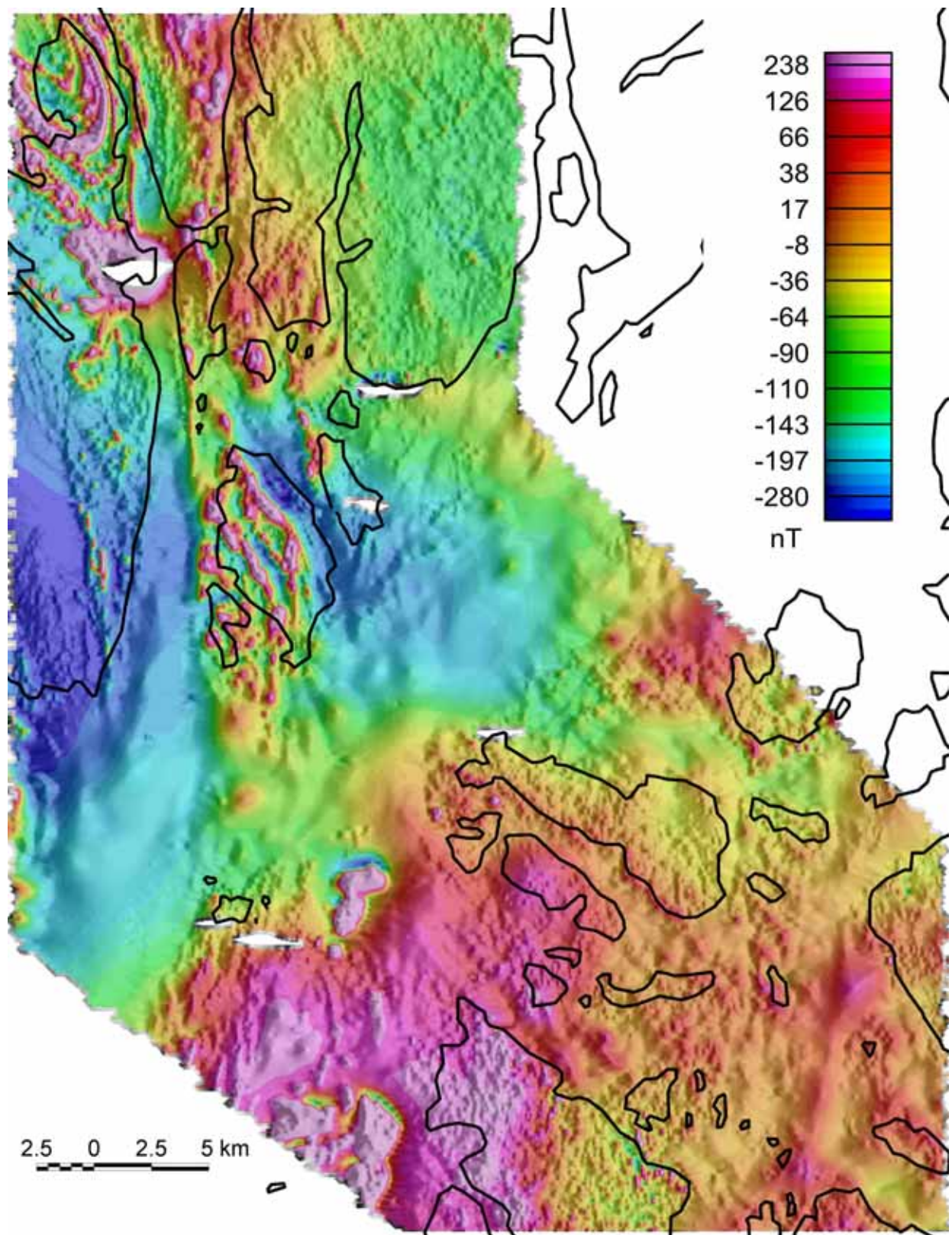


Figure 4.1. Aeromagnetic map from the outer Bokn fjord area. A shaded relief version of the 8-km high-pass filtered topography and bathymetry superimposed on a colour version of the same dataset.



## 4.2 Interpretation of deep weathering and magnetic dislocations

A new method, referred to as the Amager Method (AeroMagnetic and Geomorphological Relations), has been developed to map the occurrence of deep clay alteration in the bedrock of the Oslo Region (Olesen et al. in press).

### 4.2.1 Scientific background

Structural weakness zones contain clay minerals such as kaolinite and smectite and are to a large extent the result of chemical weathering during tropical conditions in the Mesozoic. Lidmar-Bergström (1989) proposed that the joint valley landscape of southwestern Sweden was formed during Neogene exhumation of the Fennoscandian Shield. She studied how the glacial erosion of a thick Jurassic saprolite along regional fault zones had caused the formation of extensive valleys in the northern Scania region. This system of joint valleys could be traced north along the west coast of Sweden all the way to Lake Mjøsa in Norway and south-westwards along the coast of southern Norway (see Figure. 4.2).

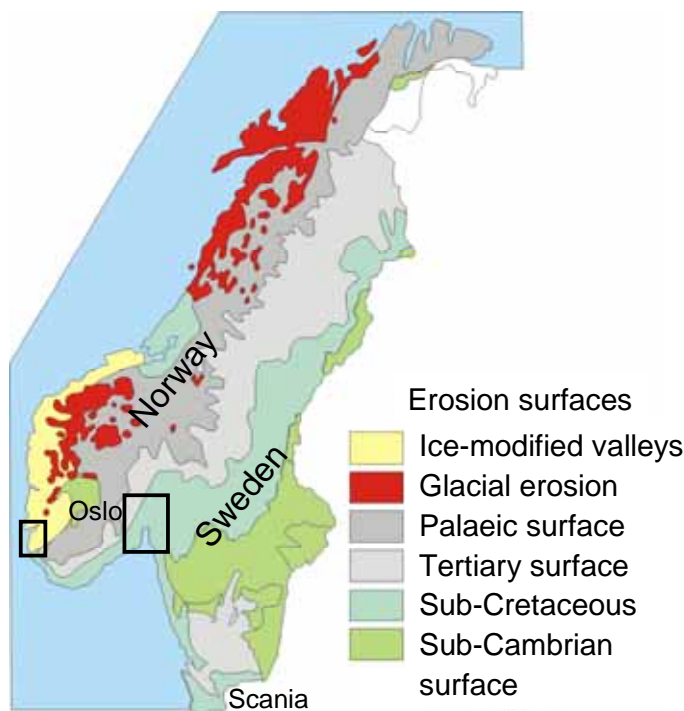


*Figure 4.2. Geomorphological map of western Fennoscandia (Lidmar-Bergström et al. 1999). The sub-Cretaceous etch-surface extends from Scania northwards along the coasts of western Sweden and southern Norway. The black frames denote the greater Oslofjord region and the ROGAS area. Note that the sub-Cretaceous etch-surface has been eroded in the area to the north of Egersund in Rogaland. There are therefore some uncertainties about how much is remaining of the deep weathering in this area.*

The weathering penetrated deeper into pre-existing fracture zones and was preserved below Late Jurassic and Cretaceous sediments. Subsequent exhumation, particularly during the extensive Pleistocene glaciations removed most of the deep weathering. Clay zones occurring to depths of 200-300 metres were, however, preserved.

The weakness zones in this sub-Cretaceous etch-surface consist partly of clay minerals such as kaolinite and smectite and are to a large extent the result of chemical weathering during tropical conditions in the Jurassic (Lidmar-Bergström 1989). The weathering occurred originally across the entire paleo-surface, but gradually penetrated deeper into the pre-existing fracture zones (Figure 4.3).

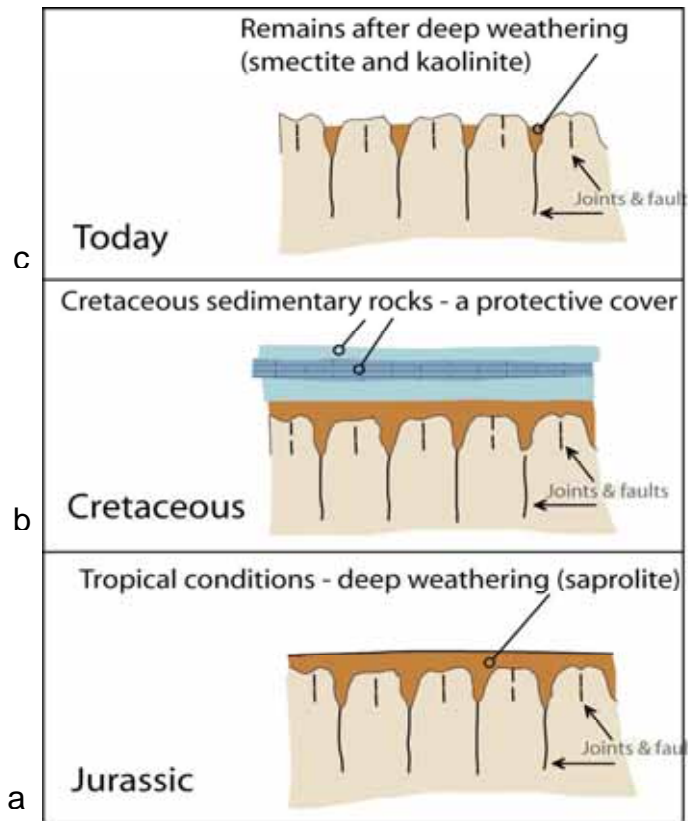


Figure 4.3. Schematic illustration of the process leading to the present day deep weathering products. A) Jurassic weathering (etching) across the entire paleo-surface with deeper penetration into pre-existing fracture zones. B) Preservation of chemical weathering below shales and carbonates deposited during the Late Jurassic and Cretaceous transgression. C) Uplift and erosion during the extensive Pleistocene glaciations. The bulk of the chemical weathering was removed leaving an immature etch surface landscape with joints and faults.

The chemical weathering was preserved below shales and carbonates deposited during the Late Jurassic and Cretaceous transgression (c. 400 metre higher sea level). Exhumation of south-eastern Norway was initiated during the Early Cenozoic and the uplift and erosion accelerated during the extensive Pleistocene glaciations. Although the glacial erosion removed the bulk of the chemically weathered materials, the clay zones were preserved to depths of 200-300 metres along the fracture zones.

The exhumation and erosion history of western Norway is, however, different from south-eastern Norway as illustrated by Lidmar-Bergström et al. (1999) in Figure 4.2. The innermost part of the coastal area is dominated by glacially eroded valleys and fjords while the outermost coastal areas was mostly formed by an erosion mechanism involving freezing, thawing and wave-abrasion (e.g. Holtedahl 1953). The chances for finding remnants of the deep weathering are therefore largest in the outermost strandflat area, i.e. outer Jæren-Boknfjord and Karmøy areas.

During tropical weathering, iron oxides such as magnetite alter to hematite and iron-hydroxides at the same time as silicate minerals are converted into clay minerals (e.g. Henkel & Guzmán 1977, Grant 1984). The deep weathering will therefore create a negative deviation in the Earth's magnetic field. It is generally observed that the thick layer of weathered rock (saprolite) in tropical areas can be subdivided into several weathering zones (Acworth 1987). The deeper zone is often dominated by a granular friable layer of disintegrated crystal aggregates and rock fragments while a more shallow zone has massive accumulation of secondary minerals (clays) in which some stable primary minerals may be present in their original form.



#### 4.2.2 Deep weathering

**The topography grid** was produced using digital hypsographic and hydrographic vector data (see section 5.2 for details). The final grid shown in Figure 4.4 was displayed using the shaded-relief technique with illumination from the east. To enhance the high wave number component of the compiled dataset, a shaded relief version (in grey-tones) of the 1 km Gaussian high-pass filtered grid has been produced and superimposed on the coloured map.

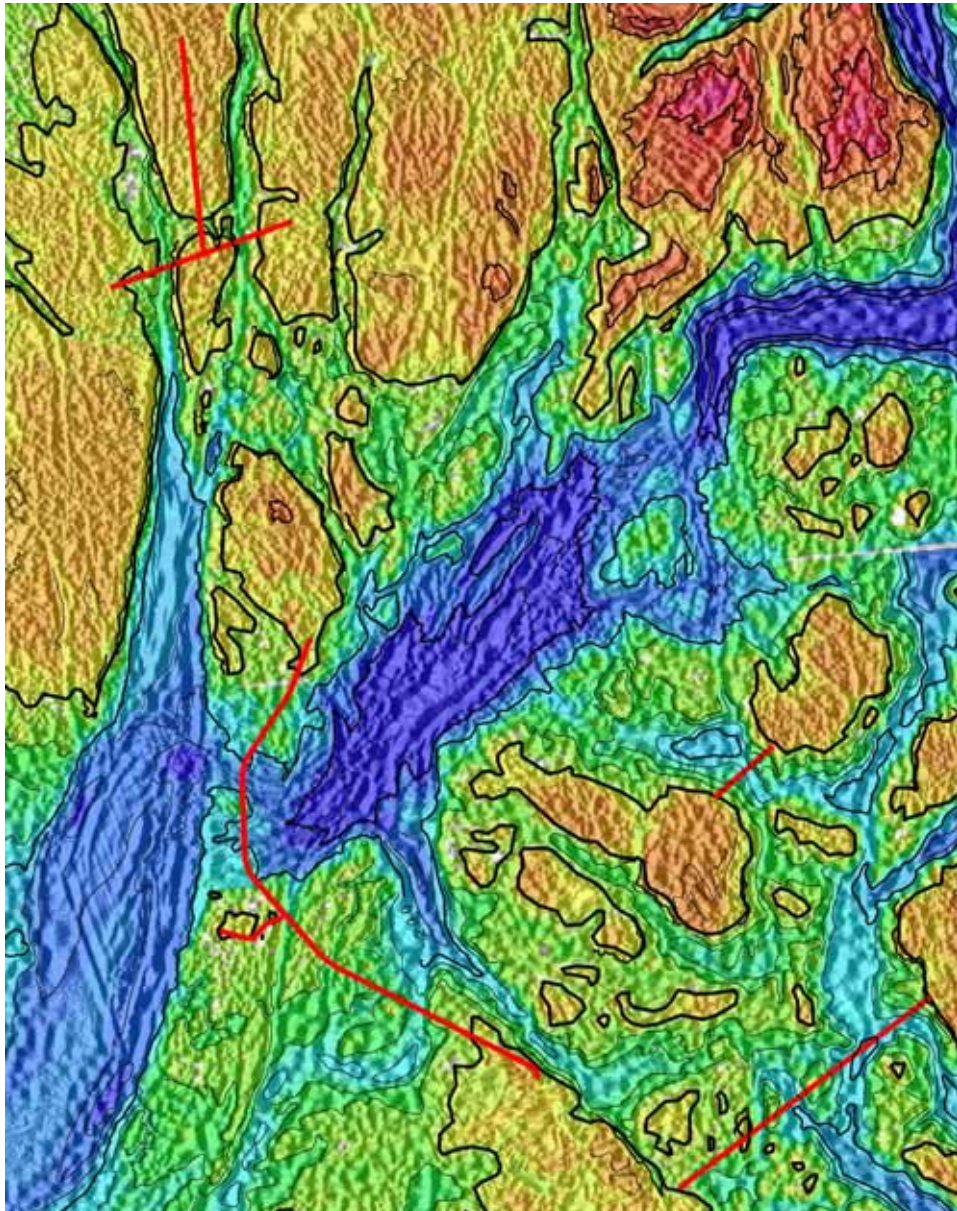


*Figure 4.4. Topography and bathymetry from the outer Bokn fjord area. A shaded relief version of the 1-km high-pass filtered topography and bathymetry superimposed on a colour version of the same dataset.*

**The magnetic profiles** were merged into a regular grid of 50x50 metres cells using the bicubic spline gridding algorithm (Geosoft 2004). To enhance the high wave-number component of the compiled dataset, a shaded relief version (in grey-tones) of the 8 km Gaussian high-pass filtered



grid has been produced and superimposed on the coloured total field map (Figure 4.1). We have also produced an analytic signal grid (total gradient amplitude), which enhances the high-frequency content of the data (Figure 4.5).

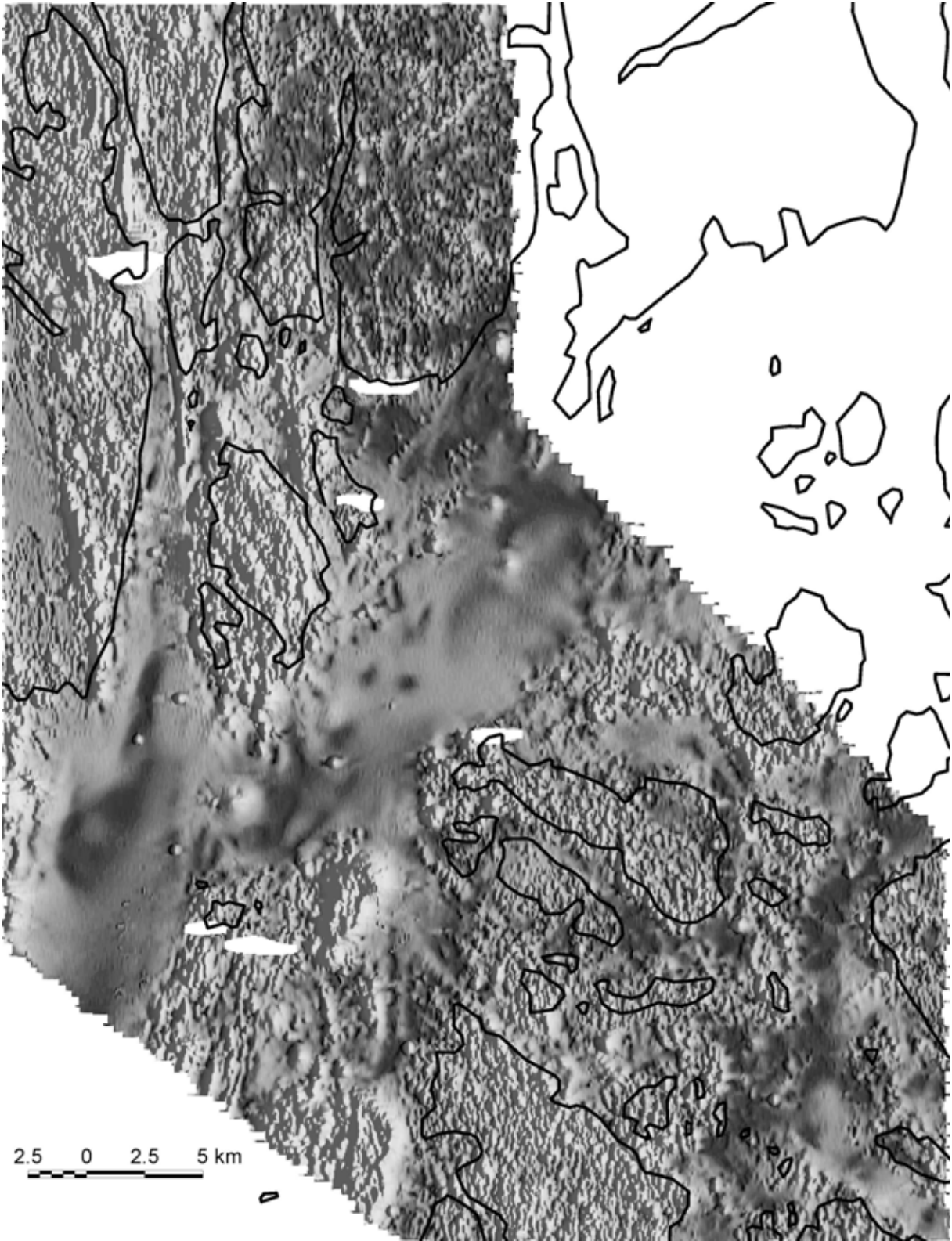


Figure 4.5. An analytic signal map (total gradient amplitude map) of the aeromagnetic grid.

The magnetic field has been reduced to the magnetic pole using a frequency-domain filtering package (Geosoft 2005). We have further carried out a 1 km Gaussian high-pass filtering of both the magnetic (Figure 4.6a) and topography/bathymetry grids (Figure 4.6b). Coinciding negative anomalies in the two high-pass filtered datasets are used as indications of deep weathering. The resulting signal is classified as 'probable' or 'possible' weathering depending on the signal to noise ratio. Pronounced anomalies with amplitudes below -5 m and -5 nT, respectively, are classified as 'probable', while less pronounced anomalies between -5 m and -2 m and between -5 nT and -2 nT, respectively, are classified as 'possible'.

#### 4.2.3 Magnetic dislocations

Total magnetic field (figure 4.1) and 1 km high pass filtered data (figure 4.6a) are used to delineate magnetic dislocations (Henkel 1991). We have also lent support from the topography/bathymetry map (figure 4.6b) when identifying the most pronounced dislocations. Magnetic dislocations are identified as

- 1) Offset of linear magnetic anomalies.
- 2) Linear termination of the magnetic anomaly pattern
- 3) Linear gradients
- 4) Linear minima

and can be interpreted as bedrock borders, faults and fractured zones. Magnetic dislocations are shown in figure 4.6c, and also in the final interpretation map.

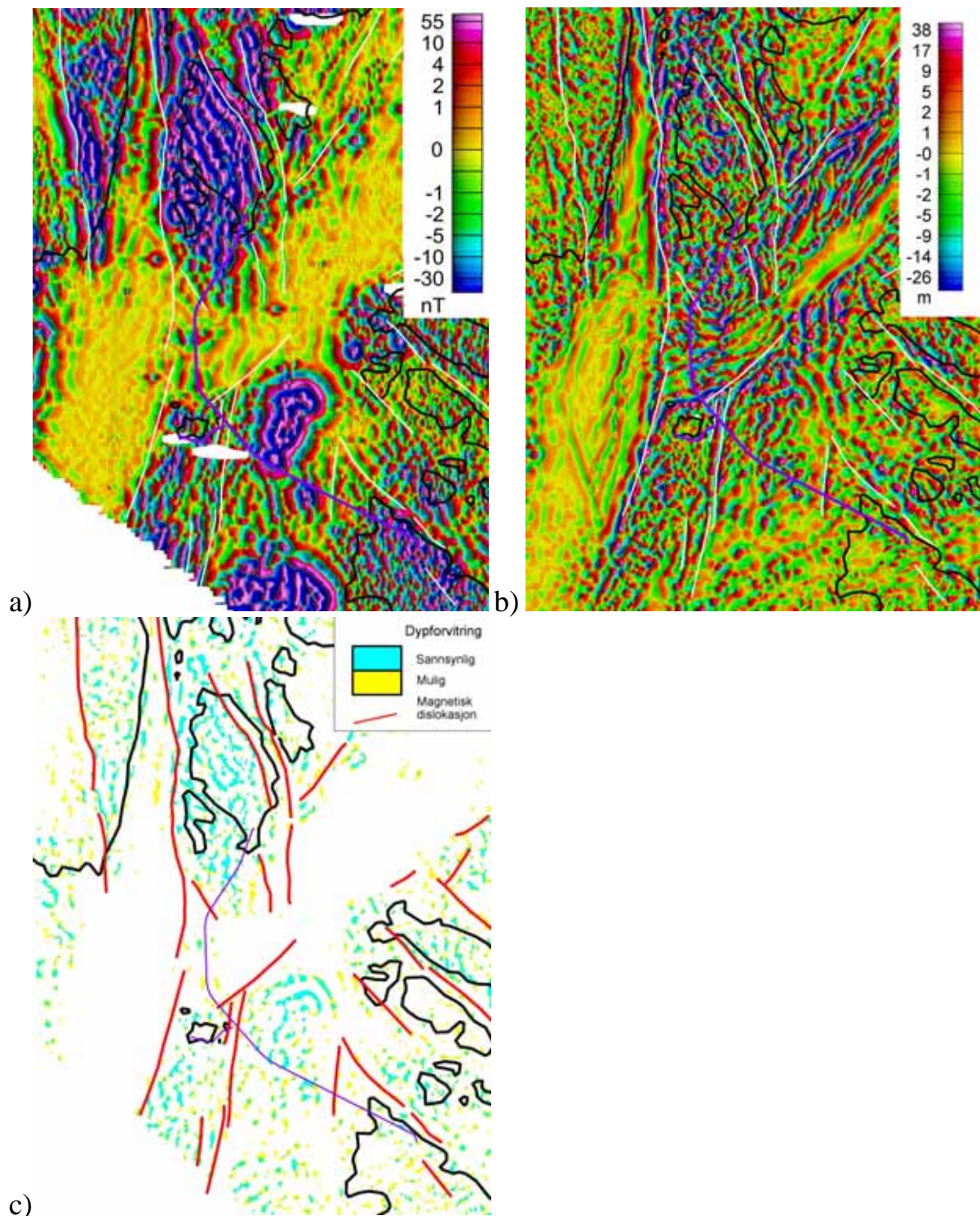


Figure 4.6. Interpretation map of outer Bokn fjord area. a) 1 km highpass filtered aeromagnetic data. b) 1 km highpass filtered topography/bathymetry. c) Predicted zones of deep weathering based on the processed magnetic and topographic data in Figures a) and b) above are shown in blue 'probable (sannsynlig)' and yellow 'possible (mulig)'. Interpreted magnetic dislocations (possibly weak zones) are marked with white and red lines in figure a/b and c respectively.



### 4.3 Modelling of magnetic data

The magnetic total field presented in figure 4.1 reveal some strong magnetic anomalies close to the tunnel line between Randaberg and Kvitsøy. The shape of these anomalies indicates that they might be caused by shallow magnetic material of the same kind as exposed at Karmøy outcropping at the sea bottom. In that case, the tunnel might end up following a thrust plane, which could cause serious construction problems. To get better control on the geology, magnetic modelling along three lines was performed (see figure 4.7).

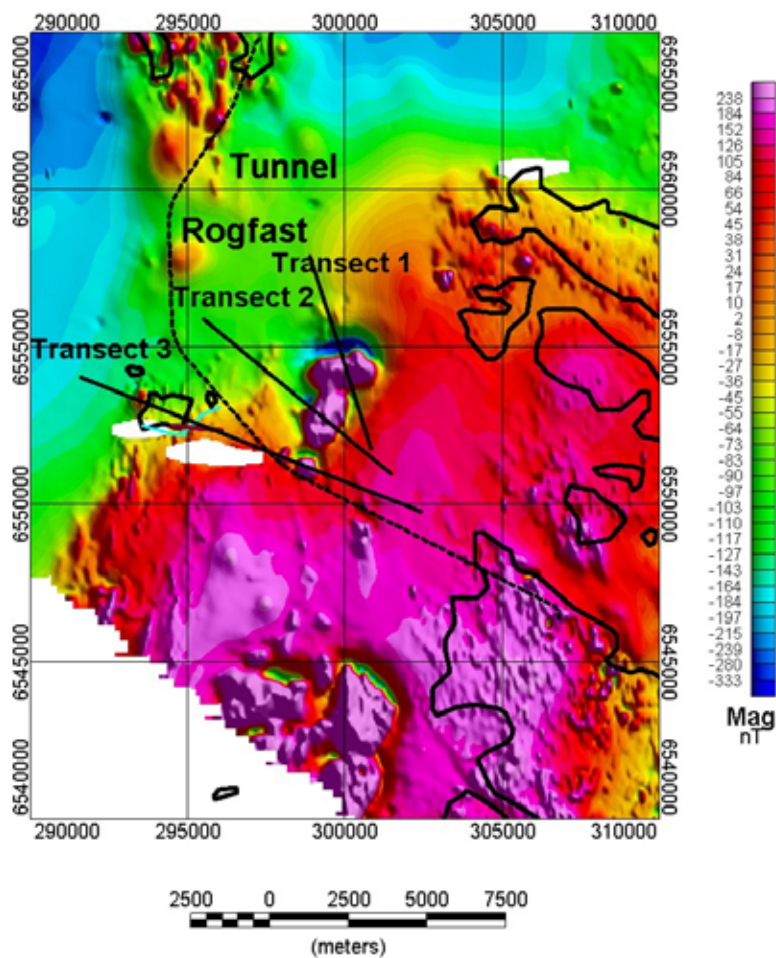


Figure 4.7. Location of aeromagnetic interpretation profiles (transects).

#### 4.3.1 Modelling software and input parameters

Magnetic modelling was performed applying the interactive forward modelling software GM-SYS (Northwest Geophysics & Ass. 2004). The program uses parallel vertical cross-sections with a polygonal structure and triangulates between the sections. Bodies of different magnetisation are defined, and the shape and magnetic properties are changed until model response fits with the measured data.

In figures 4.8, 4.9 and 4.10, five different bodies are defined. These are described as follows:

- Blue: Seawater. Magnetic susceptibility 0 ( $10^{-6}$  SI units)
- Yellow: Phyllites, greenstones, nonmagnetic gabbros of different nappe complexes. Magnetic susceptibility 500 ( $10^{-6}$  SI) (average value, see section 3.1)
- Orange: Autochthonous Precambrian basement. Magnetic susceptibility 2000( $10^{-6}$  SI)
- Brown: Magnetic body, possible ultramafic rocks belonging to the Hardanger nappe. Magnetic susceptibility 100.000 ( $10^{-6}$  SI)
- Green: Possible deep weathering. Magnetic susceptibility ( $10^{-6}$  SI)

Seawater depth is taken from the known bathymetry in the area.

#### 4.3.2 Results of magnetic modelling

Results of the modelling along the three transects are presented in figures 4.8, 4.9 and 4.10. Black dots represents measured data, black line calculated data from model while red curve is the difference between these two.

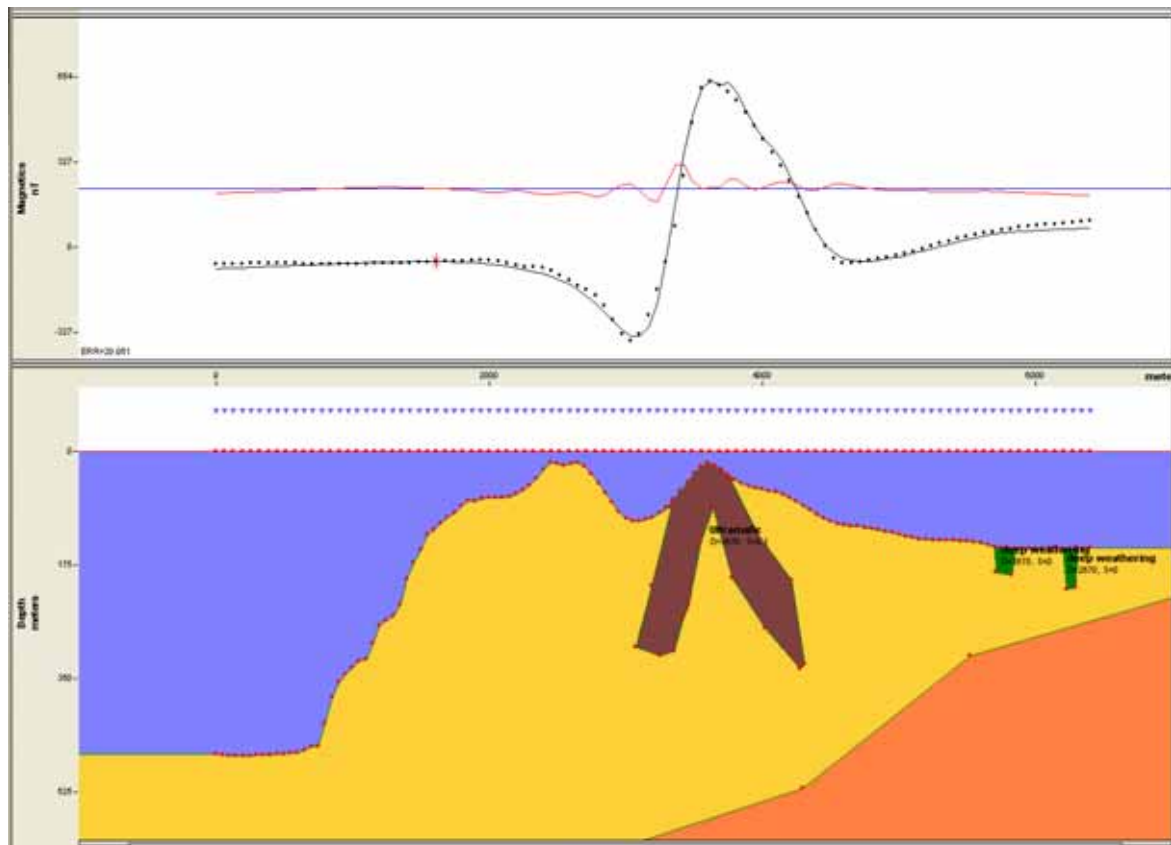


Figure 4.8. Magnetic modelling along transect 1.

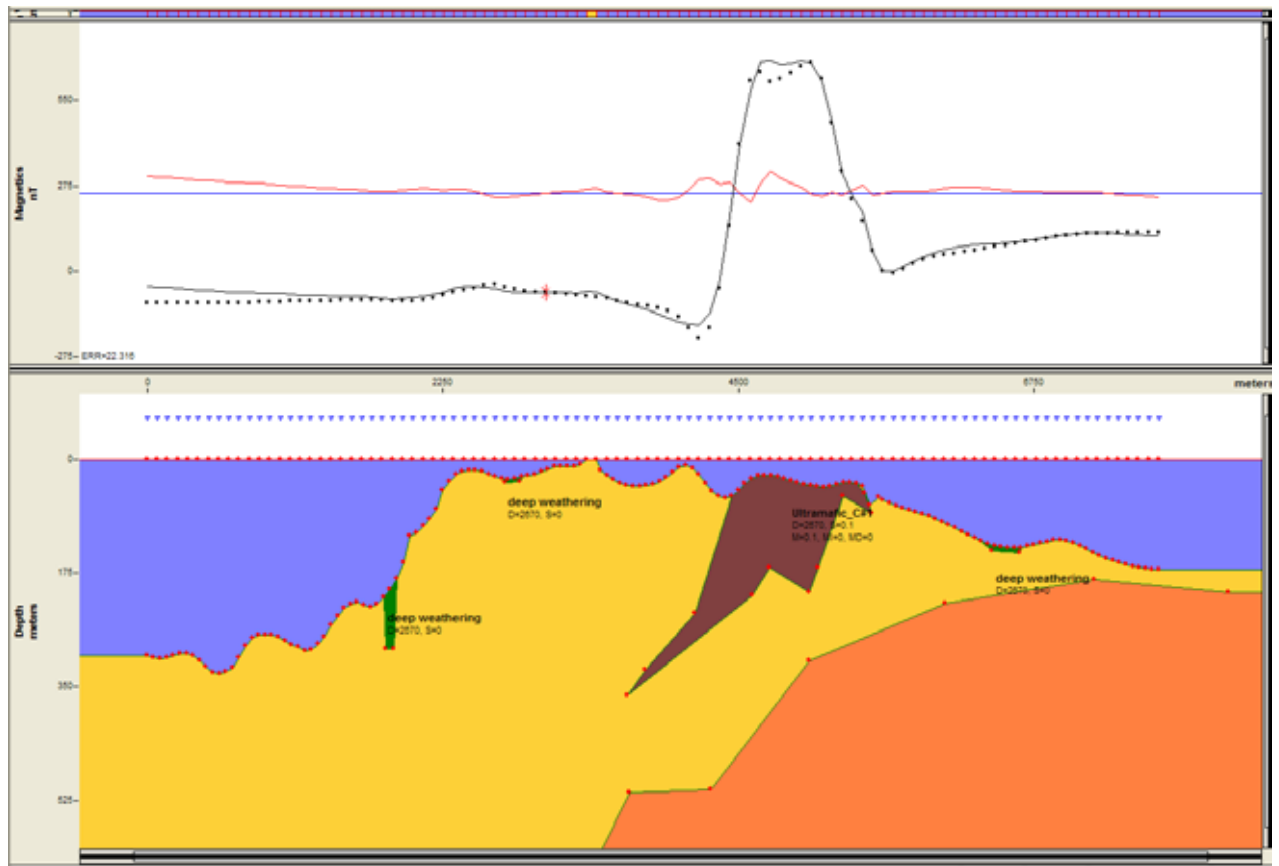


Figure 4.9. Magnetic modelling along transect 2.

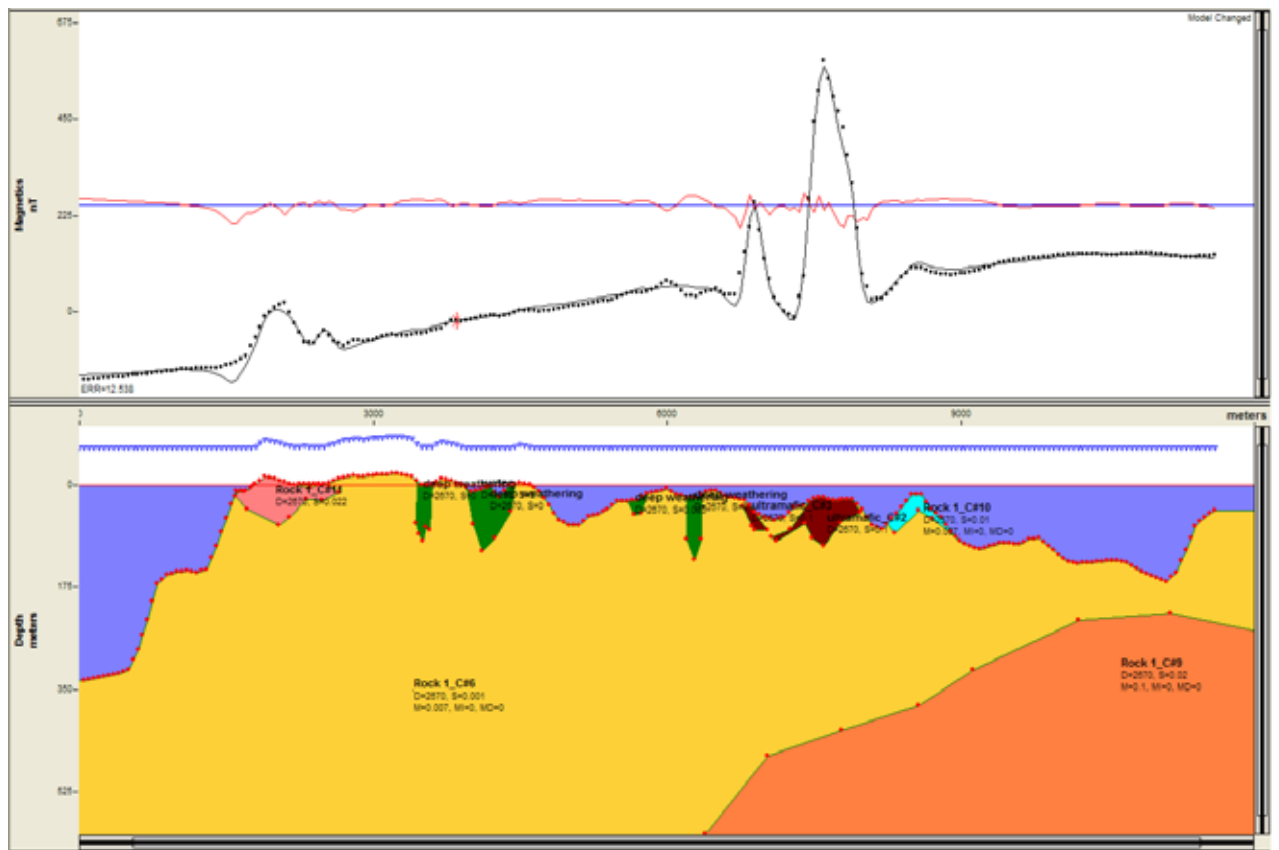


Figure 4.10. Magnetic modelling along transect 3.

To explain the regional trend in the magnetic field, it was necessary to introduce a magnetic basement, which is dipping down towards the north and west. Since we have no petrophysical data of the basement in the area, the value used in the model is just a guess. As a result, the depth to magnetic basement is uncertain.

The main reason for doing this modelling was to estimate the depth extent of the magnetic bodies indicated between Randaberg and Kvitsøy. Along transects 1 and 2, outside the tunnel trace, the depth extent is on the order of 350 metres below sea level. At transect 1, which runs more or less along the tunnel trace, the depth extent is limited to approximately 120 metres below sea level. At this site, the tunnel is planned to go deeper than 200 metres below sea level, and it will probably not cut the magnetic body.

The green bodies in the modelled profiles were introduced to simulate deep weathering. Unfortunately, in this area the contrast in magnetic susceptibility is too low to give any idea of how deep a possible weathering can go.

## **4.4 Discussion of magnetic interpretation**

### **4.4.1 Deep weathering**

The less strict criteria of -2m and -2 nT reveal potential weathering in relatively low-magnetic bedrock but in addition produce some artefacts that are unlikely to be related to clay alteration since some of them occur as isolated patches spread out in the terrain. The application of the more strict thresholds (-5m and -5 nT) in the filtering process provides a result that coincides with more linear zones and could therefore represent zones of deep weathering in the bedrock.

A set of dislocations in the aeromagnetic anomaly map has been observed. Three main orientations occur: N-S, NW-SE and NE-SW. We think that the majority of the dislocations represent fault and weakness zones in the crystalline bedrock. The linear aeromagnetic and topographic anomalies (Figure 4.6) may also, however, have other origins and could be related to:

- a) dikes and sills
- b) layered intrusions

The Amager method has proven capable of detecting c. 90 % of the known fracture zones in the Lieråsen and Romeriksporten railway tunnels and Oslofjorden and Hvaler road tunnels in south-eastern Norway (Olesen et al. 2004a,b, in press). Modelling of the observed magnetic field indicated that some of the low-magnetic zones continue to a depth of c. 300 metres below the surface. We concluded that aeromagnetic data should be acquired prior to planning of long tunnels in bedrock with tropical weathering or hydrothermal alteration. We have therefore tested the Amager method in the outer Boknfjord area.

The Amager method will not produce valid results in bedrock with very low magnetisation since there will be no magnetic ferro-oxides to oxidize to low-magnetic ferro-hydroxides. If the deep weathering has been removed by glacial erosion in a fjord, valley or a strand flat the conditions for an aeromagnetic mapping of these zones are of course not fulfilled. It is therefore important that an experienced geologist or geophysicist assess the magnetisation of the bedrock from either petrophysical measurements in the field or laboratory measurements on collected bedrock samples or by a careful inspection of the aeromagnetic map. It is also

crucial that the results from the present study are compared with the observed clay zones in the existing Rennfast tunnels to check the validity of the method.

The original application of the Amager method (Olesen 2004a,b) involved utilisation of a 50x50 metre grid acquired by gridding the 20-metre contours on the 1:50.000 scale topography map series of Norway. The results from processing of the improved topography dataset from 1:5.000 and 1:10.000 scale maps (Olesen et al. in press) revealed some more details but did not deviate significantly from the initial interpretation. This conclusion shows that the method is quite robust and is not fully dependant on a high-resolution topography/bathymetry dataset to produce reliable results.

The Amager method is supposed to work in Fennoscandian bedrock that was exposed to Mesozoic weathering and exhumed during the Neogene. Lidmar-Bergström et al. (1999) have identified two such areas in Norway; the Skagerrak-Kattegat coast (including the greater Oslofjord region) and the Fosen Peninsula-Trondheimfjord area in Mid Norway (Fig. 4.2).

#### 4.4.2 Magnetic modelling

In the magnetic modelling, a susceptibility of 100000 ( $10^{-6}$  SI units) was used in the most magnetic bodies. This value is based on one single laboratory measurement and 12 in situ measurements at one exposure. To test the sensitivity of the method, we tried to model the same profiles with a reduction of 20% in the susceptibility of the most magnetic body. This did not influence on the depth extent significantly. Based on this, we conclude that the depth estimates are reasonable.

The most magnetic modelled bodies are supposed to be ultramafic part of the Karmøy ophiolite in the Hardangerfjord nappe. From the petrophysical analysis and what we can see from the magnetic map at Karmøy, we know that the ophiolite also consists of nonmagnetic rocks like gabbro (sample ASO-3, Appendix A2) and others. The total thickness of the Karmøy ophiolite in the sea between Randaberg and Kvitsøy can be greater than indicated in the modelling.

In order to find the thickness of the nonmagnetic nappe bedrocks in the area, an Euler deconvolution (Reid et al 1990, Thomson 1982) analysis was performed on the magnetic data. By this method it is possible to calculate the depth down to a magnetic body. This analyse gave interesting results describing the variations in depth to magnetic bedrock, however, the data were far to uncertain to be used in the planning of a great tunnel project. Magnetic anomalies between Kvitsøy and Vestre Bokn seem to be caused by magnetic bodies at a depth of 300 to 500 metres.



## 5 DIGITAL TOPOGRAPHY AND BATYMETRY

### 5.1 Data sets and acquisition

The following datasets were used in this study:

- High-resolution bathymetry from south of Kvitsøy, obtained from Blom as randomly spaced xyz points
- High-resolution bathymetry from north of Kvitsøy, obtained from Statens kartverk, sjøkartverket as randomly spaced xyz points
- Low-resolution bathymetry from Statens kartverk as a grid with 50 metre pixels
- Low-resolution topography from Statens kartverk as a grid with 25 metre pixels
- High-resolution topography from FKB (felles kart base) as vector contours with 1 metre spacing

### 5.2 Data processing

Vector topographic data including elevation contours, spot heights and hydrographic features were used to build a triangular irregular network (TIN). This TIN was then interpolated onto a regularly spaced grid with 5 metre pixels. Randomly spaced topographic data from Blom and Sjøkartverket were interpolated onto a 1 metre grid using a minimum curvature algorithm. All high- and low-resolution datasets were then merged into a single topographic model.

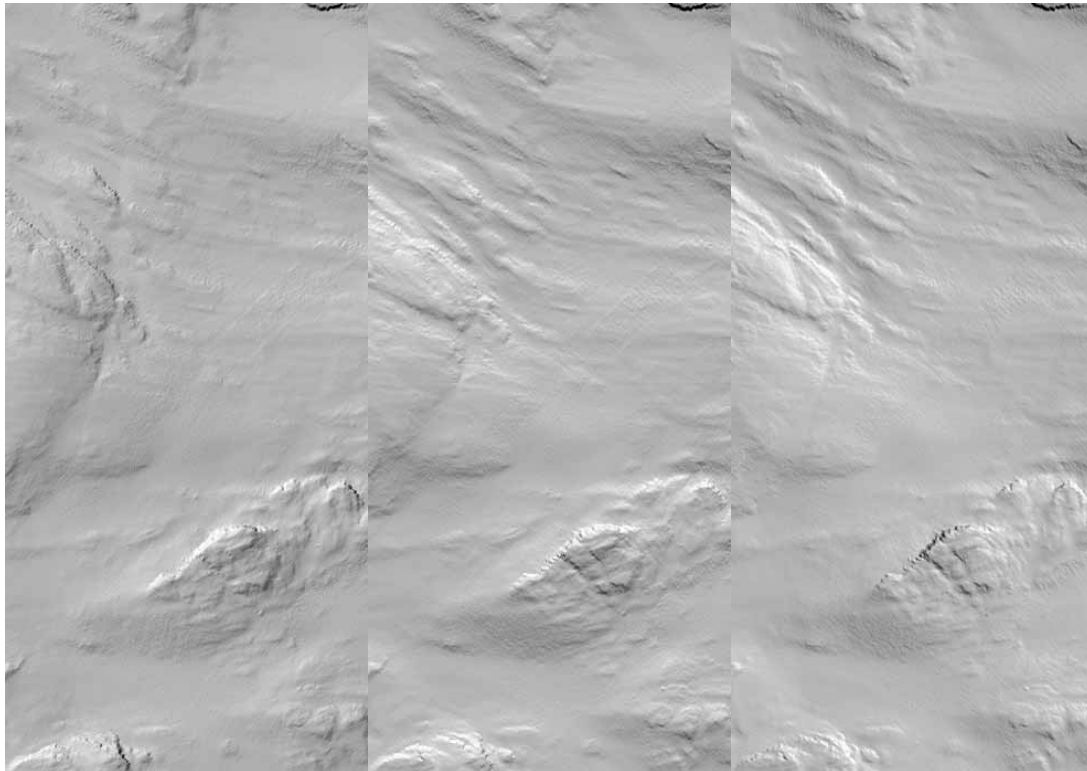


**Figure 5.1.** Shaded images produced by artificial illumination of the digital topographic model. Each image covers the same area using a different sun-angle. The left image has lighting from the NW. The middle image has lighting from the N. The right image has lighting from the NE.

Artificial illumination of the topographic model produces a shaded image that is easier to interpret than actual height values. By varying the 'sun-angle,' various images can be made. The choice of sun angle is important, as features perpendicular to the illumination direction are highlighted while those parallel to this direction tend to be subdued (Figure 5.1). For this study, three images were interpreted, with illumination from northwest, north and northeast.

### 5.3 Lineament analysis

Linear and curvilinear features were digitised based upon subjective interpretation of the images. Most features represent probable faults or fracture zones. Some features were identified as submarine landslide scarps (Figure 5.2) or glacial scour marks (Figure 5.3). These were excluded from further analyses.

We must emphasise the importance of acquiring the highest resolution topographic data available. High-resolution data was available along most of the tunnel trace but not over the entire study area. In some cases, lineaments appear to stop at the edge of the high-resolution data (Figure 5.4). Many of these lineaments probably continue but are not visible using lower-resolution data.

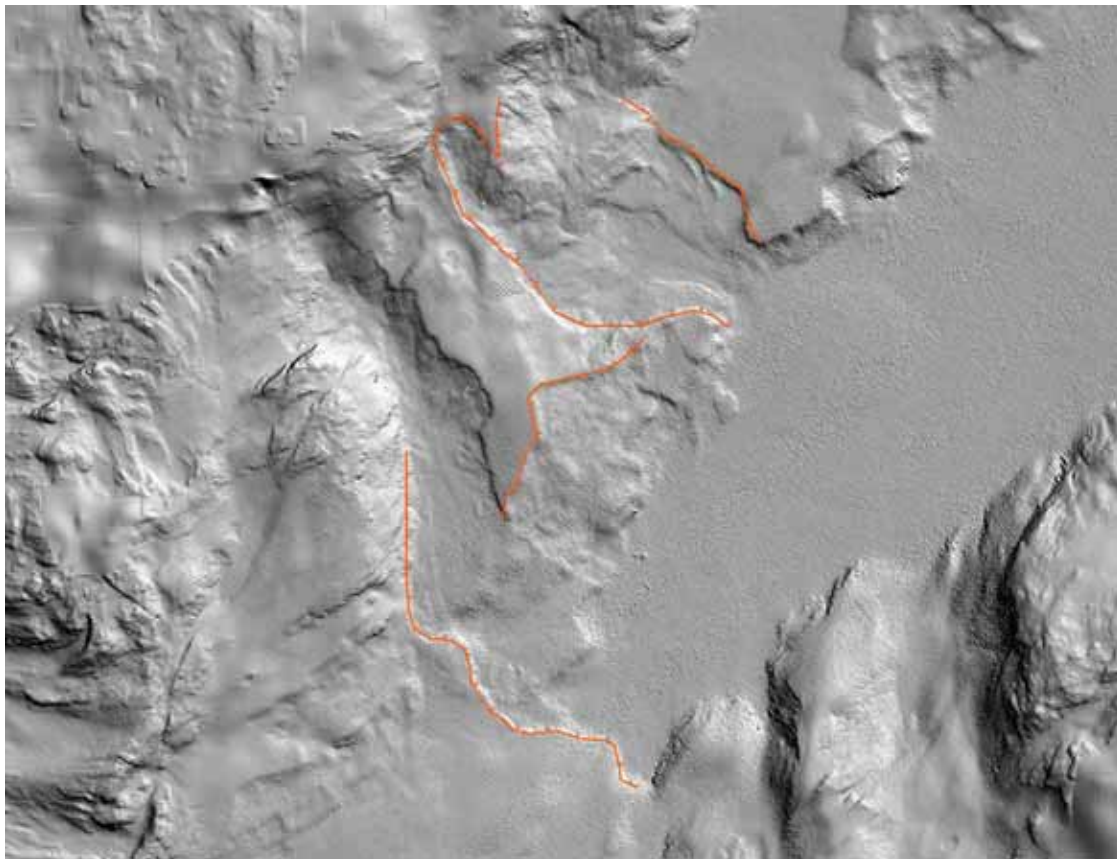


Figure 5.2. Submarine landslide scarps.

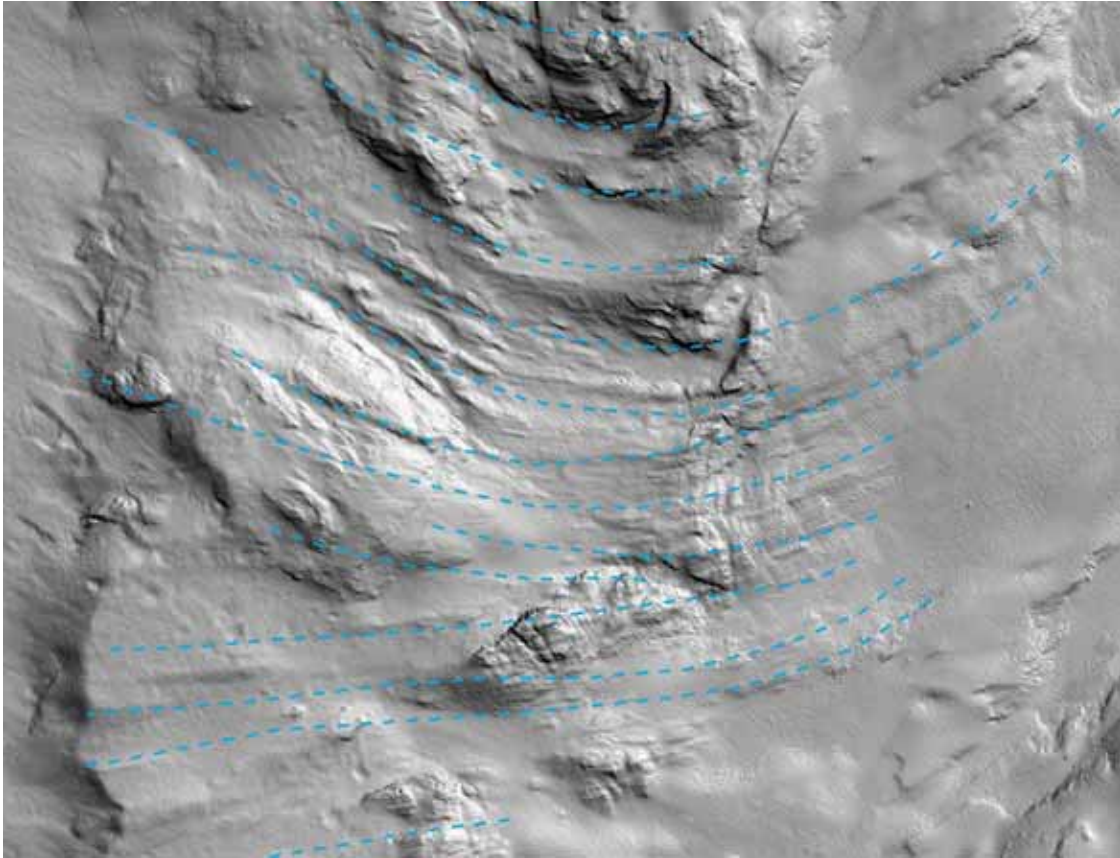


Figure 5.3. *Glacial ice scours.*

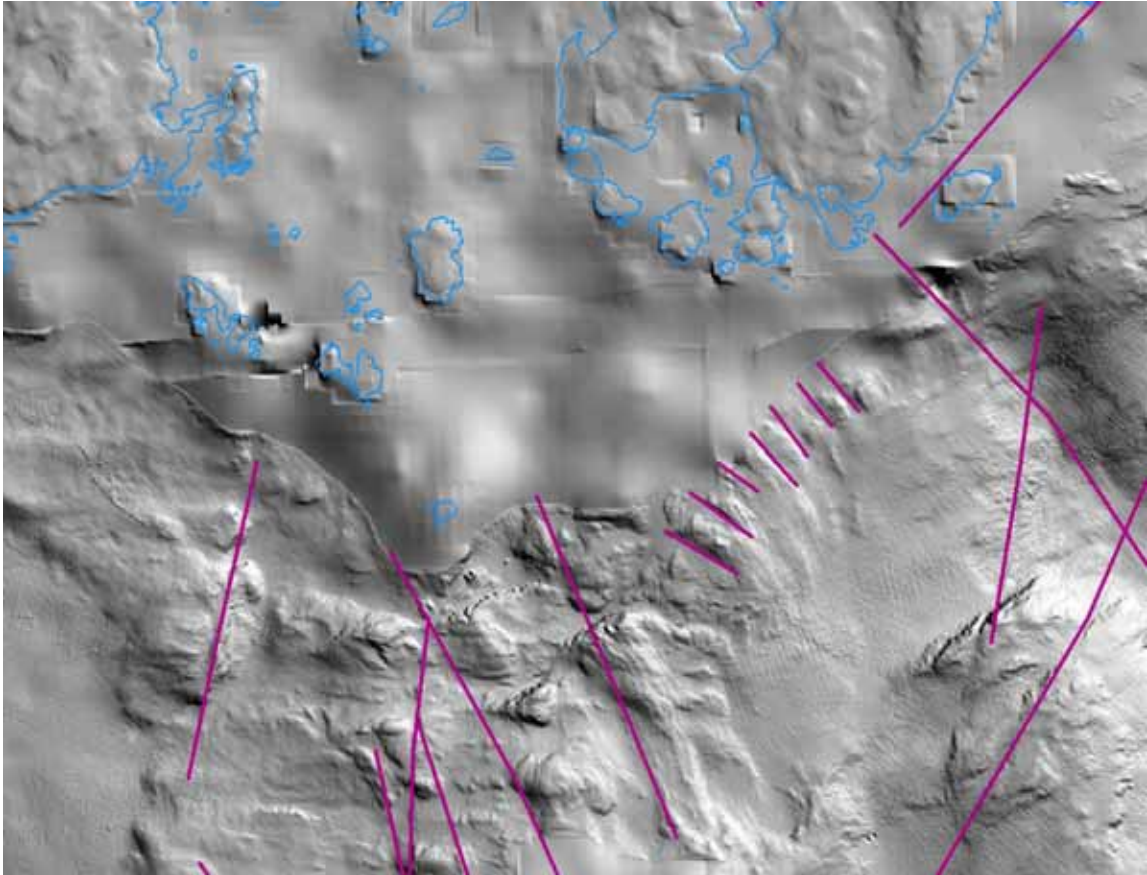


Figure 5.4. *Many lineaments seen in the high-resolution data are not visible where only low-resolution data is available. This does not mean that these features do not continue.*

Directional analysis was done using the intercept method (Launeau & Robin 1996). The technique is based on counting the number of times a set of parallel test lines intercepts a set of objects along a number of directions. The number of intercepts is a periodic function of  $\alpha$ , the counting direction, and can be represented by a Fourier series (Launeau & Robin 1996). From this Fourier series, a 'rose of directions' can be calculated. By truncating the Fourier series at a level such that the resulting curve matches the main features of the data curve, we are able to obtain a measure of directional intensity that is both weighted by lineament length, and smoothed to remove noise.

Figure 5.5 shows the results of the lineament analysis. The main directions are very similar to those obtained from the Landsat imagery. Differences are due to the fact that a smaller area was analysed at higher resolution than the satellite study.

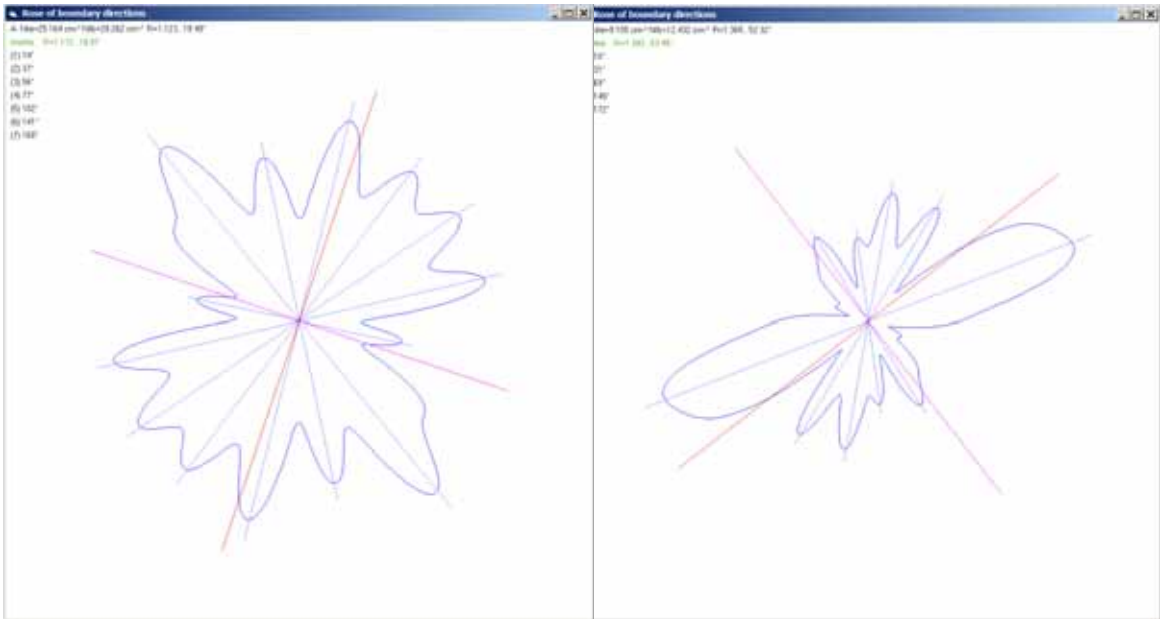


Figure 5.5. Rose of directions of lineaments interpreted using the topographic model (left) and satellite image (right).

In order to be confident that the subjective manual lineament interpretation had highlighted all the lineaments populations, a fully automatic lineament extraction was performed (Figure 5.6). This resulted in many short, small lineaments. However, the directional analysis shows the same features as for the manual interpretation.





## 6 STRUCTURAL AND GEOLOGICAL STUDIES

This chapter describes the results of follow up studies conducted by Aline Saintot (May 2006), Øystein Nordgulen (June 2006) and Arne Solli (September 2006).

### 6.1 General description

#### 6.1.1 Visited sites

More than 40 sites (figure 6.1) have been visited in order to better characterise the structural geology of the area. In Appendix B, all measurements and related stereoplots and comments are listed at each visited sites. Field studies have been performed in four geographically distinct zones (figure 6.1) and will be presented accordingly in the following sub-sections: field studies in the Randaberg region, on Kvitsøy, at Vestre Bokn and at Bru-Sokn-Mosterøy-Rennesøy.

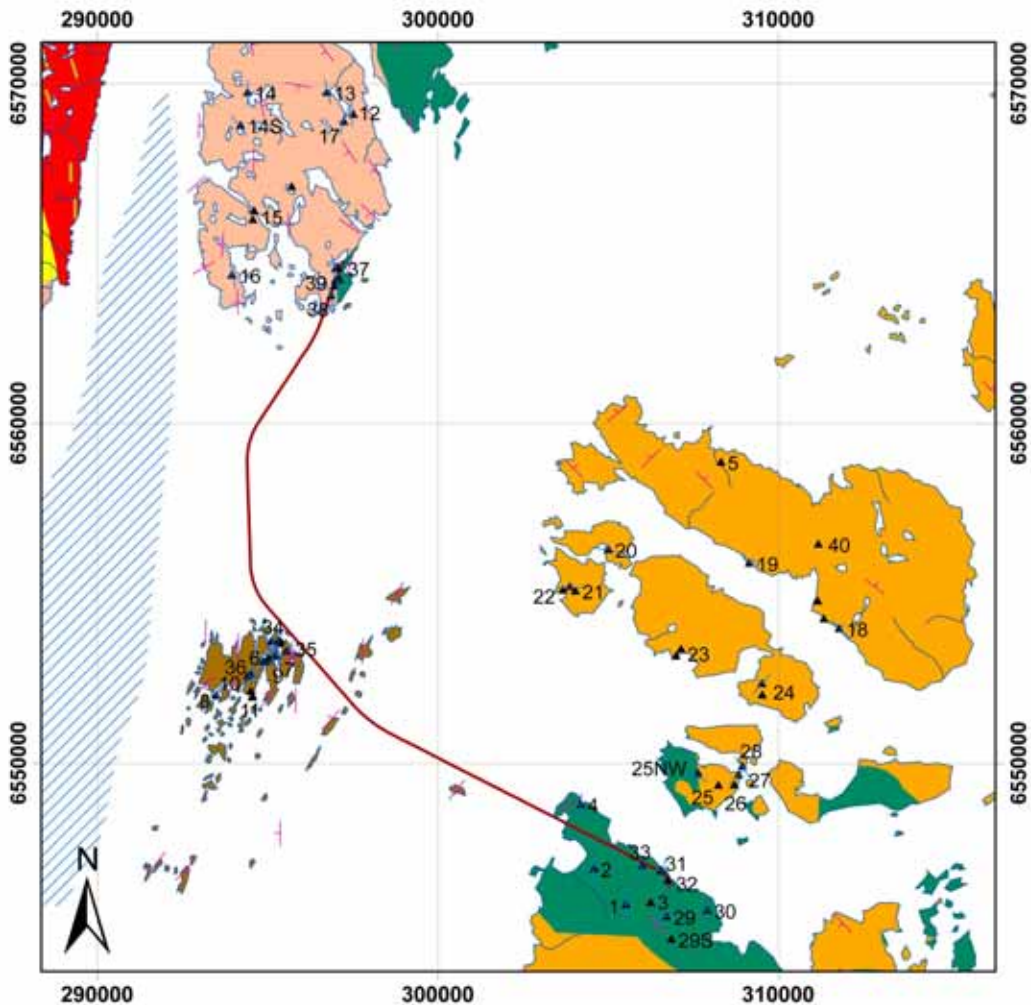


Figure 6.1. Locations of field sites. The geological maps of Stavanger and Haugesund (scale 1:250000) as background. In pink: attitude of foliations as on the geological maps; in dark purple: attitude of foliations as observed at studied sites.

The field study focused on structural geology and brittle tectonics. As such, 507 planar structures have been measured and an overview of their attitude is given on left rose diagram in figure 6.2. A large set of fractures is close to N-S (from NNW-SSE to NNE-SSW). Two other trends are well identified as NE-SW and WNW-ESE. The fractures are steep. The total set of data has been split in two sub-sets: fractures without striae on their surfaces and striated faults (388 and 119 data respectively), rose diagrams at the centre and to the right of figure 6.2. It follows that (1) the WNW-ESE set corresponds to fractures on which striae has not been observed; (2) the NE-SW set is composed of both types of data (fractures displaying slickensides or not) and (3) the NNW-SSE to NNE-SSW set is mainly the striated faults.

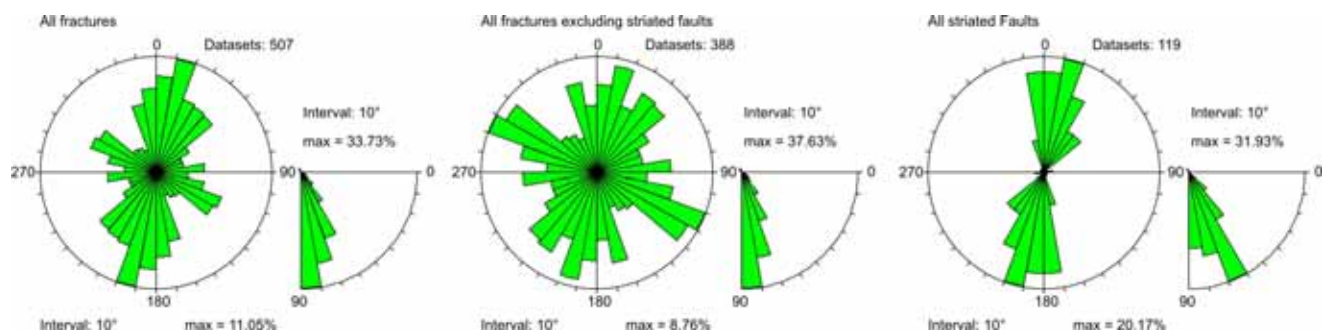


Figure 6.2. An overview of all brittle data collected on the field.

### 6.1.2 Keys to read stereoplots in the following sections

At the scale of the outcrops, a systematic analysis of brittle structures has been made. It includes the analyses of fault slip data, which comprises an analysis of strikes and dips of fault sets and of azimuth and plunges of their striae. It allows the characterisation of the kinematics of fault trends (even major fault trends). Figure 6.3 give the keys for reading stereoplots of fault slip data sets. The other brittle structures have been also taken into account and plotted as such: undistinguished fractures/diacleases/joints in black, tension gashes in blue (only used if minerals have clearly grown into the fractures, this implies an opening of the fractures under tension), metamorphic foliation and lineation in green, fold planes and axes in red (Figure 6.4).

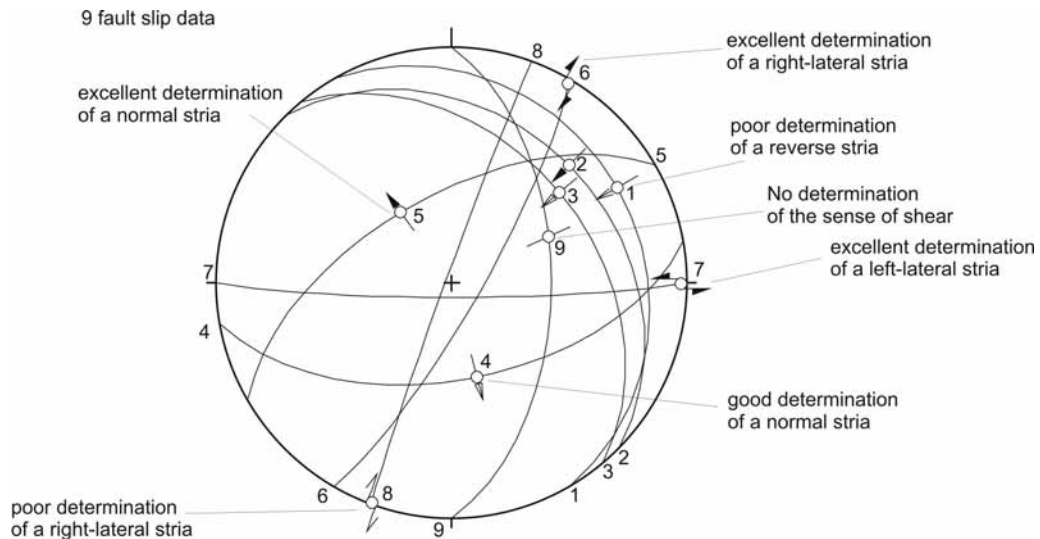


Figure 6.3. Example of stereonet for fault slip data, Schmidt's projection, lower hemisphere. Keys for striae: outward directed arrow: normal striae (numbers 4 and 5 on stereonet); inward directed arrow: reverse striae (numbers 1, 2 and 3); couple of arrows: strike-slip striae (numbers 6, 7 and 8); full black arrow: excellent constraints on the sense of shear (numbers 2, 5, 6 and 7); empty arrow: good constrains on the sense of shear (numbers 3 and 4); simple arrow: poor constrains on the sense of shear (numbers 1 and 8); thin line: no determination of the sense of shear (number 9).

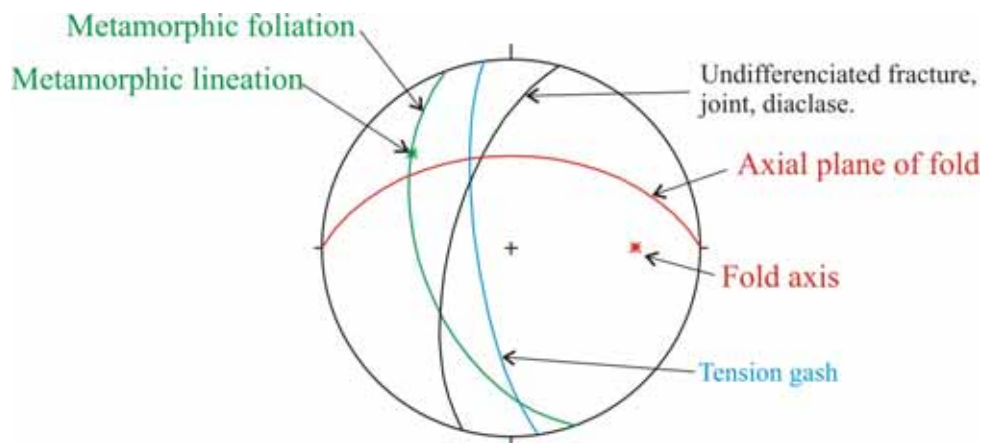


Figure 6.4 Example of stereonet for structures other than fault slip data, Schmidt's projection, lower hemisphere. Undistinguished fractures/diaclasses/joints in black, tension gashes in blue, metamorphic foliation and lineation in green, fold planes and axes in red.



## 6.2 Structural field studies

All detailed field observations are listed in Appendix B. In the following, a summary of all observations is presented together with photo documentation.

### 6.2.1 Field studies at Randaberg

10 sites have been visited in the Randaberg area (figure 6.5). All of them are the quartz-rich Ryfylke schist.

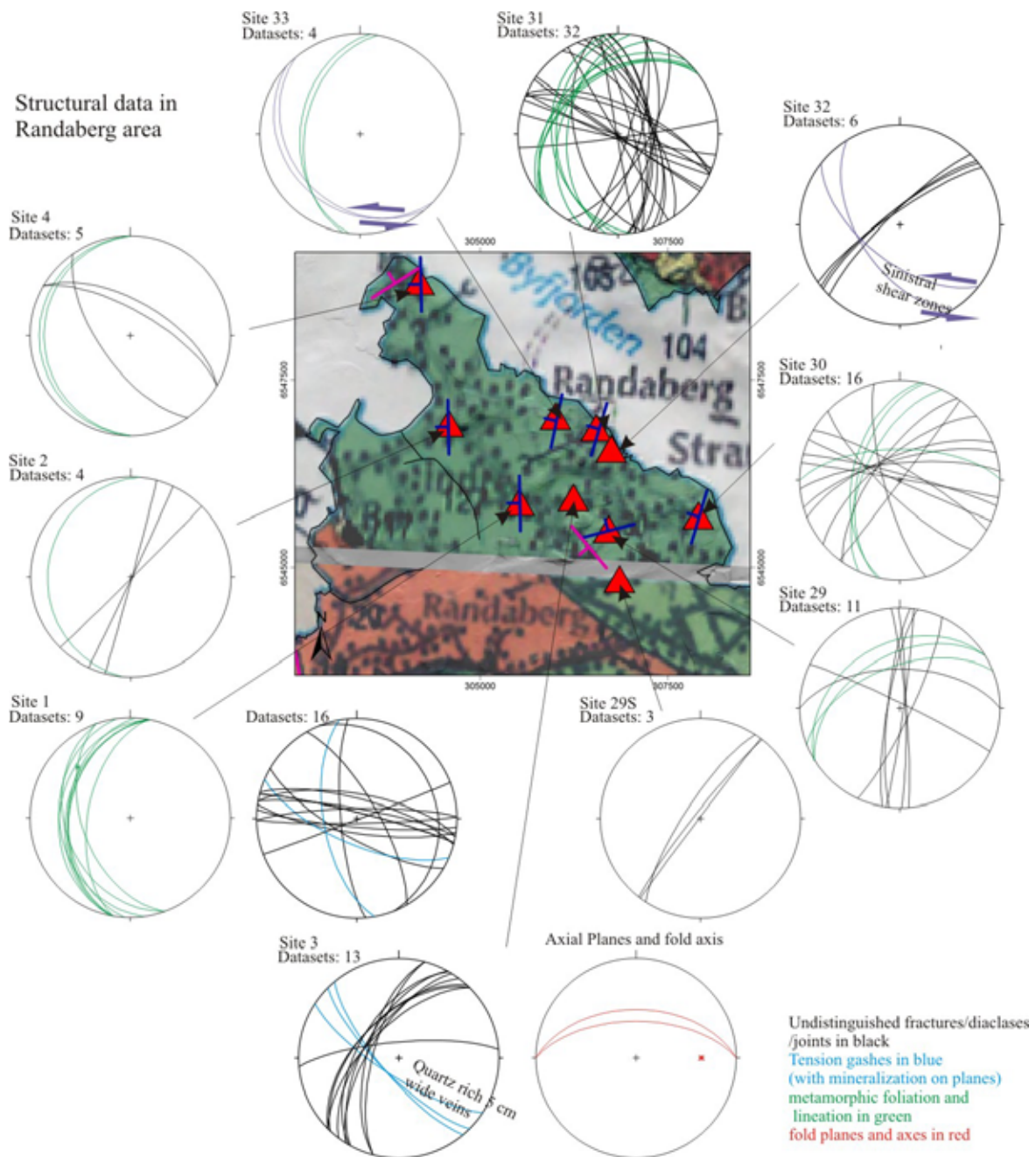


Figure 6.5. Stereonets of structural data in Randaberg region.

The metamorphic foliation is shallow and dipping to W and NW at the 10 sites in Randaberg region (stereoplots on Figure 6.5). In some places, the micaschists are folded and the fold wavelength does not exceed few centimetres (site 3). Ductile shallow SW-dipping shear zone are present at sites 32 and 33.

Most of the joints are steep (dipping 60°) to vertical. A trend of WNW-ESE (NW-SE to E-W) steep joints is clearly displayed throughout the area (see stereoplots on Figure 6.5, and examples on Figure 6.6). Some NW-SE structures are filled fractures (sites 1, 3, Figure 6.7). Other sets of steep joints strike roughly N-S to NE-SW (see stereoplots on Figure 6.5 and examples on Figure 6.8).



Figure 6.6. Site 1: left, large E-W joints; right, NNW-SSE and E-W joints, probably conjugate system of joints.



Figure 6.7. Site 3. 5 cm wide quartz-rich veins trending NW-SE, steeply dipping SW (width along yellow lines on pictures) and cutting across the fabric of the micaschist host-rock and NE-SW large joints on the right picture.



*Figure 6.8. Left: NE-SW large open joints at site 2 and right: NE-SW large joints at Site 3.*



## 6.2.2 Field studies at Kvitsøy

All the sites visited on Kvitsøy are in the Torvastad and Visne Groups of the Hardangerfjord Nappe. On the western part of the island, this nappe consists of tuffs and lavas, with conglomerates, keratophyres and thin layers of marble, while on the eastern part of the island we find mainly greenstones and greenschists, with pillow- or brecciated structures, and diabase dykes.

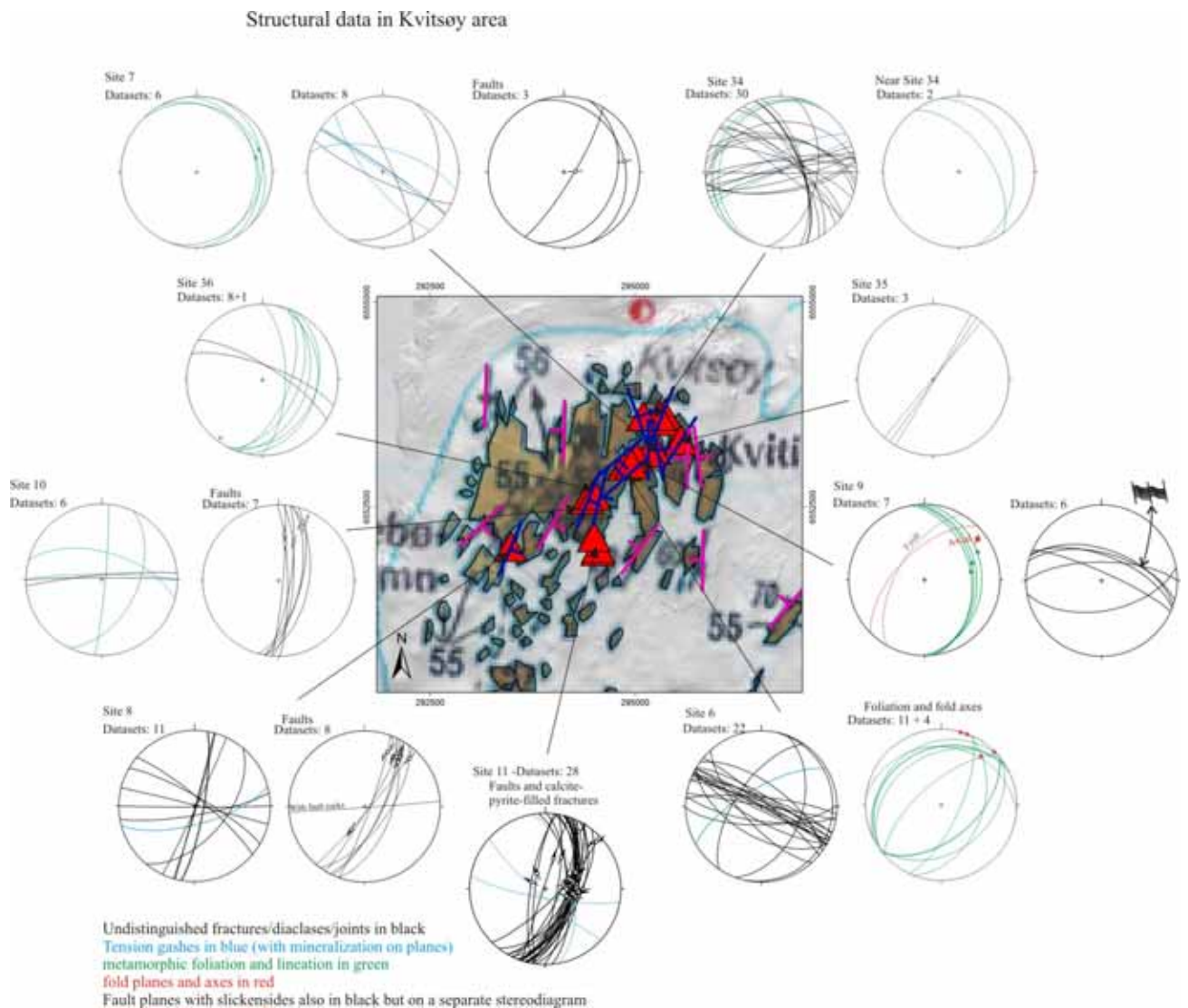
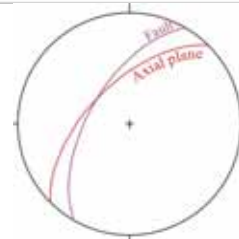


Figure 6.9. Stereonets of structural data in Kvitsøy region.

At Kvitsøy the Torvastad- and Visne Groups of the Hardangerfjord Nappe displays folds with NE-SW to NNE-SSW axes and SE- ESE-vergences (stereonets on Figure 6.9), examples on Figure 6.10). They are cylindrical, mostly closed and with a maximum wavelength of some metres.





*Figure 6.10. Top left: view to the SW of folds with NE-SW axes (site 6). Middle: view to the SSW of folds with NNE-SSW axes (site 6). Bottom: view to NE of SE-vergent folds and associated, probably reverse, faults, scheme and stereonet of the structures (west of Site 9).*

The two main sets of steep brittle structures are E-W to WNW-ESE and NNE-SSW (stereonet on Figure 6.9). The E-W to WNW-ESE trend and especially the WNW-ESE trend is of regional importance (see analyses of large regional lineaments in sub-section 5.3). In the field, it mostly corresponds to joints (Figure 6.11). However, occasionally it is the trend of other types of planar structures of local importance.



*Figure 6.11. View to the SE of large WNW-ESE steep open joints (site 6).*

At site 9, the rocks are highly hatched by E-W micro-fault planes along which developed drag-fold-like structures (Figure 6.12). Of more importance, at site 8, is the presence of such an E-W trending fault zone, 10 cm wide, filled with a breccia and its quartz veins (Figure 6.13).



*Figure 6.12. Drag-fold-like structures along E-W fractures dipping 70° N that may indicate reverse ductile shears and displacements to the south (site 9).*



*Figure 6.13. An E-W trending fault zone filled with fault rocks, 10 cm wide (site 8).*

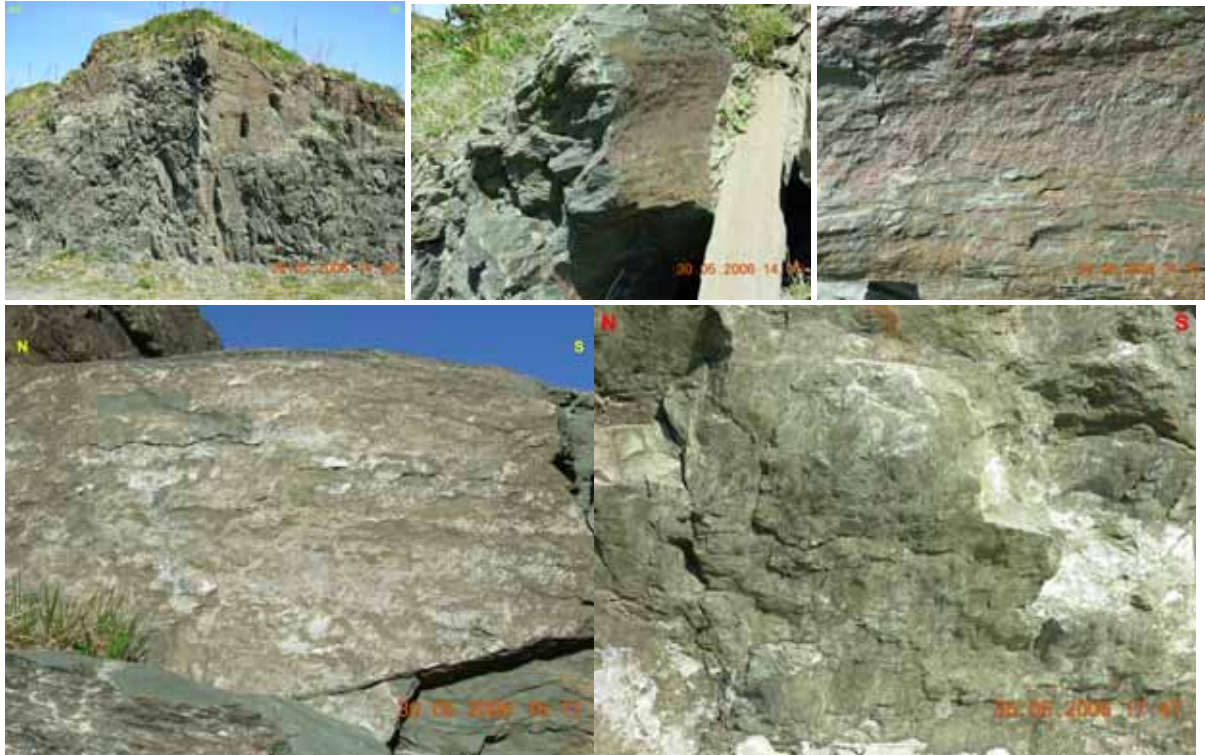
The NNE-SSW (N-S to NE-SW) is highly represented by some strike-slip (Figure 6.14) and many normal faults at the scale of the outcrops (at sites 7, 8, 10 and 11; see stereonets on Figure 6.9 and pictures on Figure 6.15.). This trend belongs to the regional trend displayed through analyses of large regional lineaments (see in sub-section 5.3). The field study in Kvitsøy has been of primary importance for the regional analysis and the characterisation of the NNE-SSW steep and large regional structures as a majority of normal faults. It may reflect the deformation occurring when the Kamsundet rift basin developed along its eastern bordered Kvitsøy fault zone.





Figure 6.14. Examples of strike-slip faults. Top left: view to the W of a large NE-SW strike-slip fault plane and top right: of the left-lateral striae and the lunate fractures observed on the plane (site 8). Middle left: NNE-SSW strike-slip fault and its damaged mineralized zone and middle right: the strike-slip striae on the same plane (site 10). Bottom: horizontal calcite steps of a NE-SW left-lateral fault (site 11).





*Figure 6.15. Top: View of the outcrop with, from left to right, the dense network of NNE-SSW/NE-SW fractures, a NE-SW striated normal fault and the striated surface of the normal fault (site 8). Bottom left: NNE-SSW west dipping normal fault (site 11). Bottom right: NNE-SSW east dipping normal fault and R-Riedel and calcite steps as kinematic indicators (site11).*

### 6.2.3 Field studies at Vestre Bokn

The sites visited at Vestre Bokn are either on the autochthonous basement (mainly foliated granites, granitic gneiss, migmatites, migmatitic gneiss and foliated and gneissic granodiorites) or on the quartz-rich Ryfylke schist (encountered only in the south-easternmost part of the Vestre Bokn; Figure 6.16).

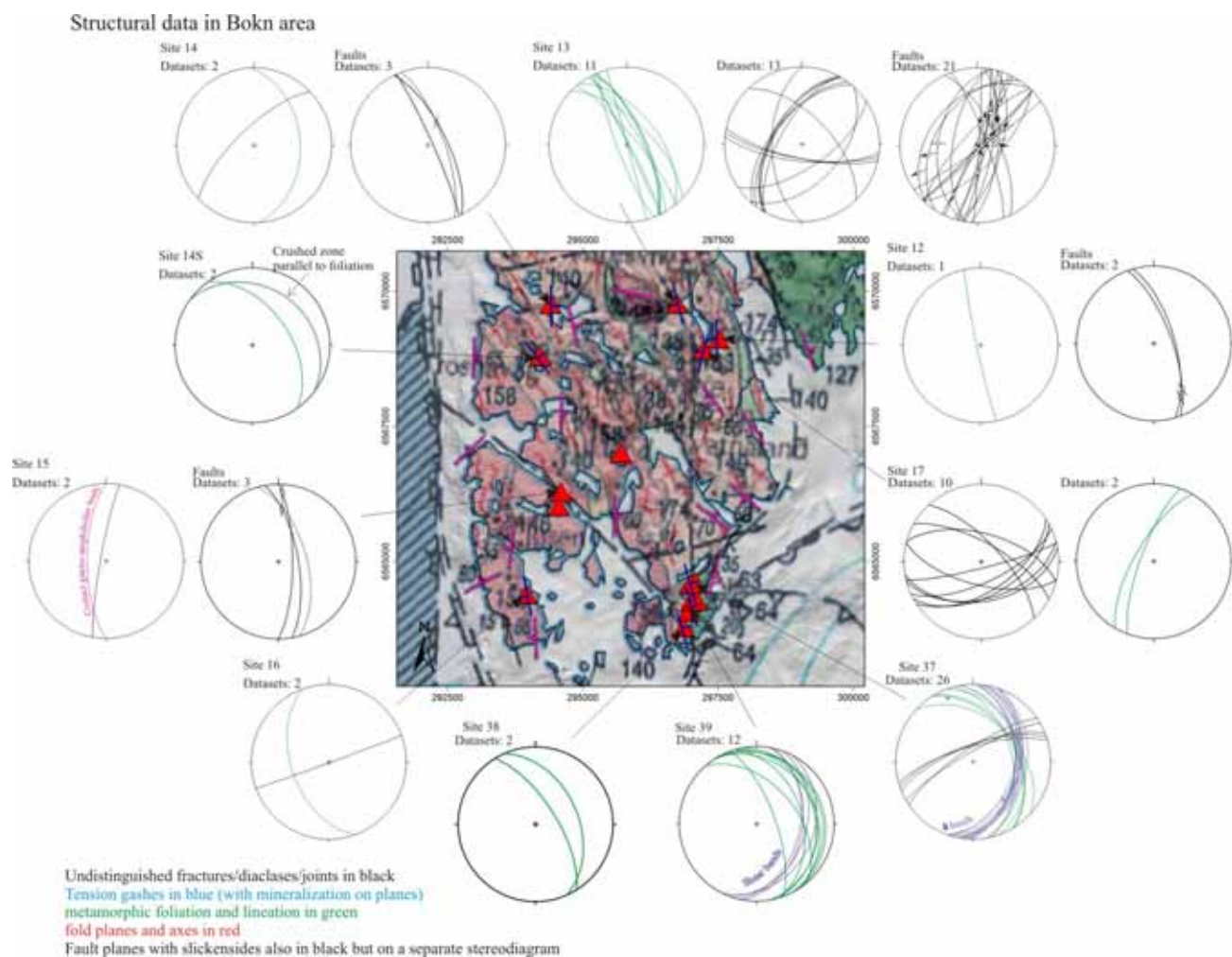


Figure 6.16. Stereonets of structural data in the Vestre Bokn region.

At Vestre Bokn, the foliation of the autochthonous rocks is generally steep and trends NNW-SSE on average (stereonets on Figure 6.16). Contact between amphibolite bodies and surrounding gneiss forms large discontinuities (as displayed on Figure 6.17). Also, on the north-western part of the area, where the foliation is less steep and ENE-dipping, a 1 m wide crushed zone has developed along the foliation (Figure 6.18).





*Figure 6.17. N-S trending steep contact between foliated granodiorite (light grey) and an amphibolite band (brownish) (site 15).*



*Figure 6.18. Highly fractured NE-dipping zone along the foliation (site 14S).*

The foliation of the Ryfylke schist is 30° to 40° ENE-dipping (sites 37 and 39, stereonets on Figure 6.16). 30° to 40° E-dipping ductile shear bands and associated lineations have been observed and are likely related to the thrusting of the phyllite unit onto the autochthon. Two main sets of steep fractures characterise the area: the first set is roughly E-W trending joints and second set is NNW-SSE to NE-SW trending fractures (Figure 6.16). The nearly E-W striking set of joints is found in sites 13 and 17, in the west-northern part of the Vestre Bokn (Figure 6.16). At both sites, they form a conjugate system of joints (with 60° between the conjugate planes, see stereonets on Figure 6.16 and picture on Figure 6.19).



*Figure 6.19. Two sets of roughly E-W striking joints forming a conjugate system with a N-dipping one and a S-dipping other one (foliation is roughly parallel to picture surface) (site 17).*

The other set of steep fractures trending NNW-SSE at sites 12 and 14 (Figure 6.20), N-S at site 15 (Figure 6.21), NNW-SSE to NE-SW at site 13 (Figure 6.22) mostly corresponds to strike-slip and normal faults.





*Figure 6.20. NNW-SSE large steep fault plane (top left: view to west) displaying strike-slip slickensides (top right) (site 12). Bottom: two views of a 1, 5 m wide NNW-SSE steep fault zone filled with fault rocks (site 14).*





*Figure 6.21. Large N-S strike-slip fault plane (site 15).*



*Figure 6.22. Large 40° NW-dipping fault displaying oblique normal slickensides (site 13) (view from below).*

## 6.2.4 Field studies at Bru-Sokn-Mosterøy-Rennesøy

It is mainly units of the Boknafjord nappe that crop out on the Bru-Sokn-Mosterøy-Rennesøy group of islands. On Bru, the Boknafjord nappe has been thrust onto the Ryfylke schist.

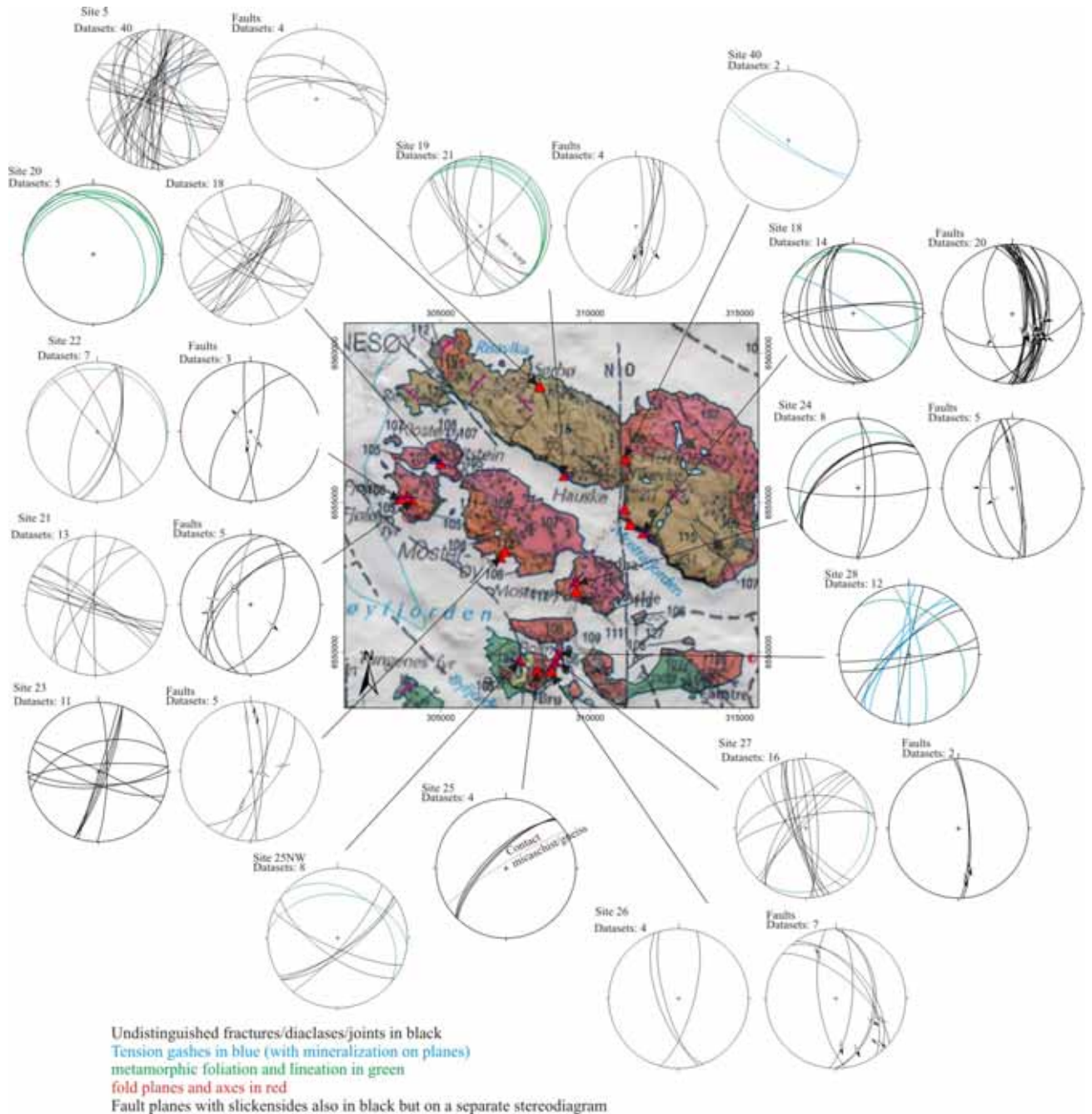
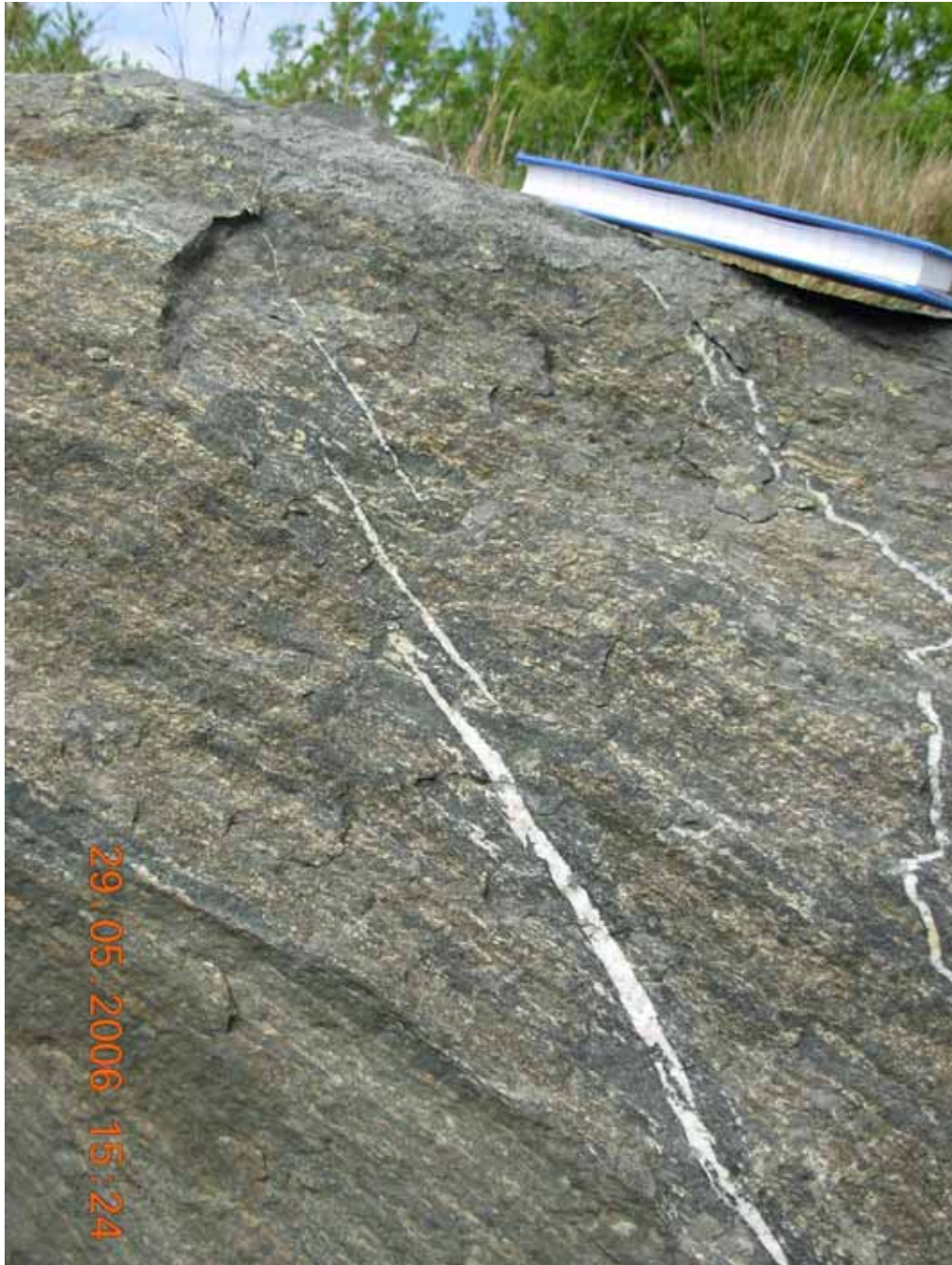


Figure 6.23. Stereonets of structural data in Bru-Sokn-Mosterøy-Rennesøy group of islands.

The metamorphic foliation is gently dipping at all sites, generally to the N and NE (Figure 6.23). The most relevant structures found in the entire group of islands are the widespread set of roughly N-S extensional structures (Figure 6.23) including joints, mineralised tension



gashes (Figure 6.24) and above all normal faults (Figure 6.25 and Figure 6.26). Kinematic indicators on fault surfaces were not rare. Normal sense of shear was more common than strike-slip (Figure 6.27). At site 24, both kind of slickensides are present on the same large fault mirror, arguing for a polyphase tectonic history (Figure 6.28).



*Figure 6.24. Eastward dipping NNW-SSE quartz filled en echelon tension gashes (site 5).*



*Figure 6.25. Top: views of the attitude of the eastward dipping N-S normal faults and of their frequency (every 1,5 m) (site 18). Bottom left: 15 cm down offset of a white quartz layer along such a normal fault (site 18). Bottom right: downward offset of layers along NNE-SSW normal fault (site 19).*





Figure 6.26. View to the N of spectacular extensional structures trending NNE-SSW (site 22); left: network of west dipping extensional fractures; right: normal fault zone.



Figure 6.27. Top left: normal slickensides on a NNE-SSW west-dipping fault (site 21). Top right: normal striae and steps on an east dipping fault mirror (view to the east) (site 18). Bottom: Examples of right-lateral slickensides on N-S trending planes (site 27).





*Figure 6.28. View to the NE: large N-S vertical fault plane (with various trends and types of slickensides displaying a polyphase tectonic history) (site 24).*

WNW-ESE to NW-SE steep to vertical joints are well developed in Rennesøy, Fjøløy and Klosterøy (sites 5, 19, 20, 21, 23, 25NW, 40; Figure 6.29). This trend is of regional importance as it divides the group of islands. Its topographic signature is very well seen at site 19, where a large scarp developed along a pre-existing NW-SE joint (Figure 6.30). At sites 5 and 26, this trend is represented by 50°-60° dipping fault planes with slickensides (Figure 6.31).



*Figure 6.29. View to the NE of the outcrop at site 20 with the vertical joints striking NE-SW; here, they are linked to vertical joints striking NW-SE to form a perpendicular system of joints (the two sets are underlined in red).*



*Figure 6.30. A scarp originated from large NW-SE joints (view to the NW) (site 19).*



Figure 6.31. Northward dipping WNW-ESE fault plane, highlighted in yellow (site 5). NW-SE large fault plane, dipping  $50^\circ$  eastward and developed along the metamorphic foliation (site 26).

#### 6.2.5 Conclusion on structural field analyses

The foliation is generally gently dipping in the allochthonous units (outcropping at Kvitsøy, from Bru to Rennesøy and at Randaberg) whereas it can be steep in the autochthonous basement (Bokn). The main result of the field analyses is the widespread occurrence of NNW-SSE to NE-SW striking faults. Besides another set of planar brittle structures are WNW-ESE and mostly corresponds to joints.

The allochthonous unit at Kvitsøy displays cylindrical, mainly close folds of a maximal wavelength of some metres. It also appears highly weathered.

### 6.3 Geological mapping

To examine rock types and possible fracture zones about 15 islands in the fjord between Randaberg and Kvitsøy were visited (on a one day helicopter trip). The rocks can be divided into two groups:

Localities 4-8 (Figure 6.32) consist of rather massive plutonic rocks, mostly of gabbroic composition, but also some ultramafic rock and diorites. These rocks are intruded by later trondhjemites and mafic dykes and are thought to belong to the Karmøy ophiolite. The rocks are found in the eastern area and occur only on small islands and skerries rounded by waves and ice. No large fractures are found on these islands. About 15 measurements on smaller brittle structures gave no preferred orientation.

Close to Kvitsøy, there is a row of elongated islands (localities 9-18, figure 6.32). These islands consist of supracrustal schistose rocks such as mica schist, chlorite schist and minor bands of marble. There are also some volcanic rocks in the sequence. All these rocks are characterized by a strong foliation in NNE-SSW direction with a dip steep towards the west.



About 20 measurements on brittle structures on these islands show that there is a preferred orientation on the joints and fractures in the E-W direction nearly perpendicular to the foliation.

All this new information is included in the upgraded geological map presented in section 7.

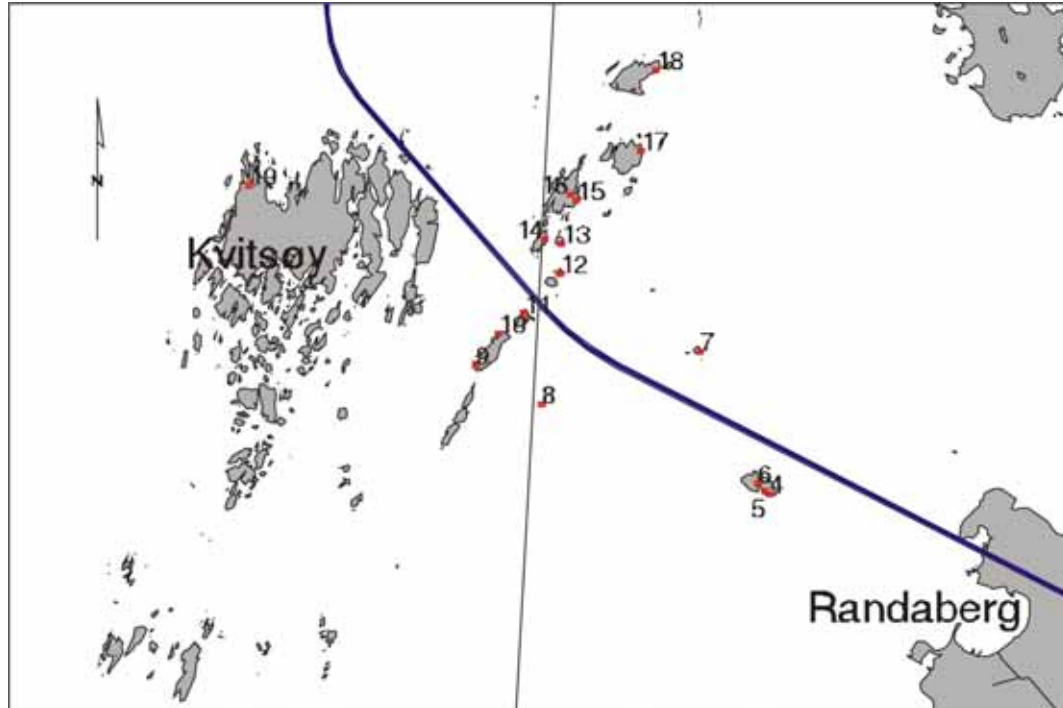


Figure 6.32. Localities visited in the fjord between Randaberg and Kvitsøy. The tunnel trace in blue.

## 7 SYNTHESIS OF DATA AND NEW GEOLOGICAL MODEL

The new geologic and tectonic map of the whole area, and sections along the planned tunnel in the areas Randaberg - Kvitsøy and Kvitsøy – Vestre Bokn, have been compiled using field observations, maps of bathymetric lineaments, of magnetic anomalies and associated transects, and to some extent seismic data.

### 7.1 Tectonic map

The basement and the lowest allochthonous cover units (Ryfylke Schist and Storheia nappe) of the Randaberg area are overlain by the Hardangerfjord nappe. The latter is composed of at least two tectonic units: the Torvastad group and the subjacent Karmøy Ophiolite. The Torvastad group crops out on Kvitsøy and also on the group of islands just east of Kvitsøy (from Gjerdholmen to Eime). Further to the east there are intrusive rocks assigned to the Karmøy Ophiolite. The Karmøy Ophiolite includes some ultramafic bodies identified both in the field (at Nordre Svartaskjær) and on the magnetic anomaly map and modelled on magnetic profiles (see figure 4.8 to 4.10 in section 4.3). Nevertheless, the unit is mainly

composed of mafic to intermediate rocks (such as gabbros and diorites that crop out on Kråka and Alstein islands) (see section 6.3).

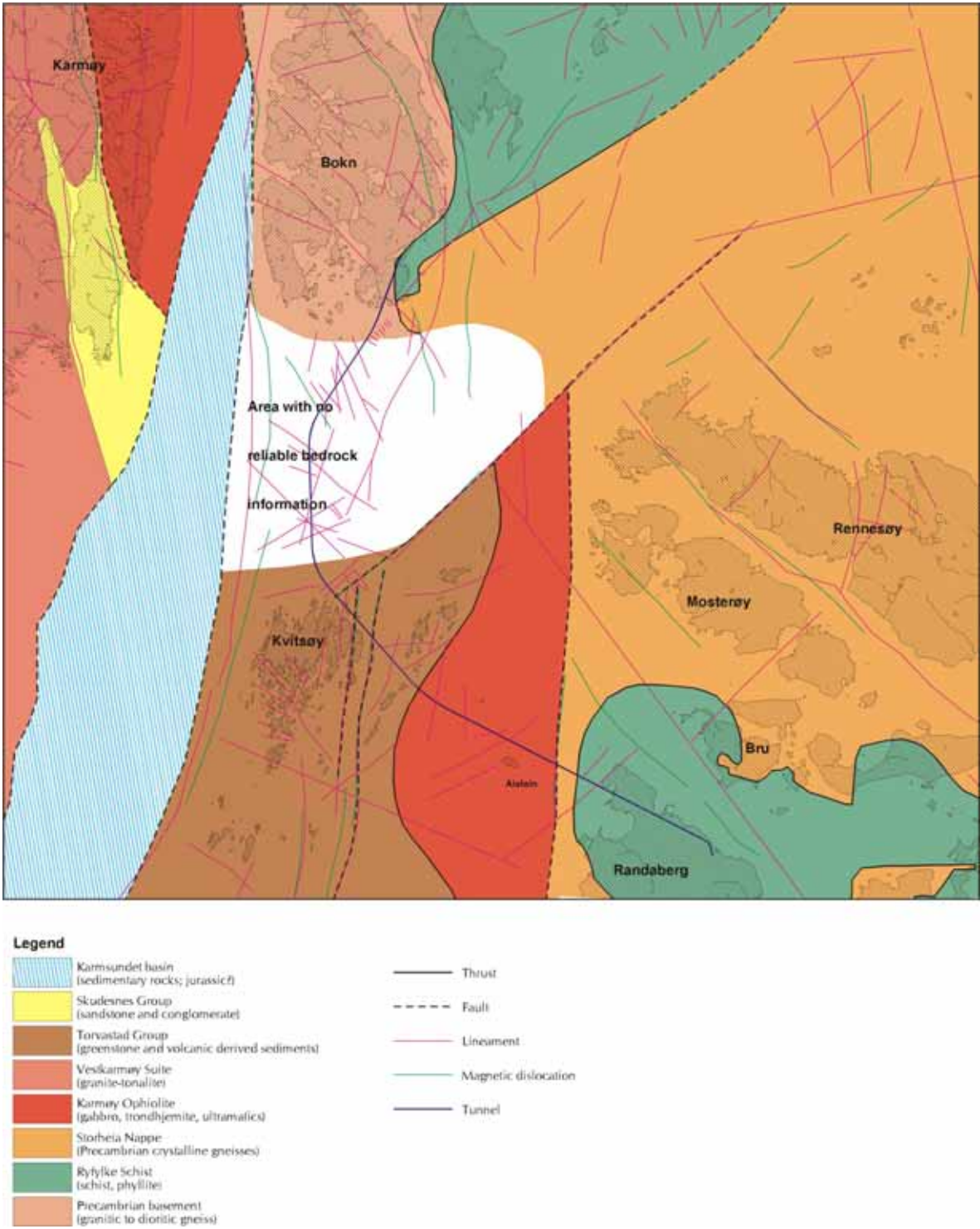


Figure 7.1. New tectonic map of the Boknafjorden region.



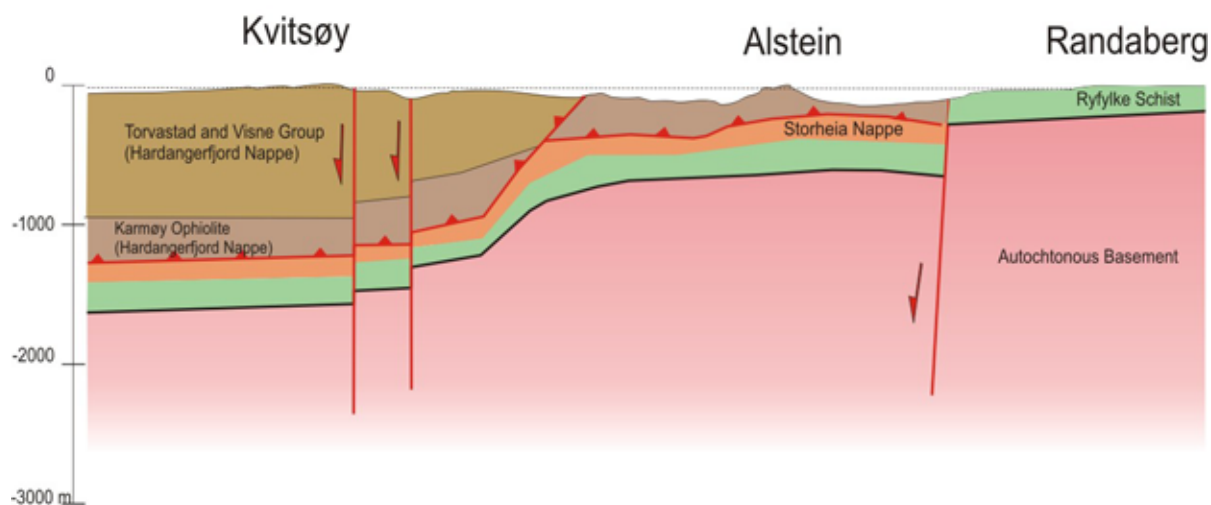
## 7.2 Profile Randaberg to Kvitsøy

Three major N–S-oriented, steep normal fault zones have been added along the profiles of figure 7.2. To trace them, constraints from magnetic data, seismic, bathymetry and field analyses have been all been taken into account. Thus, individual faults are defined by a linear magnetic dislocation, a bathymetric lineament, and a drop in seismic velocity. The field studies in the area clearly indicate a normal component of displacement along these faults. One of the N-S normal faults, situated close to the mainland at Randaberg, has a downward displacement to the west. The two other faults are close to each other and occur between Kvitsøy and the group of island just east of Kvitsøy. The relative sense of displacement (i.e. down towards the west or the east), is uncertain; this is shown in the two different models on figure 7.2).

Another important fault zone is obviously the tectonic contact between the two units of the Hardangerfjord nappe (Karmøy Ophiolite and Torvastad group) that strikes NNE-SSW along the tunnel (see on map figure 7.1). The structure is not highlighted by a bathymetric lineament and magnetic dislocation, which constrained the three N-S steep normal fault zones discussed above. However, the structure can be seen as the top of a magnetic body dipping towards northwest. The high magnetic anomaly on the east and at depth is believed to be the basement (and maybe the two allochthonous Storheia Nappe and Ryfylke Schist).

In the sections shown on Fig. 7.2, the contact between the Torvastad Group (of Kvitsøy) and the Karmøy Ophiolite (of Alstein area) is interpreted as either a thrust plane or as a normal fault (Models A and B, respectively). In the first case, the data are explained by a step-like geometry of the thrust plane of the Hardangerfjord nappe onto the autochthonous basement (model A on figure 7.2; with imbricated thrusts). In the second case, the contact is shown as a west-dipping normal fault with the two N-S faults close to Kvitsøy as nearly antithetic normal faults. (Note the differences in thickness of the units in Kvitsøy due to the changing of displacement along the N-S vertical faults from profile A to B). In both sections, the Storheia nappe and Ryfylke Schist are shown schematically as continuous units. However, the westward extent and thickness of these units are highly uncertain, and they may have been completely excised offshore at Randaberg, placing the Hardangerfjord nappe directly on top of the Precambrian basement. The thickness of the Hardangerfjord nappe is also very approximate. In the Alstein area, the thrust plane has been drawn along the boundary between the low-magnetic Karmøy Ophiolite unit (of the Hardangerfjord nappe) and subjacent high-magnetic rock bodies thought to represent the Precambrian basement (with or without the Storheia Nappe and Ryfylke Schist). The new sections of figure 7.2 are mainly shown to emphasize the location of the major fault zones. The different sections presented on figure 2.3 (Ch 2.4.1) mainly focus on the uncertainties in the thickness of units, especially on the northwestern part of the profile.

### A: Step-like geometry of thrust plane



### B: Normal fault

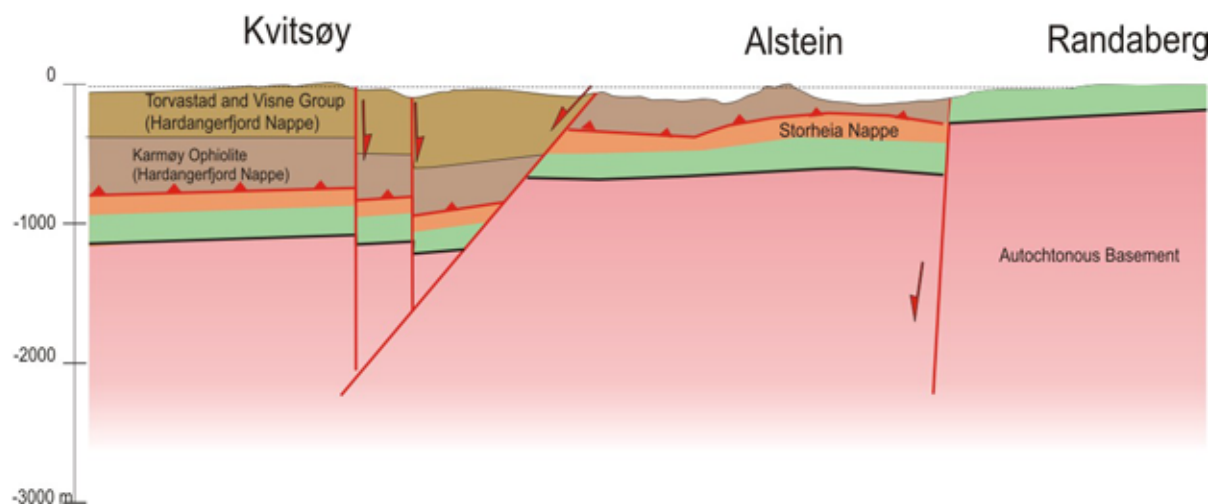


Figure 7.2. New profiles with location of major fault zones. The nature and thickness of the tectonic units at depth are still speculative (see figure 2.3 – the four profiles in 'geological setting' section).

### 7.3 Profile Kvitsøy to Vestre Bokn

The scarcity of data prevents a detailed geological section between Kvitsøy and Bokn. However, the interpretation of bathymetry, geophysics and the available structural data strongly suggests that there is a NE–SW-oriented, major fault and fracture zone along Boknafjorden (figure 7.3). Belonging to this zone are several fairly short NE–SW segments close to Kvitsøy and a larger scarp along the fjord towards the northeast (see lineament on figure 7.1). The geophysical data suggest deep weathering and a drop in seismic velocity along these structures. (Note that it is offset to the south relative to the deepest axis of the fjord.)

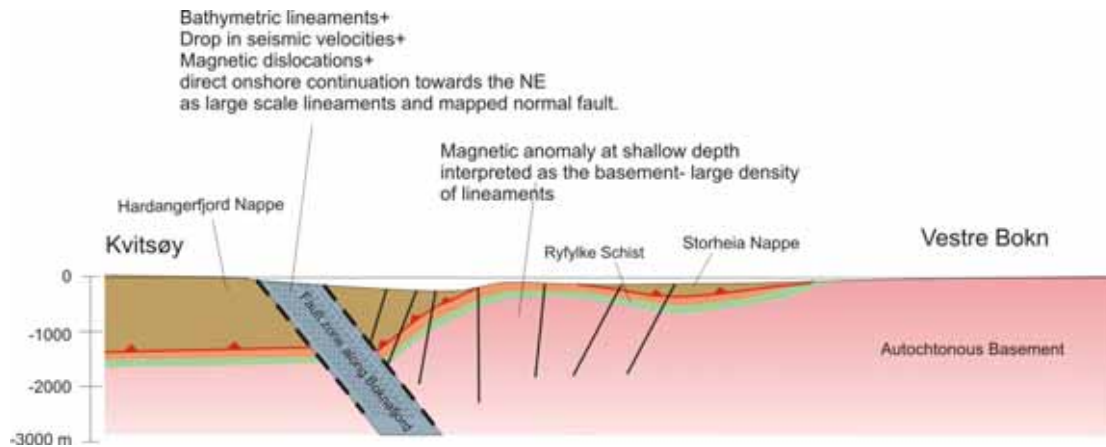


Figure 7.3. Proposed geological profile from Kvitsøy to Bokn. The thickness and nature of the unit involved on the structures are speculative. The presence of a large fault zone is highly probable (its interpretation as a north-dipping normal fault flanked by a roll-over anticline is based on a regional knowledge of large NE-SW structures better known further to the north).

On a regional scale, this NE-SW zone along Boknafjorden is also observed onshore further to the northeast. At the map sheet Sauda 1: 250.000, this zone is mapped as a normal fault (Sigmond 1975). It is one of the largest NE-SW lineaments extracted from satellite images by Gabrielsen et al. (2002), and was probably initiated in Precambrian times (purple lineaments on figure 7.4). Its trace is segmented making a wide zone at the sub-surface (figure 7.4).

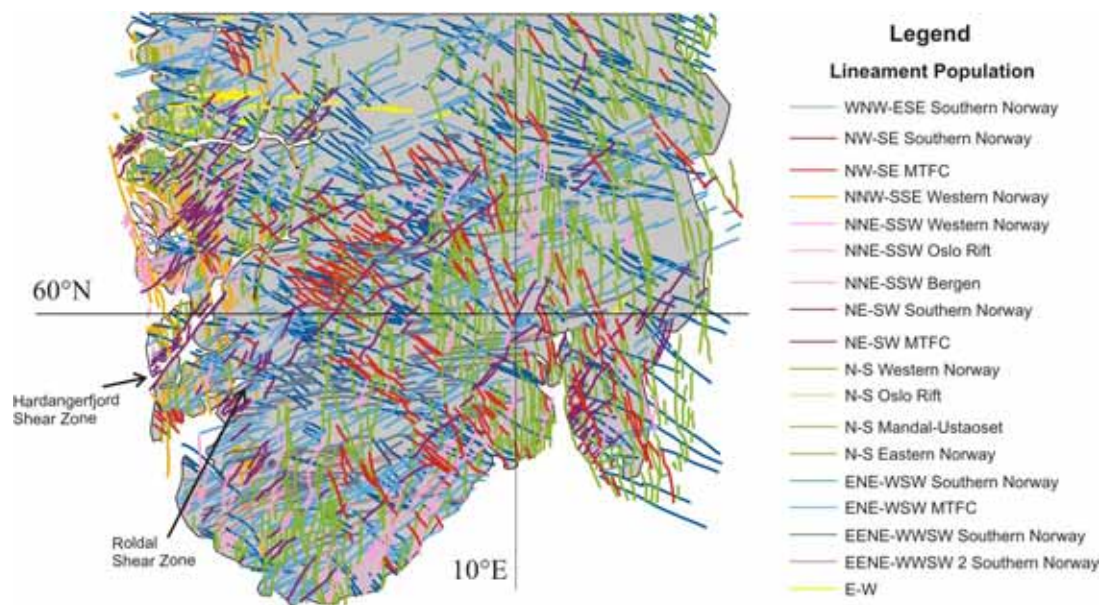


Figure 7.4: Lineament map of Norway with NE-SW lineaments (in purple). Note the large extent of the trace of the NE-SW lineament from Boknafjord towards the NE. (Extracted from Fig. 2 in Gabrielsen et al. 2002).

## 7.4 Conclusion on new geological model

Our proposed model between Randaberg and Kvitsøy indicates a thrust plane between Karmøy Ophiolite and the underlying Storheia nappe at a depth of a few hundreds metres. To make sure that the tunnel will not go along this thrust plane, drilling from the small island Alstein is highly recommended. North of Kvitsøy, a NE – SW trending fault zone along the southern edge of the Boknafjord is indicated, and drilling from one of the islands north of Kvitsøy is also recommended here.

## 8 CONCLUSIONS AND RECOMENDATIONS

Analysis of the new airborne magnetic data, petrophysical data, digital topography/bathymetry and geological follow up work have revealed new information about the bedrock geology in the Boknafjord area. Results from digital structural analysis have already been used in the planning of seismic follow up studies. Magnetic dislocations coincide with lineaments from bathymetric studies, and seem to give information on the most pronounced faults in the area. Based on the magnetic data, depth extent of magnetic bodies at the sea bottom between Randaberg and Kvitsøy are calculated.

Geological follow up studies discovered outcropping rock of the Karmøy ophiolite complex at the islands between Randaberg and Kvitsøy. North of Kvitsøy lack of exposures and magnetic signature made it difficult to reveal new information. A new geological map with profiles has been produced, introducing a thrust plane at a few hundred metres depth between Randaberg and Kvitsøy. A major NE-SW trending fault zone is proposed just north of Kvitsøy. To avoid unexpected problems during the construction work, a vertical drillhole from the island Alstein, and a long drillhole along the tunnel trace from an island north of Kvitsøy are highly recommended.

The Boknfjord area is located outside the Cretaceous etch surface as identified by Lidmar-Bergström et al. (1999) and consequently, there are some uncertainties about the applicability of the Amager method. The obtained results in Figure 4.6 (also presented at map 2006.076-01) indicate that deep weathering may indeed occur in the area. Due to low magnetic susceptibility in the bedrock, it is not possible to calculate the depth extent of the possible weathering.

The study by Olesen et al. (in press) in the greater Oslo region shows, however, that there may also be other causes of coincident topography and magnetic lows than deep weathering. It is important therefore, that the interpretations are checked by ground truth (e.g. resistivity measurements, refraction seismics or drilling) before being introduced in the planning of the tunnel construction. It is also important to study the geomorphology to estimate the glacial erosion of the area. If the erosion is deeper than 300 metres the chances of encountering deep weathered clay zones are significantly reduced.

This project was proposed to evaluate modern geological mapping tools for tunnel planning. So far, interesting results are acquired, but these results has to be checked against other data as refraction seismics, drilling and of cause the tunnel construction to get a fully evaluation of the methods.



## 9 REFERENCES.

- Acworth, R.I. 1987: The development of crystalline basement aquifers in a tropical environment. *Quarterly Journal of Engineering Geology* 20, 265-272.
- Anundsen, K., 1989. Late Weischelian relative sea levels in south-west Norway: observed strandlines and neotectonic activity. *Geol. Fören. Stockh. Förh.* 111, 288-292.
- Bystrøm s. 2006: Sluttrapport. Produksjon av flygmagnetiske mätdata för projekt ROGAS-06. Report from SGU dated 2006.08.18 (90 pp.).
- Bøe, R., Hovland, M., Instanes, A., Rise, L. and Vasshus, S., 2000. Submarine slide scars and mass movements in Karmsundet and Skudenesfjorden, southwestern Norway; morphology and evolution. *Marine Geology*, 167(1-2): 147-165.
- Bøe, R., Sorensen, S. and Hovland, M., 1992. The Karmsundet Basin, SW Norway; stratigraphy, structure and neotectonic activity. In: L.N. Jensen, F. Riis and R. Boyd (Editors), Post-Cretaceous uplift and sedimentation along the western Fennoscandian Shield. *Norsk Geologisk Tidsskrift*. Universitetsforlaget, Oslo, Norway, pp. 281-283.
- Gabrielsen, R.H., Braathen, A., Dehls, J. and Roberts, D., 2002. Tectonic lineaments of Norway. *Norsk Geologisk Tidsskrift*, 82(3): 153-174.
- Ganerød, G.V., Rønning, J.S., Dalsegg, E., Elvebakk, H., Holmøy, K., Nilsen, B. and Braathen, A. 2006: Comparison of geophysical methods for sub-surface mapping of faults and fracture zones in a section of the Viggja road tunnel, Norway. *Bull. Eng. Geol. and the Environment*, p. 231 – 243.
- Geosoft 2004: OASIS Montaj v6.0 Mapping and processing system, The core software platform for working with large volume spatial data. Quick start tutorials. *Geosoft Incorporated*, 258
- Geosoft 2005: Montaj MAGMAP filtering, 2-D frequency domain processing of potential field data, Extension for Oasis Montaj v6.1. *Geosoft Incorporated*, 66 pp.
- Grant, F.S. 1984: Aeromagnetics, geology and ore environments, I. Magnetite in igneous, sedimentary and metamorphic rocks: an overview. *Geoexploration*, v. 23, p. 303-333.
- Henkel, H. 1991: Magnetic crustal structures in Northern Fennoscandia. In Wasilewski, P. & Hood, P. (eds.) *Magnetic anomalies - land and sea. Tectonophysics* 192, 57-79.
- Henkel, H. & Guzmán, M. 1977: Magnetic features of fracture zones. *Geoexploration* 15, 173-181.
- Holtedahl, O. 1953: Norges geologi, Bind II. *Norges geologiske undersøkelse* 164, 587-1118.
- Jorde, K., Sigmond, E.M.O. og Thorsnes, T. 1995. STAVANGER, Berggrunnsgeologisk kart 1:250 000, NGU.
- Larsen, Ø., Fossen, H., Langeland, K. & Pedersen, R.B., 2003. Kinematics and timing of polyphase post-Caledonian deformation in the Bergen area, SW Norway. *Norwegian Journal of Geology*, 83: 149-165.
- Launeau, P., and Robin, P.Y.F., 1996. Fabric analysis using the intercept method: *Tectonophysics*, v. 267, p. 91-119.
- Lidmar-Bergström, K. 1989: Exhumed Cretaceous landforms in south Sweden. *Zeitschrift für Geomorphologi, N.F. Suppl.* 72, 21-40.
- Lidmar-Bergström, K., Olsson, C.D. & Roaldset, E. 1999: Relief features and palaeoweathering remnants in formerly glaciated Scandinavian basement areas. In: Thiry, M. & Simon-Coinçon, R. (eds.), *Palaeoweathering, palaeosurfaces and Related Continental Deposits. International Association of Sedimentologists, Special Publications* 27, 275-301.
- Nordgulen, Ø. & Dehls, J.F. 2003: Bruk av digitale høydedata i strukturgeologisk analyse: Eksempel fra Oslo kommune. NGU Rapport 2003.013
- Northwest Geophysical & Ass. 2004: GM-SYS. Gravity/Magnetic Modelling Software, User's Guide ver. 4.9. Northwest Geophysical Associates, Inc OR 97333 USA.

- Olesen, O., Dehls, J.F., Ebbing, J. Kihle, O. & Lundin, E. in press: Aeromagnetic mapping of deep-weathered fracture zones in the Oslo Region – a new tool for improved planning of tunnels. *Nor. Journ. of Geology*.
- Olesen, O. 2004a: Problemene skyldes dypforvitring. *GEO* 7, 18-20.
- Olesen, O. 2004b: Ny metode for kartlegging av dypforvitring. *GEO* 7, p. 20.
- Ragnhildstveit, J., Naterstad, J., Jorde, K. Og Egeland, B. 1998: Geologisk kart over Norge, berggrunnskart Haugesund - M 1:250000, NGU
- Reid, A.B., Allsop, J.M., Granser, H., Millett, A.J. & Sommerton, I.W. 1990: Magnetic interpretation in three dimensions using Euler deconvolution. *Geophysics* 55, 80-91.
- Sigmond, E.M., 1975. Geologiske Kart over Norge, berggrunnskart SAUDA, 1:250 000. NGU.
- Thompson, D.T. 1982. EULDPH: A new technique for making computer-assisted depth estimates from magnetic data. *Geophysics* 47, 31-37.
- Torsvik, T.H. & Olesen O. 1988: Petrophysics and Paleomagnetism initial report of the Norwegian Geological Survey Laboratory. NGU Report 88.171.
- Valle, P., Faerseth, R.B. and Fossen, H., 2002. Devonian-Triassic brittle deformation based on dyke geometry and fault kinematics in the Sunnhordland region, SW Norway. *Norsk Geologisk Tidsskrift*, 82(1): 3-17.

Acknowledgements. – The Norwegian Mapping Authority made digital topography data available to us through the Norge Digital portal. The Geological Survey of Sweden acquired and processed the aeromagnetic data. The study has been financed by the Norwegian Road Authorities ("Statens vegvesen Region vest" and "Statens vegvesen Vegdirektoratet").

## Appendix A1:

**Petrophysical data (density, magnetic susceptibility and magnetic remanence) on samples collected by Rune Stumo, "Statens vegvesen Region vest".**

Sample	Location	UTM Zone	UTM X	UTM Y	Rock Name	Volume cm <sup>3</sup>	Density kg/m <sup>3</sup>	Suscep 10 E-6 SI	Remanence
1	Karmøy sør	32V	6564960	283760	Anatektisk granodi/metased.	91.86	2797	30232	205
2	Karmøy sør	32V	6564960	283762	Anatektisk granodi/metased.	216.06	2745	2943	34
3	Karmøy sør	32V	6564959	283765	Anatektisk granodi/metased.	164.12	2711	895	10
4	Karmøy sør	32V	6562506	286545	Granitt	105.09	2661	237	10
5	Karmøy sør	32V	6562572	286528	Granitt	70.92	2900	542	10
6	Karmøy sør	32V	6562918	287392	Konglomerat	132.97	2772	289	0
7	Karmøy sør	32V	6562937	287406	Konglomerat	176.47	2812	371	4
8	Karmøy sør	32V	6562938	287372	Konglomerat	235.68	2804	422	0
9	Karmøy sør	32V	6570219	289959	Grønnstein/metagabbro	225.78	2858	471	0
10	Karmøy sør	32V	6570265	289968	Grønnstein/metagabbro	126.47	2895	536	0
11	Karmøy øst	32V	6574743	290400	Grønnstein	70.44	2884	770	14
12	Karmøy øst	32V	6574753	290384	Grønnstein	72.32	2970	656	10
13	Karmøy øst	32V	6581492	289659	Metasandstein/andesitt	187.15	2908	14055	204
14	Karmøy øst	32V	6581508	289666	Metasandstein/andesitt	118.17	2990	1741	82
15	Røksund	32V	6582926	293122	Glimmergneis	201.79	2622	202	5
16	Røksund	32V	6582938	293125	Glimmergneis	204.14	2596	244	0
17	Fosen	32V	6580251	293444	Glimmergneis	144.29	2618	329	12
18	Fosen	32V	6580245	293442	Glimmergneis	137.26	2707	1746	96
19	Fosen	32V	6580238	293441	Glimmergneis	141.9	2825	446	5
20	Fosen	32V	6577182	293007	Metasandstein	177.62	2633	89	0
21	Fosen	32V	6577185	292998	Glimmergneis	143.7	2748	283	0
22	Fosen	32V	6577188	292992	Glimmergneis	177.45	2708	268	4
23	Hetland	32V	6583998	298312	Glimmerskifer	231.12	2711	264	3
24	Haukås	32V	6584009	298317	Granodiorittisk gneis	139.79	2726	259	0
25	Haukås	32V	6584030	298333	Granittisk gneis	171.43	2684	119	6
26	Ådland	32V	6579977	297917	Kvartsdiorittisk gneis	143.04	2846	901	1818
27	Ådland	32V	6579983	297929	Kvartsdiorittisk gneis	235.93	2740	345	0
28	Ådland	32V	6579949	297911	Mylonitt	134.32	2761	337	5
29	Ådland	32V	6579948	297922	Mylonitt	213.32	2694	148	0
30	Lervik	32V	6577292	299303	Mylonitt	192.02	2633	59	4
31	Lervik	32V	6577308	299307	Mylonitt	171.92	2654	224	4
32	Lervik	32V	6577292	299317	Mylonitt	309.46	2669	153	3
33	Lervik	32V	6576947	299096	Glimmerskifer (grt)	91.1	2688	347	0
34	Lervik	32V	6576951	299084	Glimmerskifer (grt)	129.1	2718	648	364
35	Lervik	32V	6576948	299121	Glimmerskifer (grt)	141.56	2741	447	10

36	Ogn	32V	6574644	298295	Granittisk gneis	215.79	2626	94	5
37	Ogn	32V	6574644	298295	Granittisk gneis	207.3	2621	76	0
38	Ogn	32V	6574638	298318	Granittisk gneis	230.96	2621	69	3
39	Ogn	32V	6574632	298339	Mylonitt	292.64	2637	100	2
40	Østre Bokn	32V	6569501	299170	Fyllitt	135.01	2746	586	66
41	Østre Bokn	32V	6569516	299133	Fyllitt	107.87	2677	377	149
42	Østre Bokn	32V	6569509	299111	Fyllitt	211.26	2711	631	251
43	Vestre Bokn	32V	6564556	297089	Fyllitt	109.12	2713	435	7
44	Vestre Bokn	32V	6564567	297088	Fyllitt	115.25	2722	412	6
45	Vestre Bokn	32V	6564469	297074	Meta-arkose	97.22	2630	47	7
46	Vestre Bokn	32V	6564476	297066	Meta-arkose	124.44	2637	91	0
47	Vestre Bokn	32V	6564433	297111	Mylonitt	254.44	2652	89	0
48	Vestre Bokn	32V	6564429	297115	Mylonitt	206.17	2739	680	91
49	Vestre Bokn	32V	6564392	297161	Fyllitt	252.2	2738	421	4
50	Vestre Bokn	32V	6564385	297178	Fyllitt	194.04	2723	396	4
51	Vestre Bokn	32V	6564376	297198	Fyllitt	177.74	2783	572	12
52	Rennesøy nord	32V	6560389	305408	Glimmerskifer	180.62	2777	288	16
53	Rennesøy nord	32V	6560374	305407	Glimmerskifer (and?)	227.65	2810	765	106
54	Rennesøy nord	32V	6560375	305434	Glimmerskifer (and?)	269.87	2917	544	33
55	Rennesøy øst	32V	6556514	315348	Granittisk gneis	170.88	2593	53	4
56	Rennesøy øst	32V	6556509	315349	Granittisk gneis	174.12	2655	130	4
57	Mosterøy	32V	6553374	307126	Glimmerskifer	107.06	2810	338	9
58	Mosterøy	32V	6553385	307127	Glimmerskifer	282.49	2755	272	3
59	Mosterøy	32V	6553386	307136	Glimmerskifer	187.87	2827	361	0
60	Mosterøy sør	32V	6552982	309700	Granodiorittisk gneis	163.23	2686	111	0
61	Mosterøy sør	32V	6553008	309712	Granodiorittisk gneis	254.82	2684	115	3
62	Mosterøy sør	32V	6553004	309722	Mylonitt	166.65	2698	122	0
63	Randaberg kirke	32V	6546719	306631	Fyllitt	182.95	2658	235	89
64	Randaberg kirke	32V	6546721	306629	Fyllitt	206.1	2668	943	142
65	Randaberg kirke	32V	6546726	306611	Fyllitt	217.05	2752	1511	645
66	Randaberg nord	32V	6547532	305567	Fyllitt	89.86	2850	604	26
67	Randaberg nord	32V	6547508	305585	Fyllitt	206.06	2816	8747	2820
68	Randaberg nord	32V	6547501	305590	Fyllitt	255.35	2813	531	5



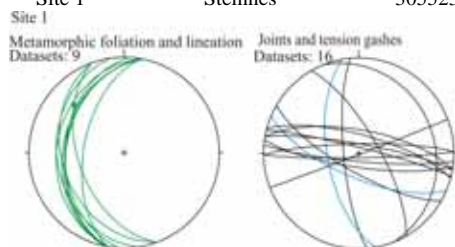
## Appendix A2:

Petrophysical data (density, magnetic susceptibility and magnetic remanence) on samples collected by NGU (AS= Aline Saintot, ØN= Øystein Nordgulen and ASO= Arne Solli).

Sample	Location	UTM	UTM X	UTM Y	Rock Name	Volume	Density	Suscept	Remanence
						cm3	kg/m3	10 E-6 SI	
AS-1	Randaberg-1	32 V	305523	6545870	micaschistes	206.6	2815	416	11
AS-2	Randaberg-2	32V	304583	6546924	Quarts micashist	349.22	2847	518	3
AS-3B	Randaberg-3	32 V	306242	6545928	micaschistes	266.95	2785	322	0
AS-5	Kvitsøy-7	32 V	295239	6553199	greenstones	363.4	2895	971	3
AS-6	Kvitsøy-8	32 V	293483	6552019	greenstones	246.99	2904	641	3
AS-7	Kvitsøy-9	32 V	295167	6553170	greenstones	184.35	2910	920	4
AS-8	Kvitsøy-10	32 V	294411	6552600	greenstones	253.45	2906	624	21
AS-9	Vestre Bokn -12	32 V	297512	6569121	foliated granite/granitic gneiss	259.17	2655	87	0
AS-10	Vestre Bokn -15	32 V	294597	6566281	granodiorite	282.82	2827	5622	497
AS-4	Rennesøy-5	32 V	308308	6558885	amphibolite	367.91	3027	559	2
AS-11	Rennesøy-18	32 V	311782	6553993	amphibolite	156.88	2972	21807	311
AS-12	Fjøløy-22	32 V	303868	6555223	gneiss	164.46	2669	110	6
AS-13	Mosterøy-24	32 V	309517	6552036	micagneiss	182.94	2793	346	0
ØN-1	Kvitsøy-Fergekai	32 V	294551	6552003		221.8	3002	1040	60
ØN-2	Kvitsøy	32 V	294500	6552137		193.8	2934	723	0
ASO-1	Egerholmen	32V	299717	6543429	Dioritt	261.02	3079	520	4
ASO-2	N. Svartaskjær	32V	299459	6544555	Ultrabasitt	231.56	2662	112094	652
ASO-3	Alstein	32V	300746	6549082	Gabbro	375.86	2963	704	2
ASO-4	Kråka	32V	299753	6551092	Gabbro	316.91	3027	61996	119
ASO-5	Gåsholmen	32V	297514	6550353	Trondhemitt	167.52	2975	337	6
ASO-6	Bussholmen	32V	296584	6550905	Klorittskifer	159.58	2835	496	0
ASO-7	Lyngholmen	32V	297569	6552682	Fylitt	226.10	2509	190	5
ASO-8	Eime	32V	299134	6555063	Fylitt	283.81	2960	1283	4

## Appendix B: Structural observations.

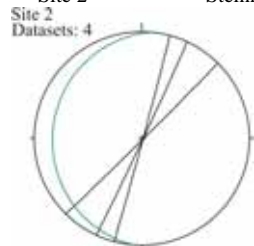
Site number	Locality	UTM32V X	UTM32V Y	Rocks	Type structure	strike	Dip direction	Dip	Azimuth or pitch
Site 1	Steinnes	305523	6545870	micaschists	MF		280	55	
Site 1	Steinnes	305523	6545870	micaschists	MF		282	36	
Site 1	Steinnes	305523	6545870	micaschists	MF		280	39	
Site 1	Steinnes	305523	6545870	micaschists	MF		273	38	
Site 1	Steinnes	305523	6545870	micaschists	MF		281	38	
Site 1	Steinnes	305523	6545870	micaschists	MF ML		250	50	N134
Site 1	Steinnes	305523	6545870	micaschists	MF		280	30	
Site 1	Steinnes	305523	6545870	micaschists	MF		250	35	
Site 1	Steinnes	305523	6545870	micaschists	MF		262	30	
Site 1	Steinnes	305523	6545870	micaschists	J		14	85	
Site 1	Steinnes	305523	6545870	micaschists	J		10	70	
Site 1	Steinnes	305523	6545870	micaschists	J		265	77	
Site 1	Steinnes	305523	6545870	micaschists	J		188	78	
Site 1	Steinnes	305523	6545870	micaschists	J		185	83	
Site 1	Steinnes	305523	6545870	micaschists	J		210	74	
Site 1	Steinnes	305523	6545870	micaschists	JX		203	69	
Site 1	Steinnes	305523	6545870	micaschists	JX		260	63	
Site 1	Steinnes	305523	6545870	micaschists	J		60	73	
Site 1	Steinnes	305523	6545870	micaschists	J		10	82	
Site 1	Steinnes	305523	6545870	micaschists	J		179	86	
Site 1	Steinnes	305523	6545870	micaschists	J		359	82	
Site 1	Steinnes	305523	6545870	micaschists	J		15	74	
Site 1	Steinnes	305523	6545870	micaschists	J		68	21	
Site 1	Steinnes	305523	6545870	micaschists	J		159	90	
Site 1	Steinnes	305523	6545870	micaschists	J		14	85	



The metamorphic foliation is 40 degrees W-dipping in average. Two sets of roughly vertical joints are present trending NNW-SSE and E-W.

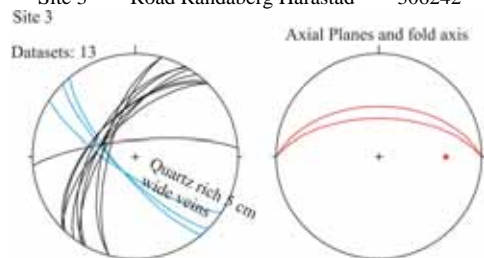
Site 2	Steinnes	304583	6546924	quartz-micaschists	Large joints		115	90	
Site 2	Steinnes	304583	6546924	quartz-micaschists	Large joints		135	90	
Site 2	Steinnes	304583	6546924	quartz-micaschists	opened fracture		105	90	

Site 2	Steinnes	304583	6546924	quartz-micaschists	MF	275	18
--------	----------	--------	---------	--------------------	----	-----	----



Flat metamorphic foliation and of vertical NNE-SSW joints.

Site 3	Road Randaberg Harastad	306242	6545928	micaschists- microfolded	J	315	64
Site 3	Road Randaberg Harastad	306242	6545928	micaschists- microfolded	J	313	56
Site 3	Road Randaberg Harastad	306242	6545928	micaschists- microfolded	quartz-rich JV	225	75
Site 3	Road Randaberg Harastad	306242	6545928	micaschists- microfolded	quartz-rich JV	230	75
Site 3	Road Randaberg Harastad	306242	6545928	micaschists- microfolded	J	307	62
Site 3	Road Randaberg Harastad	306242	6545928	micaschists- microfolded	quartz-rich JV	213	75
Site 3	Road Randaberg Harastad	306242	6545928	micaschists- microfolded	J	300	56
Site 3	Road Randaberg Harastad	306242	6545928	micaschists- microfolded	J	285	69
Site 3	Road Randaberg Harastad	306242	6545928	micaschists- microfolded	J	299	61
Site 3	Road Randaberg Harastad	306242	6545928	micaschists- microfolded	J	355	77
Site 3	Road Randaberg Harastad	306242	6545928	micaschists- microfolded	J	302	66
Site 3	Road Randaberg Harastad	306242	6545928	micaschists- microfolded	J	315	56
Site 3	Road Randaberg Harastad	306242	6545928	micaschists- microfolded	J	285	64
Site 3	Road Randaberg Harastad	306242	6545928	micaschists- microfolded	Microfold axis	270	35-40
Site 3	Road Randaberg Harastad	306242	6545928	micaschists- microfolded	Microfold axial plane	360	50-60

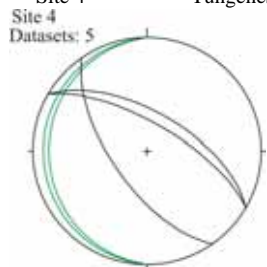


NE-SW to NNE-SSW trend of joints is observed. The micaschists at site 3 displayed south-vergent micro-folding with a wavelength of few centimetres. NW-SE steep quartz rich and 5cm wide veins cut across the micaschist fabric.

Site 4	Tungeneset	304191	6548813	micaschists	large joints	30	70
Site 4	Tungeneset	304191	6548813	micaschists	MF	270	15
Site 4	Tungeneset	304191	6548813	micaschists	MF	270	10
Site 4	Tungeneset	304191	6548813	micaschists	J	30	62
Site 4	Tungeneset	304191	6548813	micaschists	opened fracture	235	65
Site 4	Tungeneset	304191	6548813	micaschists			



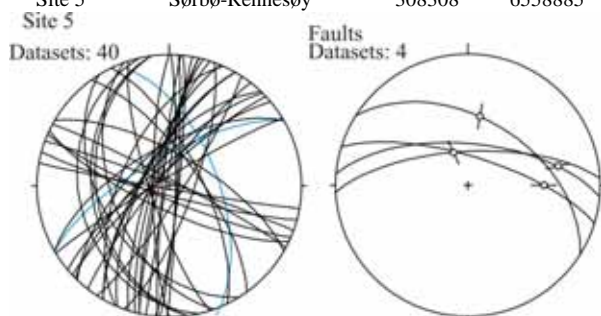
Site 4	Tungeneset	304191	6548813	micaschists
Site 4	Tungeneset	304191	6548813	micaschists
Site 4	Tungeneset	304191	6548813	micaschists
Site 4	Tungeneset	304191	6548813	micaschists
Site 4	Tungeneset	304191	6548813	micaschists
Site 4	Tungeneset	304191	6548813	micaschists



The metamorphic foliation is flat dipping westward. Large NW-SE steep joints are observed.

Site 5	Sørbø-Rennesøy	308308	6558885	amphibolite facies	quartz JX en echelon	70	60
Site 5	Sørbø-Rennesøy	308308	6558885	amphibolite facies	J	317	82
Site 5	Sørbø-Rennesøy	308308	6558885	amphibolite facies	J	64	70
Site 5	Sørbø-Rennesøy	308308	6558885	amphibolite facies	J	300	73
Site 5	Sørbø-Rennesøy	308308	6558885	amphibolite facies	J	91	86
Site 5	Sørbø-Rennesøy	308308	6558885	amphibolite facies	J	54	72
Site 5	Sørbø-Rennesøy	308308	6558885	amphibolite facies	J	320	78
Site 5	Sørbø-Rennesøy	308308	6558885	amphibolite facies	J	314	68
Site 5	Sørbø-Rennesøy	308308	6558885	amphibolite facies	J	262	41
Site 5	Sørbø-Rennesøy	308308	6558885	amphibolite facies	J	288	78
Site 5	Sørbø-Rennesøy	308308	6558885	amphibolite facies	J	275	86
Site 5	Sørbø-Rennesøy	308308	6558885	amphibolite facies	Quartz JX	330	72
Site 5	Sørbø-Rennesøy	308308	6558885	amphibolite facies	J	96	84
Site 5	Sørbø-Rennesøy	308308	6558885	amphibolite facies	J	94	85
Site 5	Sørbø-Rennesøy	308308	6558885	amphibolite facies	J	280	88
Site 5	Sørbø-Rennesøy	308308	6558885	amphibolite facies	J	250	54
Site 5	Sørbø-Rennesøy	308308	6558885	amphibolite facies	J	257	32
Site 5	Sørbø-Rennesøy	308308	6558885	amphibolite facies	J	262	44
Site 5	Sørbø-Rennesøy	308308	6558885	amphibolite facies	J	123	82
Site 5	Sørbø-Rennesøy	308308	6558885	amphibolite facies	J	283	84
Site 5	Sørbø-Rennesøy	308308	6558885	amphibolite facies	J	30	70
Site 5	Sørbø-Rennesøy	308308	6558885	amphibolite facies	J	308	83
Site 5	Sørbø-Rennesøy	308308	6558885	amphibolite facies	J	238	47
Site 5	Sørbø-Rennesøy	308308	6558885	amphibolite facies	J	300	74
Site 5	Sørbø-Rennesøy	308308	6558885	amphibolite facies	J	330	66
Site 5	Sørbø-Rennesøy	308308	6558885	amphibolite facies	J	285	80
Site 5	Sørbø-Rennesøy	308308	6558885	amphibolite facies	J	315	75

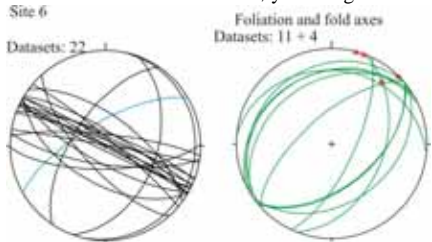
Site 5	Sørbø-Rennesøy	308308	6558885	amphibolite facies	J	252	78	
Site 5	Sørbø-Rennesøy	308308	6558885	amphibolite facies	J	205	75	
Site 5	Sørbø-Rennesøy	308308	6558885	amphibolite facies	J	195	84	
Site 5	Sørbø-Rennesøy	308308	6558885	amphibolite facies	J	270	80	
Site 5	Sørbø-Rennesøy	308308	6558885	amphibolite facies	J	294	60	
Site 5	Sørbø-Rennesøy	308308	6558885	amphibolite facies	J	203	82	
Site 5	Sørbø-Rennesøy	308308	6558885	amphibolite facies	J	28	86	
Site 5	Sørbø-Rennesøy	308308	6558885	amphibolite facies	J	329	85	
Site 5	Sørbø-Rennesøy	308308	6558885	amphibolite facies	J	20	88	
Site 5	Sørbø-Rennesøy	308308	6558885	amphibolite facies	J	283	82	
Site 5	Sørbø-Rennesøy	308308	6558885	amphibolite facies	J	293	73	
Site 5	Sørbø-Rennesøy	308308	6558885	amphibolite facies	J	110	75	
Site 5	Sørbø-Rennesøy	308308	6558885	amphibolite facies	J	190	88	
Site 5	Sørbø-Rennesøy	308308	6558885	amphibolite facies	F	32	48	75W
Site 5	Sørbø-Rennesøy	308308	6558885	amphibolite facies	F	5	64	35E
Site 5	Sørbø-Rennesøy	308308	6558885	amphibolite facies	F	357	69	82W
Site 5	Sørbø-Rennesøy	308308	6558885	amphibolite facies	F	17	72	45E



Two sets of vertical fractures are predominant. They trend NNE-SSW and WNW-ESE. Another trend is NNW-SSE and the fractures dip of both direction: ENE and WSW. En echelon tension gashes have developed. A large fault with striae of undetermined sense of shear strikes WNW-ESE and dips 60 degrees to the north.

Site 6	Between Kvitsøy-Kviting	294868	6553015	greenstones	MF	320	20	
Site 6	Between Kvitsøy-Kviting	294868	6553015	greenstones	MF	327	34	
Site 6	Between Kvitsøy-Kviting	294868	6553015	greenstones	MF	335	26	
	West side of the bridge:				fold axes	greenstones		0
Site 6	Between Kvitsøy-Kviting	294868	6553015	greenstones	MF	140	52	
Site 6	Between Kvitsøy-Kviting	294868	6553015	greenstones	MF	141	53	
Site 6	Between Kvitsøy-Kviting	294868	6553015	greenstones	MF	144	37	
Site 6	Between Kvitsøy-Kviting	294868	6553015	greenstones	Quartz JX	330	70	
Site 6	Between Kvitsøy-Kviting	294868	6553015	greenstones	J	40	84	
Site 6	Between Kvitsøy-Kviting	294868	6553015	greenstones	J	209	75	
Site 6	Between Kvitsøy-Kviting	294868	6553015	greenstones	Fold axis	015-020		0
Site 6	Between Kvitsøy-Kviting	294868	6553015	greenstones	J	210	57	

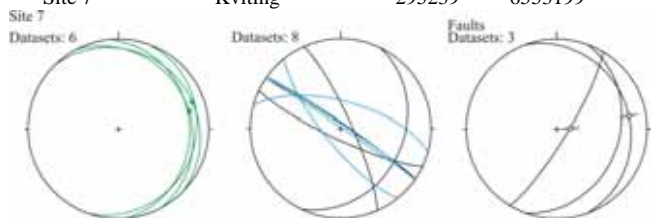
Site 6	Between Kvitsøy-Kviting	294868	6553015	greenstones	J	228	70
Site 6	Between Kvitsøy-Kviting	294868	6553015	greenstones	J	179	70
Site 6	Between Kvitsøy-Kviting	294868	6553015	greenstones	J	25	82
Site 6	Between Kvitsøy-Kviting	294868	6553015	greenstones	J	24	90
Site 6	Between Kvitsøy-Kviting	294868	6553015	greenstones	J	20	85
Site 6	Between Kvitsøy-Kviting	294868	6553015	greenstones	J	36	65
Site 6	Between Kvitsøy-Kviting	294868	6553015	greenstones	J	10	90
Site 6	Between Kvitsøy-Kviting	294868	6553015	greenstones	J	30	90
Site 6	Between Kvitsøy-Kviting	294864	6553005	greenstones	J	207	90
Site 6	Between Kvitsøy-Kviting	294864	6553005	greenstones	J	30	85
Site 6	Between Kvitsøy-Kviting	294864	6553005	greenstones	J	31	78
Site 6	Between Kvitsøy-Kviting	294864	6553005	greenstones	J	6	80
Site 6	Between Kvitsøy-Kviting	294864	6553005	greenstones	J	188	74
Site 6	Between Kvitsøy-Kviting	294864	6553005	greenstones	J	206	86
Site 6	Between Kvitsøy-Kviting	294864	6553005	greenstones	J	21	79
Site 6	Between Kvitsøy-Kviting	294864	6553005	greenstones	Fold axis	39	18
Site 6	Between Kvitsøy-Kviting	294864	6553005	greenstones	outcrop with irregular west-verging folds		
Site 6	Between Kvitsøy-Kviting	294953	6553030	greenstones	MF	111	44
Site 6	Between Kvitsøy-Kviting	294953	6553030	greenstones	MF	6	24
Site 6	Between Kvitsøy-Kviting	294953	6553030	greenstones	MF	330	26
Site 6	Between Kvitsøy-Kviting	294953	6553030	greenstones	MF	319	66
Site 6	Between Kvitsøy-Kviting	294953	6553030	greenstones	MF	115	70
Site 6	Between Kvitsøy-Kviting	294953	6553030	greenstones	J	304	62
Site 6	Between Kvitsøy-Kviting	294953	6553030	greenstones	J	110	45
Site 6	Between Kvitsøy-Kviting	294953	6553030	greenstones	J	102	6



WNW-ESE vertical large joints are the predominant brittle structures. The unit displayed NNE-SSW to NE-SW folds and tension gash might have developed parallel to axial plane in response to folding.

Site 7	Kviting	295239	6553199	greenstones	J	205	80	
Site 7	Kviting	295239	6553199	greenstones	F	70	20	N080
Site 7	Kviting	295239	6553199	greenstones	J	66	80	
Site 7	Kviting	295239	6553199	greenstones	F	121	80	83E
Site 7	Kviting	295239	6553199	greenstones	F	110	31	
Site 7	Kviting	295239	6553199	greenstones	J	34	86	
Site 7	Kviting	295239	6553199	greenstones	JX	35	85	

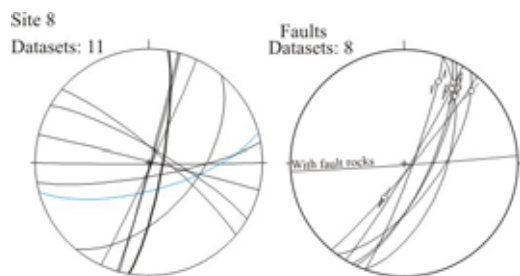
Site 7	Kviting	295239	6553199	greenstones	J	116	31	
Site 7	Kviting	295239	6553199	greenstones	Quartz pyrite JX	15	65	
Site 7	Kviting	295239	6553199	greenstones	Pyrite J	231	75	
Site 7	Kviting	295239	6553199	greenstones	Quartz pyrite JX	34	89	
Site 7	Kviting	295239	6553199	greenstones	MF ML	45	15	N070
Site 7	Kviting	295239	6553199	greenstones	MF	110	15	
Site 7	Kviting	295239	6553199	greenstones	MF	85	22	



The foliation gently dips ENE. Vertical NW-SE joints and tension gashes are present. Three E- to ESE-dipping faults with dip-slip striae have been observed without determining the sense of shear on them.

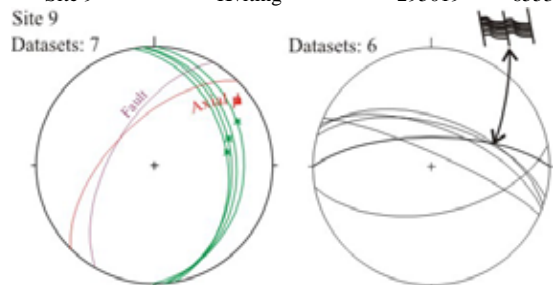
Site 7	Kviting	295239	6553199	greenstones	MF ML	62	21	N076
Site 8	Ystabohamn	293483	6552019	greenstones	Large joints	180	90	
Site 8	Ystabohamn	293483	6552019	greenstones	FN?	110	60	30N
Site 8	Ystabohamn	293483	6552019	greenstones	J	40	81	
Site 8	Ystabohamn	293483	6552019	greenstones	FS?	126	65	16N
Site 8	Ystabohamn	293483	6552019	greenstones	FS	121	86	23N
Site 8	Ystabohamn	293483	6552019	greenstones	FS	115	72	19N
Site 8	Ystabohamn	293483	6552019	greenstones	F	117	71	29N
Site 8	Ystabohamn	293483	6552019	greenstones	F with fault rocks	176	90	
Site 8	Ystabohamn	293483	6552019	greenstones	Surface	130	55	
Site 8	Ystabohamn	293483	6552019	greenstones	JX	165	70	
Site 8	Ystabohamn	293483	6552019	greenstones	FS	110	84	23N
Site 8	Ystabohamn	293483	6552019	greenstones	FN	130	85	62W
Site 8	Ystabohamn	293483	6552019	greenstones	J	115	88	
Site 8	Ystabohamn	293483	6552019	greenstones	J	170	80	
Site 8	Ystabohamn	293483	6552019	greenstones	J	100	80	
Site 8	Ystabohamn	293483	6552019	greenstones	J	14	90	
Site 8	Southern part of outcrop:							
Site 8	Ystabohamn	293483	6552019	greenstones	J	30	80	
Site 8	Ystabohamn	293483	6552019	greenstones	J with infill	105	90	
Site 8	Ystabohamn	293483	6552019	greenstones	J with infill	106	88	





Two sets of steep fractures. The first roughly trends E-W and the second one NE-SW to NNE-SSW. The first set mostly corresponds to joints aside from an E-W damaged fault zone 10 cm wide. Frequent striae have been observed on the second set of fractures, both of normal and left-lateral sense of shear.

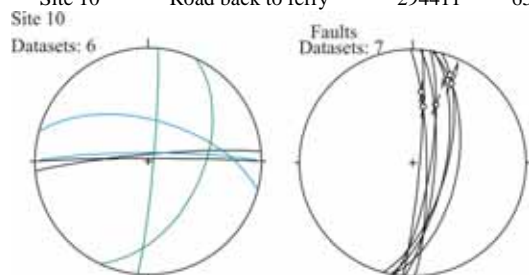
Site 9	Kviting	295167	6553170	greenstones	MF ML	84	35	N070
Site 9	Kviting	295167	6553170	greenstones	MF	85	31	
Site 9	Kviting	295167	6553170	greenstones	MF ML	91	25	N062
Site 9	Kviting	295167	6553170	greenstones	J	24	81	
Site 9	Kviting	295167	6553170	greenstones	MF ML	80	38	N080
Site 9	Kviting	295167	6553170	greenstones	J	15	60	
Site 9	Kviting	295167	6553170	greenstones	J	19	56	
Site 9	Kviting	295167	6553170	greenstones	micro-drag folds along E-W microfaults, dipping 70°N			
Site 9	Kviting	295167	6553170	greenstones	J	170	57	
Site 9	Kviting	295167	6553170	greenstones	J	21	63	
Site 9	Kviting	295019	6553107	greenstones	fold axis	045	0	
Site 9	Kviting	295019	6553107	greenstones	axial plane	315	60-70	
Site 9	Kviting	295019	6553107	greenstones	F	300	60	



Where the foliation gently dips to the east, WNW-ESE joints have been measured. Evidences of reverse shears as drag-fold like structures, are present along steep north dipping fractures. They indicate southward reverse displacements. Just going westward of site 9, SE-vergent folds and faults are observed.

Site 10	Road back to ferry	294411	6552600	greenstones	MF	115	50	
Site 10	Road back to ferry	294411	6552600	greenstones	F	100	57	28N
Site 10	Road back to ferry	294411	6552600	greenstones	J	0	88	
Site 10	Road back to ferry	294411	6552600	greenstones	J	355	85	
Site 10	Road back to ferry	294411	6552600	greenstones	FN?	105	65	19N
Site 10	Road back to ferry	294411	6552600	greenstones	Quartz JX	0	84	

Site 10	Road back to ferry	294411	6552600	greenstones	F	94	74	
Site 10	Road back to ferry	294411	6552600	greenstones	F	95	85	48N
Site 10	Road back to ferry	294411	6552600	greenstones	F	101	66	
Site 10	Road back to ferry	294411	6552600	greenstones	F	89	80	38N
Site 10	Road back to ferry	294411	6552600	greenstones	F	99	77	45N
Site 10	Road back to ferry	294411	6552600	greenstones	MF	95	86	
Site 10	Road back to ferry	294411	6552600	greenstones	JX	15	60	
Site 10	Road back to ferry	294411	6552600	greenstones				
Site 10	Road back to ferry	294411	6552600	greenstones				

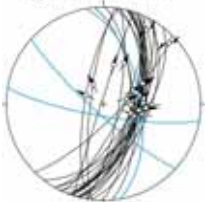


Faults developed parallel to foliation. They are N-S trending and steeply dipping east with slickensides plunging 20 to 30 degrees to the north. Some E-W fractures as tension gashes have been also observed.

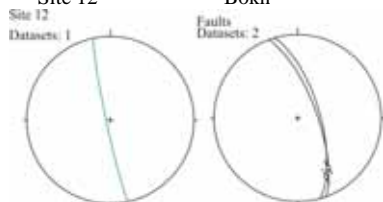
Site 11	Ferry	294543	6551967	greenstones	normal fault dipping east			
Site 11	Ferry	294543	6551967	greenstones	CN	105	62	67N
Site 11	Ferry	294543	6551967	greenstones	CN	105	62	75N
Site 11	Ferry	294543	6551967	greenstones	CN	110	60	62N
Site 11	Ferry	294543	6551967	greenstones	CS	135	77	9N
Site 11	Ferry	294543	6551967	greenstones	CN	85	64	81N
Site 11	Ferry	294543	6551967	greenstones	CS	112	57	15N
Site 11	Ferry	294543	6551967	greenstones	CN	110	67	72N
Site 11	Ferry	294543	6551967	greenstones	CN	277	79	75N
Site 11	Ferry	294543	6551967	greenstones	CN	128	57	70N
Site 11	Ferry	294543	6551967	greenstones	CN	106	60	65N
Site 11	Ferry	294543	6551967	greenstones	CN	115	74	78N
Site 11	Ferry	294543	6551967	greenstones	CN	104	60	66N
Site 11	Ferry	294543	6551967	greenstones	CN	288	88	56N
Site 11	Ferry	294543	6551967	greenstones	CN	279	74	85N
Site 11	Ferry	294543	6551967	greenstones	CN	97	54	89N
Site 11	Ferry	294543	6551967	greenstones	CN	100	77	53N
Site 11	Ferry	294551	6552003	greenstones	Calcite+pyrite JX	190	80	
Site 11	Ferry	294551	6552003	greenstones	Calcite+pyrite JX	222	82	
Site 11	Ferry	294551	6552003	greenstones	Calcite+pyrite JX	80	58	
Site 11	Ferry	294500	6552137	greenstones	SN	104	56	90

Site 11	Ferry	294500	6552137	greenstones	SN	110	62	90
Site 11	Ferry	294500	6552137	greenstones	SN	91	67	90
Site 11	Ferry	294500	6552137	greenstones	SN	120	60	73N
Site 11	Ferry	294500	6552137	greenstones	SN	117	52	73N
Site 11	Ferry	294500	6552137	greenstones	SN	120	66	68N
Site 11	Ferry	294500	6552137	greenstones	SN	100	60	90
Site 11	Ferry	294500	6552137	greenstones	SN	110	64	75N
Site 11	Ferry	294500	6552137	greenstones	SN	108	66	90

Site 11 - Datasets: 28  
Faults and calcite-  
pyrite-filled fractures



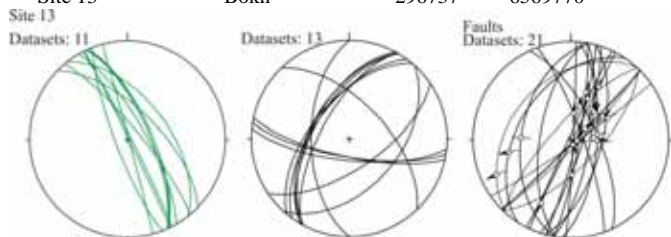
Site 12	Bokn	297512	6569121	granitic gneiss	F	74	68	25S
Site 12	Bokn	297512	6569121	granitic gneiss	F	70	71	33S
Site 12	Bokn	297512	6569121	granitic gneiss	MF	258	86	



Close to the foliation, a large fault surface crops out. Strike-slip slickensides of unknown sense of shear have been observed.

Site 13	Bokn	296737	6569770	granitic gneiss	J	132	48	
Site 13	Bokn	296737	6569770	granitic gneiss	J	46	60	
Site 13	Bokn	296737	6569770	granitic gneiss	J	300	57	
Site 13	Bokn	296737	6569770	granitic gneiss	MF	65	70	
Site 13	Bokn	296737	6569770	granitic gneiss	J	300	60	
Site 13	Bokn	296737	6569770	granitic gneiss	PN	100	83	48N
Site 13	Bokn	296737	6569770	granitic gneiss	J	306	60	
Site 13	Bokn	296737	6569770	granitic gneiss	J	298	58	
Site 13	Bokn	296737	6569770	granitic gneiss	MF	66	72	
Site 13	Bokn	296737	6569770	granitic gneiss	J	299	66	
Site 13	Bokn	296737	6569770	granitic gneiss	J	135	87	74N
Site 13	Bokn	296737	6569770	granitic gneiss	MF	66	70	
Site 13	Bokn	296737	6569770	granitic gneiss	SN	105	85	89N
Site 13	Bokn	296737	6569770	granitic gneiss	MF	60	75	
Site 13	Bokn	296737	6569770	granitic gneiss	J	146	65	

Site 13	Bokn	296737	6569770	granitic gneiss	MF	44	65	
Site 13	Bokn	296737	6569770	granitic gneiss	MF	52	56	
Site 13	Bokn	296737	6569770	granitic gneiss		105	64	84N
Site 13	Bokn	296737	6569770	granitic gneiss	CN	108	80	60N
Site 13	Bokn	296737	6569770	granitic gneiss	CN	100	74	64N
Site 13	Bokn	296737	6569770	granitic gneiss	CN	135	88	75N
Site 13	Bokn	296737	6569770	granitic gneiss	CN	313	75	65N
Site 13	Bokn	296737	6569770	granitic gneiss	CN	135	84	57N
Site 13	Bokn	296737	6569770	granitic gneiss	CN	93	88	86S
Site 13	Bokn	296737	6569770	granitic gneiss	MF	64	90	
Site 13	Bokn	296737	6569770	granitic gneiss	J	310	58	
Site 13	Bokn	296737	6569770	granitic gneiss	MF	63	87	
Site 13	Bokn	296737	6569770	granitic gneiss	J	270	58	
Site 13	Bokn	296737	6569770	granitic gneiss	MF	249	80	
					CN with offset of a			
					brown body			
Site 13	Bokn	296737	6569770	granitic gneiss		312	38	N065
Site 13	Bokn	296737	6569770	granitic gneiss	CN	303	45	N079
Site 13	Bokn	296737	6569770	granitic gneiss	MF	75	89S	
Site 13	Bokn	296737	6569770	granitic gneiss	J	186	72	
Site 13	Bokn	296737	6569770	granitic gneiss	J	192	75	
Site 13	Bokn	296737	6569770	granitic gneiss	J	189	75	
Site 13	Bokn	296737	6569770	granitic gneiss	CN	70	80	70N
Site 13	Bokn	296737	6569770	granitic gneiss	**	65	68	85S
Site 13	Bokn	296737	6569770	granitic gneiss	MF	50	80	
Site 13	Bokn	296737	6569770	granitic gneiss	PS	279	64	34S
Site 13	Bokn	296737	6569770	granitic gneiss	SS	117	89	39N
Site 13	Bokn	296737	6569770	granitic gneiss	SS	295	88	53N
Site 13	Bokn	296737	6569770	granitic gneiss	**	134	68	70S
Site 13	Bokn	296737	6569770	granitic gneiss	**	280	48	85S
Site 13	Bokn	296737	6569770	granitic gneiss	**	145	86	54N
Site 13	Bokn	296737	6569770	granitic gneiss	CN	95	68	88N

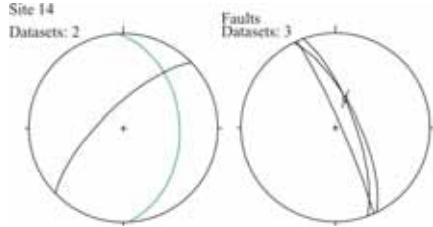


The foliation is close to the vertical and trends NNW-SSE. The most important set of fractures is NE-SW to N-S striking and displays many normal slickensides. Some few steep WNW-ESE joints are also identified.

Western scarp of Boknafjellet due to steep west dipping foliation

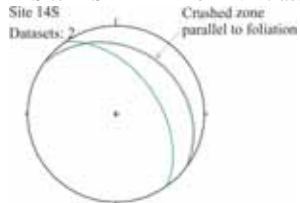


Site 14	Bokn - south of Kleiva	294408	6569766	granitic gneiss	MF	87	40	
Site 14	Bokn - south of Kleiva	294408	6569766	granitic gneiss	J	316	72	
Site 14	Bokn - south of Kleiva	294408	6569766	granitic gneiss	F	66	85	
Site 14	Bokn - south of Kleiva	294408	6569766	granitic gneiss	F	70	73	70W
Site 14	Bokn - south of Kleiva	294408	6569766	granitic gneiss	F	64	70	

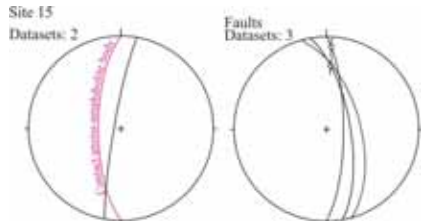


The metamorphic foliation is 40 degrees east-dipping. A 2.5 m wide NNW-SSE fault zone crops out. One of the surface into the fault zone displays slickensides dipping 70 degrees to the North. A set of NE-SW steep joints is also present.

Site 14S	Bokn-Vintrastø	294198	6568797	granitic gneiss	F	36	25	
Site 14S	Bokn-Vintrastø	294198	6568797	granitic gneiss	MF	36	25	
Site 14S	Bokn-Vintrastø	294198	6568797	granitic gneiss	MF	55	50	

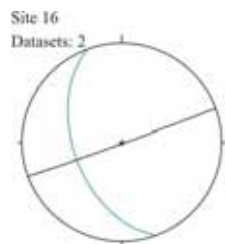


Site 15	Bokn- Sunnlandsstraumen	294597	6566281	granodioritic gneiss	J	280	84	
Site 15	Bokn- Sunnlandsstraumen	294597	6566281	granodioritic gneiss	F	90	75	12N
Site 15	Bokn- Sunnlandsstraumen	294597	6566281	granodioritic gneiss	F	80	69	35N
Site 15	Bokn- Sunnlandsstraumen	294597	6566281	granodioritic gneiss	F	75	60	
Site 15	Bokn- Sunnlandsstraumen	294556	6566021	granodioritic gneiss	Contact gneiss amphibolite	270	70	



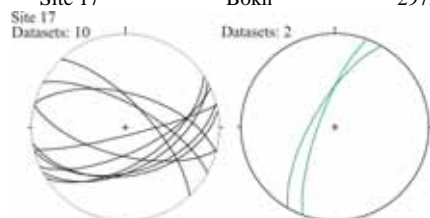
A contact between gneiss and amphibolite crops out. Its trend is N-S parallel to foliation. A large N-S steep fault surface is also present on which strike-slip slickensides have been observed.

Site 16	Road to Loten	293953	6564395	granodioritic gneiss	MF	250	50	
Site 16	Road to Loten	293953	6564395	granodioritic gneiss	vertical joints perpendicular to MF			



Vertical joint perpendicular to the WSW dipping foliation are the only identified structures.

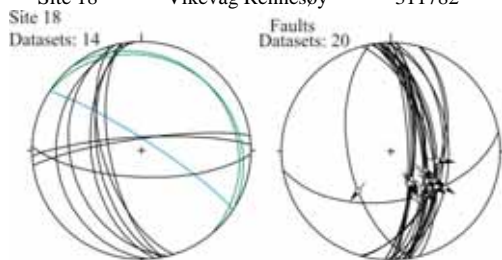
Site 17	Bokn	297236	6568912	granodioritic gneiss	MF	290	76
Site 17	Bokn	297236	6568912	granodioritic gneiss	J	15	60
Site 17	Bokn	297236	6568912	granodioritic gneiss	MF	300	70
Site 17	Bokn	297236	6568912	granodioritic gneiss	J	147	58
Site 17	Bokn	297236	6568912	granodioritic gneiss	J	194	65
Site 17	Bokn	297236	6568912	granodioritic gneiss	J	151	53
Site 17	Bokn	297236	6568912	granodioritic gneiss	J	155	68
Site 17	Bokn	297236	6568912	granodioritic gneiss	J	170	47
Site 17	Bokn	297236	6568912	granodioritic gneiss	J	166	83
Site 17	Bokn	297236	6568912	granodioritic gneiss	J	29	70
Site 17	Bokn	297236	6568912	granodioritic gneiss	J	165	50
Site 17	Bokn	297236	6568912	granodioritic gneiss	J	47	70



The foliation is steeply WNW dipping. Two sets of joints have been measured. First set is WNW-ESE trending and 60 degrees dipping N and second set is WSW-ENE trending and 60 degrees dipping S. They probably form a conjugate system of joints.

Site 18	Vikevåg Rennesøy	311782	6553993	amphibolites	MF	32	15	
Site 18	Vikevåg Rennesøy	311782	6553993	amphibolites	JX	33	82	
Site 18	Vikevåg Rennesøy	311782	6553993	amphibolites	FN	81	67	70S
Site 18	Vikevåg Rennesøy	311782	6553993	amphibolites	FN	80	58	64S
Site 18	Vikevåg Rennesøy	311782	6553993	amphibolites	FN	86	65	74S
Site 18	Vikevåg Rennesøy	311782	6553993	amphibolites	J	352	81	
Site 18	Vikevåg Rennesøy	311782	6553993	amphibolites	J	357	80	
Site 18	Vikevåg Rennesøy	311782	6553993	amphibolites	CN	88	46	63S
Site 18	Vikevåg Rennesøy	311782	6553993	amphibolites	CN	84	58	
Site 18	Vikevåg Rennesøy	311782	6553993	amphibolites	CN	259	58	66S
Site 18	Vikevåg Rennesøy	311782	6553993	amphibolites	J	267	23	
Site 18	Vikevåg Rennesøy	311782	6553993	amphibolites	CN	83	64	65S

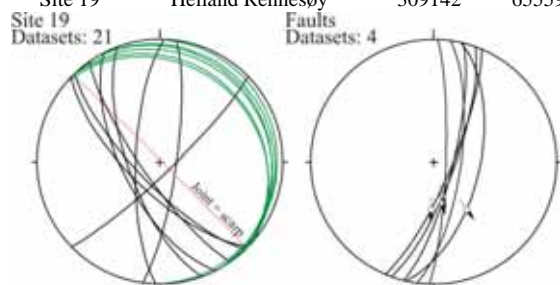
Site 18	Vikevåg Rennesøy	311782	6553993	amphibolites	FN	83	66	
Site 18	Vikevåg Rennesøy	311782	6553993	amphibolites	F	170	52	79E
Site 18	Vikevåg Rennesøy	311782	6553993	amphibolites	J	256	35	
Site 18	Vikevåg Rennesøy	311782	6553993	amphibolites	J	182	70	
Site 18	Vikevåg Rennesøy	311782	6553993	amphibolites	J	263	52	
Site 18	Vikevåg Rennesøy	311782	6553993	amphibolites	FN	92	50	85S
Site 18	Vikevåg Rennesøy	311782	6553993	amphibolites	FN	106	50	75S
Site 18	Vikevåg Rennesøy	311782	6553993	amphibolites	FN	105	52	79S
Site 18	Vikevåg Rennesøy	311782	6553993	amphibolites	J	259	66	
Site 18	Vikevåg Rennesøy	311782	6553993	amphibolites	MF	50	15	
Site 18	Vikevåg Rennesøy	311782	6553993	amphibolites	J	260	57	
Site 18	Vikevåg Rennesøy	311782	6553993	amphibolites	J	253	61	
Site 18	Vikevåg Rennesøy	311782	6553993	amphibolites	CN	81	64	55S
Site 18	Vikevåg Rennesøy	311782	6553993	amphibolites	CN	75	60	56S
Site 18	Vikevåg Rennesøy	311782	6553993	amphibolites	CN	88	77	66S
Site 18	Vikevåg Rennesøy	311782	6553993	amphibolites	CN	93	73	70S
Site 18	Vikevåg Rennesøy	311782	6553993	amphibolites	CN	90	73	66S
Site 18	Vikevåg Rennesøy	311782	6553993	amphibolites	CN	84	56	80S
Site 18	Vikevåg Rennesøy	311782	6553993	amphibolites	CN	90	64	63S
Site 18	Vikevåg Rennesøy	311782	6553993	amphibolites	CN	93	72	65S
Site 18	Vikevåg Rennesøy	311782	6553993	amphibolites	CN	90	75	66S
Site 18	Vikevåg Rennesøy	311782	6553993	amphibolites	CN	83	58	65S



The foliation is flat. The major structures are a dominant set of normal faults dipping eastward. Some conjugate fractures exist but without many observable slickensides. A set of fractures perpendicular to the normal faults developed.

Site 19	Helland Rennesøy	309142	6555915	amphibolites	large joint=scarp	45	90	
Site 19	Helland Rennesøy	309142	6555915	amphibolites	J	224	70	
Site 19	Helland Rennesøy	309142	6555915	amphibolites	J	250	69	
Site 19	Helland Rennesøy	309142	6555915	amphibolites	MF	57	8	
Site 19	Helland Rennesøy	309142	6555915	amphibolites	FN	92	82	
Site 19	Helland Rennesøy	309142	6555915	amphibolites	FN	98	72	
Site 19	Helland Rennesøy	309142	6555915	amphibolites	J	235	78	
Site 19	Helland Rennesøy	309142	6555915	amphibolites	J	136	82	
Site 19	Helland Rennesøy	309142	6555915	amphibolites	J	243	65	

Site 19	Helland Rennesøy	309142	6555915	amphibolites	MF	60	11	
Site 19	Helland Rennesøy	309142	6555915	amphibolites	MF	90	5	
Site 19	Helland Rennesøy	309142	6555915	amphibolites	MF	40	21	
Site 19	Helland Rennesøy	309142	6555915	amphibolites	MF	45	19	
Site 19	Helland Rennesøy	309142	6555915	amphibolites	J	98	79	
Site 19	Helland Rennesøy	309142	6555915	amphibolites	CN	110	76	71S
Site 19	Helland Rennesøy	309142	6555915	amphibolites	J	226	75	
Site 19	Helland Rennesøy	309142	6555915	amphibolites	CN	113	78	60S
Site 19	Helland Rennesøy	309142	6555915	amphibolites	CN	103	59	65S
Site 19	Helland Rennesøy	309142	6555915	amphibolites	CN	104	77	65S
Site 19	Helland Rennesøy	309142	6555915	amphibolites	J	272	74	
Site 19	Helland Rennesøy	309142	6555915	amphibolites	MF	46	13	

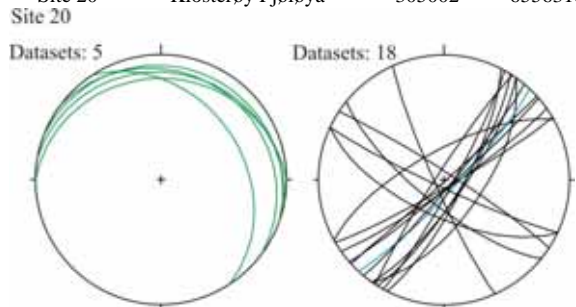


The foliation is flat. Steep NW-SE joints form the main scarp along the coast. NNE-SSW steeply eastward dipping normal faults are present.

Site 20	Klosterøy Fjøløya	305002	6556318	gneiss	J	150	85	
Site 20	Klosterøy Fjøløya	305002	6556318	gneiss	MF	20	10	
Site 20	Klosterøy Fjøløya	305002	6556318	gneiss	MF	10	15	
Site 20	Klosterøy Fjøløya	305002	6556318	gneiss	J	122	78	
Site 20	Klosterøy Fjøløya	305002	6556318	gneiss	J	219	74	
Site 20	Klosterøy Fjøløya	305002	6556318	gneiss	J	303	85	
Site 20	Klosterøy Fjøløya	305002	6556318	gneiss	MF	57	34	
Site 20	Klosterøy Fjøløya	305002	6556318	gneiss	J	125	77	
Site 20	Klosterøy Fjøløya	305002	6556318	gneiss	MF	37	15	
Site 20	Klosterøy Fjøløya	305002	6556318	gneiss	J	331	71	
Site 20	Klosterøy Fjøløya	305002	6556318	gneiss	J	125	65	
Site 20	Klosterøy Fjøløya	305002	6556318	gneiss	J	145	84	
Site 20	Klosterøy Fjøløya	305002	6556318	gneiss	J	117	77	
Site 20	Klosterøy Fjøløya	305002	6556318	gneiss	J	33	85	
Site 20	Klosterøy Fjøløya	305002	6556318	gneiss	J	138	90	
Site 20	Klosterøy Fjøløya	305002	6556318	gneiss	J	246	84	
Site 20	Klosterøy Fjøløya	305002	6556318	gneiss	JX	133	82	
Site 20	Klosterøy Fjøløya	305002	6556318	gneiss	MF	0	20	
Site 20	Klosterøy Fjøløya	305002	6556318	gneiss	J	139	85	

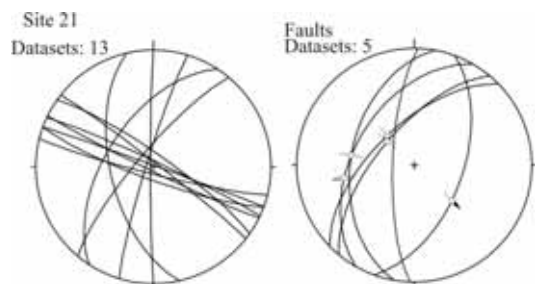


Site 20	Klosterøy Fjøløya	305002	6556318	gneiss	J	205	85
Site 20	Klosterøy Fjøløya	305002	6556318	gneiss	J	130	85
Site 20	Klosterøy Fjøløya	305002	6556318	gneiss	J	119	84
Site 20	Klosterøy Fjøløya	305002	6556318	gneiss	J	205	66



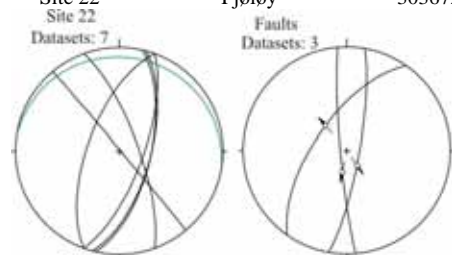
The foliation dips gently to the N. Two main sets of vertical diaclasses are present and trend NW-SE and NE-SW.

Site 21	Fjøløy	304033	6555097	gneiss	J	310	79	
Site 21	Fjøløy	304033	6555097	gneiss	J	35	81	
Site 21	Fjøløy	304033	6555097	gneiss	J	287	85	
Site 21	Fjøløy	304033	6555097	gneiss	J	38	87	
Site 21	Fjøløy	304033	6555097	gneiss	J	270	88	
Site 21	Fjøløy	304033	6555097	gneiss	PN	300	47	60S
Site 21	Fjøløy	304033	6555097	gneiss	J	303	57	
Site 21	Fjøløy	304033	6555097	gneiss	J	25	86	
Site 21	Fjøløy	304033	6555097	gneiss	F	310	65	89E?
Site 21	Fjøløy	304033	6555097	gneiss	J	20	89	
Site 21	Fjøløy	304033	6555097	gneiss	F	280	45	89S?
Site 21	Fjøløy	304033	6555097	gneiss	J	194	85	
Site 21	Fjøløy	304033	6555097	gneiss	F	316	62	89E?
Site 21	Fjøløy	304033	6555097	gneiss	J	206	87	
Site 21	Fjøløy	304033	6555097	gneiss	J	257	60	
Site 21	Fjøløy	304033	6555097	gneiss	J	200	81	
Site 21	Fjøløy	304033	6555097	gneiss	FN	272	75	
Site 21	Fjøløy	304033	6555097	gneiss	CN	110	56	76S



The foliation is close to horizontal. Apart a set of vertical WNW-ESE joints, a set of NNE-SSW faults, probably normal faults, developed.

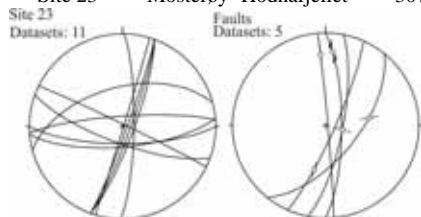
Site 22	Fjøløy	303868	6555223	eye gneiss	J	103	65	
Site 22	Fjøløy	303868	6555223	eye gneiss	J	110	71	
Site 22	Fjøløy	303868	6555223	eye gneiss	PN	100	80	80S
Site 22	Fjøløy	303868	6555223	eye gneiss	CN	265	85	74S
Site 22	Fjøløy	303868	6555223	eye gneiss	J	70	75	
Site 22	Fjøløy	303868	6555223	eye gneiss	MF	9	10	
Site 22	Fjøløy	303672	6555124	eye gneiss	J	290	65	
Site 22	Fjøløy	303672	6555124	eye gneiss	J	50	89	
Site 22	Fjøløy	303672	6555124	eye gneiss	J	105	65	
Site 22	Fjøløy	303672	6555124	eye gneiss	CN	305	65	84N



The foliation is very gently dipping north. Spectacular NNE-SSW normal faults affected the unit.

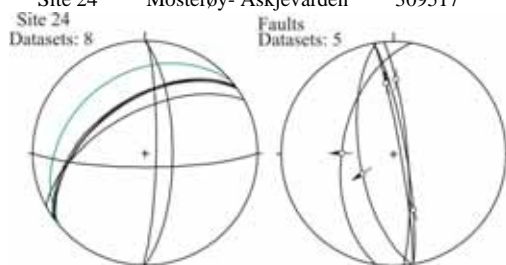
Site 23	Mosterøy- Hodnafjellet	306985	6553177	gneiss	J	110	86	
Site 23	Mosterøy- Hodnafjellet	306985	6553177	gneiss	J	180	75	
Site 23	Mosterøy- Hodnafjellet	306985	6553177	gneiss	F	114	82	50S
Site 23	Mosterøy- Hodnafjellet	306985	6553177	gneiss	F	101	75	89S
Site 23	Mosterøy- Hodnafjellet	306985	6553177	gneiss	F	129	62	62N
Site 23	Mosterøy- Hodnafjellet	306985	6553177	gneiss	J	110	80	
Site 23	Mosterøy- Hodnafjellet	306985	6553177	gneiss	J	200	75	
Site 23	Mosterøy- Hodnafjellet	306985	6553177	gneiss	J	110	83	
Site 23	Mosterøy- Hodnafjellet	306985	6553177	gneiss	J	26	88	
Site 23	Mosterøy- Hodnafjellet	306985	6553177	gneiss	J	107	90	
Site 23	Mosterøy- Hodnafjellet	306985	6553177	gneiss	CD	90	76	22N
Site 23	Mosterøy- Hodnafjellet	306985	6553177	gneiss	J	356	81	

Site 23	Mosterøy- Hodnafjellet	306985	6553177	gneiss	J	91	80	
Site 23	Mosterøy- Hodnafjellet	307143	6553377	gneiss	J	345	55	
Site 23	Mosterøy- Hodnafjellet	307143	6553377	gneiss	J	175	72	
Site 23	Mosterøy- Hodnafjellet	307143	6553377	gneiss	F	85	88	24N



Two sets of steep fractures: WNW-ESE joints and : NNE-SSW faults and joints. On the fault surfaces, both strike-slip and dip-slip slickensides are observed.

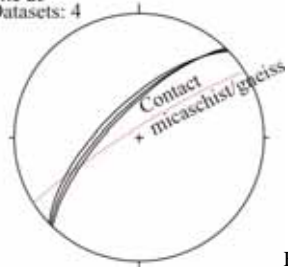
Site 24	Mosterøy- Askjevarden	309513	6552373	mica-rich gneiss	F	80	81	47S
Site 24	Mosterøy- Askjevarden	309513	6552373	mica-rich gneiss	J	90	70	
Site 24	Mosterøy- Askjevarden	309513	6552373	mica-rich gneiss	J	91	82	
Site 24	Mosterøy- Askjevarden	309513	6552373	mica-rich gneiss	J	332	60	
Site 24	Mosterøy- Askjevarden	309513	6552373	mica-rich gneiss	J	324	52	
Site 24	Mosterøy- Askjevarden	309513	6552373	mica-rich gneiss	J	325	50	
Site 24	Mosterøy- Askjevarden	309513	6552373	mica-rich gneiss	MF	320	30	
Site 24	Mosterøy- Askjevarden	309513	6552373	mica-rich gneiss	J	323	51	
Site 24	Mosterøy- Askjevarden	309513	6552373	mica-rich gneiss	contact diorite-micaschists	180	80	
Site 24	Mosterøy- Askjevarden	309517	6552036	mica-rich gneiss	PS	80	85	37N
Site 24	Mosterøy- Askjevarden	309517	6552036	mica-rich gneiss	F	85	80	35N
Site 24	Mosterøy- Askjevarden	309517	6552036	mica-rich gneiss	CN	279	52	85S
Site 24	Mosterøy- Askjevarden	309517	6552036	mica-rich gneiss	CN	261	65	80S



Foliation dips 30 degrees to the NW and joints developed along the same strike and dip 50 degrees to the NW. N-S faults are of two types. A first set comprises 50-60 degrees west-dipping normal faults. A second set consists of vertical large faults with highly oblique slickensides.

Site 25	Bru	308232	6549379	eye gneiss-conglomerates - micaschists	contact gneiss-micasch.	328	84	
Site 25	Bru	308232	6549379	eye gneiss-conglomerates - micaschists	J	315	70	
Site 25	Bru	308232	6549379	eye gneiss-conglomerates - micaschists	J	316	67	

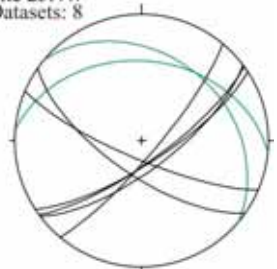
Site 25	Bru	308232	6549379	eye gneiss-conglomerates - micaschists	J	314	72
Site 25 Datasets: 4							



Fractures trend NE-SW and steeply dip NW. A vertical contact of the same strike is also observed between eye-gneiss and micaschists.

Site 25NW	North Brufjellet	307632	6549735	micaschists	MF	5	37
Site 25NW	North Brufjellet	307632	6549735	micaschists	MF	40	32
Site 25NW	North Brufjellet	307632	6549735	micaschists	J	144	76
Site 25NW	North Brufjellet	307632	6549735	micaschists	J	147	75
Site 25NW	North Brufjellet	307632	6549735	micaschists	J	130	80
Site 25NW	North Brufjellet	307632	6549735	micaschists	J	143	71
Site 25NW	North Brufjellet	307632	6549735	micaschists	J	215	68
Site 25NW	North Brufjellet	307632	6549735	micaschists	J	203	78

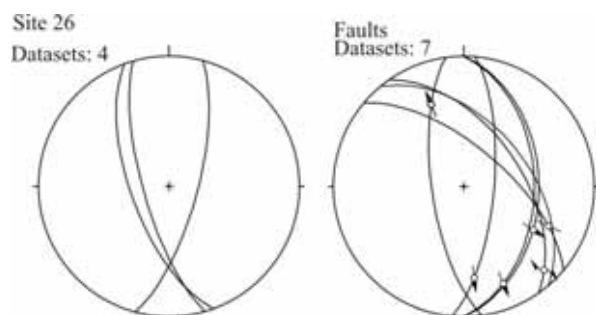
Site 25NW  
Datasets: 8



The foliation is gently dipping to the N and NE. Two sets of joints developed perpendicular to the foliation planes and respect to the strike of foliation, one trends parallel and the other one trends perpendicular.

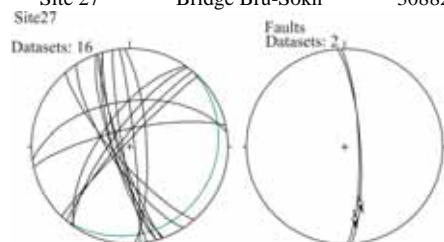
Site 26	Bru	308698	6549384	micaschists	J	250	66	
Site 26	Bru	308698	6549384	micaschists	J	254	74	
Site 26	Bru	308698	6549384	micaschists	CD	55	54	15S
Site 26	Bru	308698	6549384	micaschists	CD	95	71	32S
Site 26	Bru	308698	6549384	micaschists	J	105	72	
Site 26	Bru	308698	6549384	micaschists	PD	262	70	35N
Site 26	Bru	308698	6549384	micaschists	CD	90	45	30S
Site 26	Bru	308698	6549384	micaschists	F	50	50	
Site 26	Bru	308698	6549384	micaschists	F	40	65	32S
Site 26	Bru	308698	6549384	micaschists	CN	90	42	N122





NW-SE to N-S fractures formed and they mostly dip eastward. On some of these planes, slickensides have been measured and oblique normal shears identified. The NE-dipping planes developed along the foliation.

Site 27	Bridge Bru-Sokn	308826	6549681	gneiss grano-diorite	J	352	52	
Site 27	Bridge Bru-Sokn	308826	6549681	gneiss grano-diorite	MF	130	14	
Site 27	Bridge Bru-Sokn	308826	6549681	gneiss grano-diorite	J	251	82	
Site 27	Bridge Bru-Sokn	308826	6549681	gneiss grano-diorite	J	250	76	
Site 27	Bridge Bru-Sokn	308826	6549681	gneiss grano-diorite	J	254	80	
Site 27	Bridge Bru-Sokn	308826	6549681	gneiss grano-diorite	J	260	84	
Site 27	Bridge Bru-Sokn	308826	6549681	gneiss grano-diorite	J	305	65	
Site 27	Bridge Bru-Sokn	308826	6549681	gneiss grano-diorite	J	237	73	
Site 27	Bridge Bru-Sokn	308826	6549681	gneiss grano-diorite	J	254	76	
Site 27	Bridge Bru-Sokn	308826	6549681	gneiss grano-diorite	J	306	75	
Site 27	Bridge Bru-Sokn	308826	6549681	gneiss grano-diorite	J	229	77	
Site 27	Bridge Bru-Sokn	308826	6549681	gneiss grano-diorite	J	310	82	
Site 27	Bridge Bru-Sokn	308826	6549681	gneiss grano-diorite	CD	86	77	41S
Site 27	Bridge Bru-Sokn	308826	6549681	gneiss grano-diorite	CD	88	78	27S
Site 27	Bridge Bru-Sokn	308826	6549681	gneiss grano-diorite	J	84	86	
Site 27	Bridge Bru-Sokn	308826	6549681	gneiss grano-diorite	J	314	86	
Site 27	Bridge Bru-Sokn	308826	6549681	gneiss grano-diorite	J	87	76	
Site 27	Bridge Bru-Sokn	308826	6549681	gneiss grano-diorite	J	348	76	

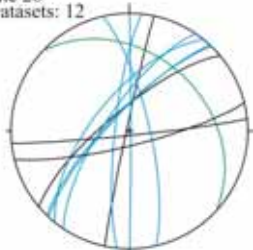


The foliation gently dips SE. Sets of steep joints trend NE-SW, NNW-SSE and ENE-WSW. Two right-lateral N-S faults have been identified.

Site 28	Bridge Bru-Sokn	308937	6549938	grano-diorite	J	282	88	
Site 28	Bridge Bru-Sokn	308937	6549938	grano-diorite	J	174	87	

Site 28	Bridge Bru-Sokn	308937	6549938	grano-diorite	J	320	75
Site 28	Bridge Bru-Sokn	308937	6549938	grano-diorite	MF	43	35
Site 28	Bridge Bru-Sokn	308937	6549938	grano-diorite	JX	304	73
Site 28	Bridge Bru-Sokn	308937	6549938	grano-diorite	JX	276	80
Site 28	Bridge Bru-Sokn	308937	6549938	grano-diorite	JX	309	65
Site 28	Bridge Bru-Sokn	308937	6549938	grano-diorite	JX	313	77
Site 28	Bridge Bru-Sokn	308937	6549938	grano-diorite	JX	90	90
Site 28	Bridge Bru-Sokn	308937	6549938	grano-diorite	JX	314	76
Site 28	Bridge Bru-Sokn	308937	6549938	grano-diorite	JX	77	76
Site 28	Bridge Bru-Sokn	308937	6549938	grano-diorite	J	166	80

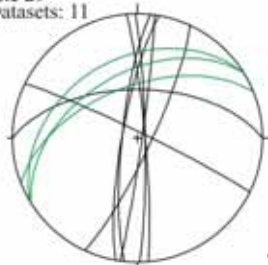
Site 28  
Datasets: 12



The foliation is 35 degrees NE dipping. Aside a set of WSW-ENE joints, a network of N-S and NE-SW steep quartz filled veins developed.

Site 29	Road Randaberg-Grødheim	306713	6545514	micaschists	J	85	85
Site 29	Road Randaberg-Grødheim	306713	6545514	micaschists	MF	328	36
Site 29	Road Randaberg-Grødheim	306713	6545514	micaschists	J	89	85
Site 29	Road Randaberg-Grødheim	306713	6545514	micaschists	J	98	87
Site 29	Road Randaberg-Grødheim	306713	6545514	micaschists	J	276	80
Site 29	Road Randaberg-Grødheim	306713	6545514	micaschists	J	280	80
Site 29	Road Randaberg-Grødheim	306713	6545514	micaschists	MF	338	56
Site 29	Road Randaberg-Grødheim	306713	6545514	micaschists	J	0	58
Site 29	Road Randaberg-Grødheim	306713	6545514	micaschists	J	26	86
Site 29	Road Randaberg-Grødheim	306713	6545514	micaschists	J	115	81
Site 29	Road Randaberg-Grødheim	306713	6545514	micaschists	MF	328	47

Site 29  
Datasets: 11

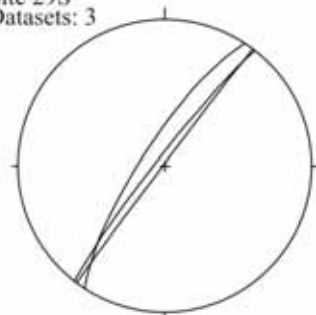


The metamorphic foliation is 45 degrees dipping to the NNW. N-S vertical joints cut across.

Site 29S	Randaberg-Rygg Road	306854	6544848	micaschists	J	307	90
----------	---------------------	--------	---------	-------------	---	-----	----

Site 29S	Randaberg-Rygg Road	306854	6544848	micaschists	J	303	77
Site 29S	Randaberg-Rygg Road	306854	6544848	micaschists	J	308	85

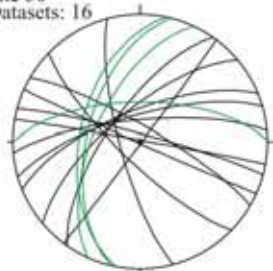
Site 29S  
Datasets: 3



Site 30	Grødheim	307904	6545695	phyllites	MF	0	65
Site 30	Grødheim	307904	6545695	phyllites	J	320	70
Site 30	Grødheim	307904	6545695	phyllites	J	338	70
Site 30	Grødheim	307904	6545695	phyllites	J	30	80
Site 30	Grødheim	307904	6545695	phyllites	J	344	73
Site 30	Grødheim	307904	6545695	phyllites	J	255	77
Site 30	Grødheim	307904	6545695	phyllites	J	305	69
Site 30	Grødheim	307904	6545695	phyllites	J	204	89
Site 30	Grødheim	307904	6545695	phyllites	J	127	90
Site 30	Grødheim	307904	6545695	phyllites	J	355	76
Site 30	Grødheim	307904	6545695	phyllites	J	15	85
Site 30	Grødheim	307904	6545695	phyllites	J	10	90
Site 30	Grødheim	307904	6545695	phyllites	J	224	77
Site 30	Grødheim	307904	6545695	phyllites	MF	282	50
Site 30	Grødheim	307904	6545695	phyllites	MF	284	55
Site 30	Grødheim	307904	6545695	phyllites	MF	295	60

NE-SW vertical joints

Site 30  
Datasets: 16



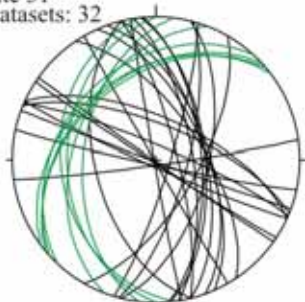
The metamorphic foliation is folded and probably subsequently the joints are widely distributed in strike.

Site 31	Ladbergvika	306424	6546977	phyllites	MF	270	38
Site 31	Ladbergvika	306424	6546977	phyllites	J	256	55

Site 31	Ladbergvika	306545	6546864	phyllites	MF	291	42
Site 31	Ladbergvika	306545	6546864	phyllites	J	22	70
Site 31	Ladbergvika	306545	6546864	phyllites	J	56	64
Site 31	Ladbergvika	306545	6546864	phyllites	J	24	66
Site 31	Ladbergvika	306545	6546864	phyllites	MF	277	48
Site 31	Ladbergvika	306545	6546864	phyllites	J	104	60
Site 31	Ladbergvika	306545	6546864	phyllites	J	70	60
Site 31	Ladbergvika	306545	6546864	phyllites	J	172	87
Site 31	Ladbergvika	306545	6546864	phyllites	J	84	62
Site 31	Ladbergvika	306545	6546864	phyllites	J	76	62
Site 31	Ladbergvika	306545	6546864	phyllites	MF	263	34
Site 31	Ladbergvika	306545	6546864	phyllites	J	192	87
Site 31	Ladbergvika	306545	6546864	phyllites	J	107	82
Site 31	Ladbergvika	306545	6546864	phyllites	J	260	90
Site 31	Ladbergvika	306545	6546864	phyllites	J	66	62
Site 31	Ladbergvika	306545	6546864	phyllites	J	204	86
Site 31	Ladbergvika	306545	6546864	phyllites	J	213	88
Site 31	Ladbergvika	306545	6546864	phyllites	MF	318	40
Site 31	Ladbergvika	306545	6546864	phyllites	J	81	69
Site 31	Ladbergvika	306545	6546864	phyllites	MF	320	42
Site 31	Ladbergvika	306545	6546864	phyllites	J	23	82
Site 31	Ladbergvika	306545	6546864	phyllites	MF	313	34
Site 31	Ladbergvika	306545	6546864	phyllites	J	200	90
Site 31	Ladbergvika	306545	6546864	phyllites	J	240	90
Site 31	Ladbergvika	306545	6546864	phyllites	J	105	72
Site 31	Ladbergvika	306545	6546864	phyllites	MF	323	38
Site 31	Ladbergvika	306545	6546864	phyllites	J	215	90
Site 31	Ladbergvika	306545	6546864	phyllites	J	120	66
Site 31	Ladbergvika	306545	6546864	phyllites	J	76	78
Site 31	Ladbergvika	306545	6546864	phyllites	J	85	64



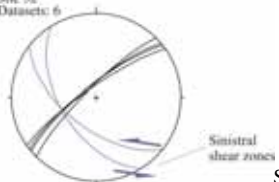
Site 31  
Datasets: 32



The metamorphic foliation is 30 degrees dipping west and NW. Vertical joints developed perpendicular to it and then trend WNW-ESE. A set of 60 degrees dipping E and N-S trending joints has been also observed

Site 32	Byfjordtunnelen	306747	6546581	phyllite	J	315	80
Site 32	Byfjordtunnelen	306747	6546581	phyllite	J	325	80
Site 32	Byfjordtunnelen	306747	6546581	phyllite	J	322	78
Site 32	Byfjordtunnelen	306747	6546581	phyllite	J	320	78
Site 32	Byfjordtunnelen	306747	6546581	phyllite	Small-scale shear zones (sinistral)	218	60
Site 32	Byfjordtunnelen	306747	6546581	phyllite	Small-scale shear zones (sinistral)	238	55

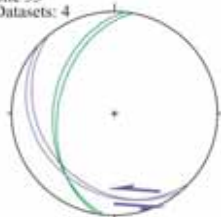
Site 32  
Datasets: 6



Shallow SW-dipping sinistral shear zones and NE-SW vertical joints.

Site 33	Todneim	306006	6547019	phyllite	MF	280	44
Site 33	Todneim	306006	6547019	phyllite	MF	276	40
Site 33	Todneim	306006	6547019	phyllite	Small-scale shear zones (sinistral)	230	29
Site 33	Todneim	306006	6547019	phyllite	Small-scale shear zones (sinistral)	223	24

Site 33  
Datasets: 4

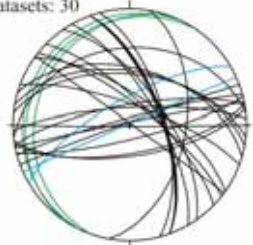


Shallow SW-dipping sinistral shear zones and shallow west dipping foliation

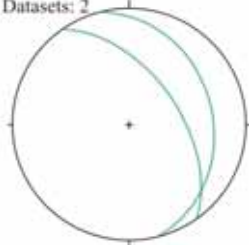
Site 34	Kvitsøy	295352	6553554	greenstones	MF	290	20
---------	---------	--------	---------	-------------	----	-----	----

Site 34	Kvitsøy	295352	6553554	greenstones	MF	304	14
Site 34	Kvitsøy	295352	6553554	greenstones	J	38	76
Site 34	Kvitsøy	295352	6553554	greenstones	J	60	70
Site 34	Kvitsøy	295352	6553554	greenstones	J	35	70
Site 34	Kvitsøy	295352	6553554	greenstones	J	10	52
Site 34	Kvitsøy	295352	6553554	greenstones	J	350	76
Site 34	Kvitsøy	295352	6553554	greenstones	J	357	78
Site 34	Kvitsøy	295352	6553554	greenstones	J	16	50
Site 34	Kvitsøy	295352	6553554	greenstones	J	6	54
Site 34	Kvitsøy	295352	6553554	greenstones	J	340	88
Site 34	Kvitsøy	295352	6553554	greenstones	J	354	34
Site 34	Kvitsøy	295352	6553554	greenstones	J	100	50
Site 34	Kvitsøy	295352	6553554	greenstones	J	36	90
Site 34	Kvitsøy	295352	6553554	greenstones	J	20	76
Site 34	Kvitsøy	295352	6553554	greenstones	J	75	65
Site 34	Kvitsøy	295360	6553633	greenstones	J	44	74
Site 34	Kvitsøy	295360	6553633	greenstones	J	70	67
Site 34	Kvitsøy	295360	6553633	greenstones	J	172	68
Site 34	Kvitsøy	295360	6553633	greenstones	J	166	80
Site 34	Kvitsøy	295360	6553633	greenstones	J	55	65
Site 34	Kvitsøy	295360	6553633	greenstones	J	170	70
Site 34	Kvitsøy	295360	6553633	greenstones	J	180	90
Site 34	Kvitsøy	295360	6553633	greenstones	J	345	85
Site 34	Kvitsøy	295360	6553633	greenstones	J	349	88
Site 34	Kvitsøy	295360	6553633	greenstones	J	70	68
Site 34	Kvitsøy	295360	6553633	greenstones	J	70	66
Site 34	Kvitsøy	295360	6553633	greenstones	Fracture & minor shear zone with quartz vein	336	90
Site 34	Kvitsøy	295360	6553633	locally some carbonate	Up to 10 cm quartz vein	330	72
Site 34	Kvitsøy	295292	6553616	greenstones	MF	76	29
Site 34	Kvitsøy	295095	6553609	greenstones	MF	55	55

Site 34  
Datasets: 30



Near Site 34  
Datasets: 2

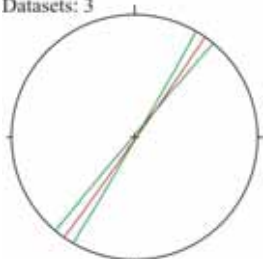


Site 35	Kvitsøy coast station	295556	6553322	calcisilicate schist	MF	120	89
---------	-----------------------	--------	---------	----------------------	----	-----	----

Site 35	Kvitsøy coast station	295556	6553322	calcsilicate schist	MF		310	89
Site 35	Kvitsøy coast station	295556	6553322	calcsilicate schist	fold axial plane		125	90
Site 35	Kvitsøy coast station	295556	6553322	calcsilicate schist	Tight upright folds with axial planes parallel to the foliation			

Site 35

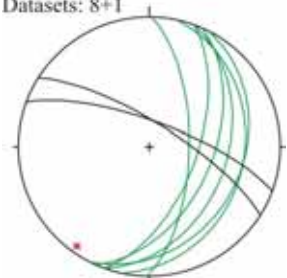
Datasets: 3



Site 36	Kvitsøy	294500	6552650	calcsilicate schist	MF		110	60
Site 36	Kvitsøy	294500	6552650	calcsilicate schist	MF		91	65
Site 36	Kvitsøy	294500	6552650	calcsilicate schist	MF		110	40
Site 36	Kvitsøy	294500	6552650	calcsilicate schist	MF		114	50
Site 36	Kvitsøy	294500	6552650	calcsilicate schist	MF		102	28
Site 36	Kvitsøy	294500	6552650	calcsilicate schist	MF		117	29
Site 36	Kvitsøy	294500	6552650	calcsilicate schist	J		20	74
Site 36	Kvitsøy	294500	6552650	calcsilicate schist	J		32	75
Site 36	Kvitsøy	294500	6552650	calcsilicate schist	fold axis	216		6

Site 36

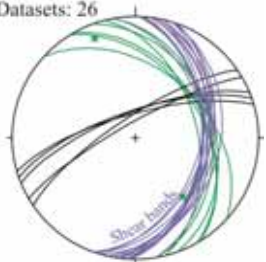
Datasets: 8+1



Site 37	Arsvåger	296990	6564580	granodioritic gneiss with layers of granite	MF		42	42
Site 37	Arsvåger	296990	6564580	granodioritic gneiss	ML	338		13
Site 37	Arsvåger	297075	6564617	phyllite with sandstone layers	MF		76	48
Site 37	Arsvåger	297075	6564617	phyllite with sandstone layers	MF		80	38
Site 37	Arsvåger	297075	6564617	phyllite with sandstone layers	MF		70	36
Site 37	Arsvåger	297075	6564617	phyllite with sandstone layers	MF		58	44
Site 37	Arsvåger	297075	6564617	phyllite with sandstone layers	MF		60	42
Site 37	Arsvåger	297075	6564617	phyllite with sandstone layers	J (spaced metre-long)		338	73

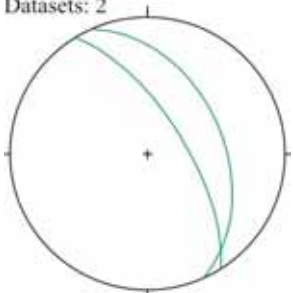
Site 37	Arsvåger	297075	6564617	phyllite with sandstone layers	J (spaced metre-long)	341	72
Site 37	Arsvåger	297075	6564617	phyllite with sandstone layers	J (spaced metre-long)	344	74
Site 37	Arsvåger	297075	6564617	phyllite with sandstone layers	J (spaced metre-long)	330	80
Site 37	Arsvåger	297075	6564617	phyllite with sandstone layers	J (spaced metre-long)	326	76
Site 37	Arsvåger	297075	6564617	phyllite with sandstone layers	Shear band	108	46
Site 37	Arsvåger	297075	6564617	phyllite with sandstone layers	Shear band	100	36
Site 37	Arsvåger	297075	6564617	phyllite with sandstone layers	Shear band	107	32
Site 37	Arsvåger	297075	6564617	phyllite with sandstone layers	Shear band	103	39
Site 37	Arsvåger	297075	6564617	phyllite with sandstone layers	Shear band	80	42
Site 37	Arsvåger	297075	6564617	phyllite with sandstone layers	Shear band	110	43
Site 37	Arsvåger	297075	6564617	phyllite with sandstone layers	Shear band	109	39
Site 37	Arsvåger	297075	6564617	phyllite with sandstone layers	Shear band	97	39
Site 37	Arsvåger	297075	6564617	phyllite with sandstone layers	Shear band	92	44
Site 37	Arsvåger	297075	6564617	phyllite with sandstone layers	Shear band	93	45
Site 37	Arsvåger	297075	6564617	phyllite with sandstone layers	Shear band	98	44
Site 37	Arsvåger	297075	6564617	phyllite with sandstone layers	Shear band	100	41
Site 37	Arsvåger	297075	6564617	phyllite with sandstone layers	Shear band	94	44
Site 37	Arsvåger	297075	6564617	phyllite with sandstone layers	lineation	142	38

Site 37  
Datasets: 26



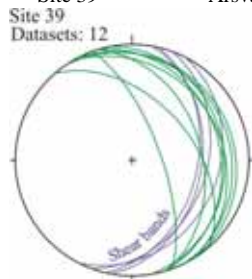
Site 38	Arsvåger	296859	6563784	granitic gneiss	MF	66	44
Site 38	Arsvåger	296859	6563784	granitic gneiss	MF	58	68

Site 38  
Datasets: 2

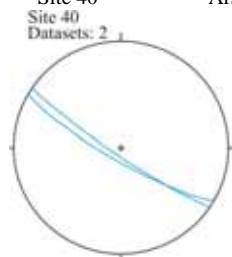




Site 39	Arsvåger	296989	6564241	granodioritic gneiss with mylonitic fabric	MF	74	25
Site 39	Arsvåger	296955	6564072	granitic gneiss	MF	73	40
Site 39	Arsvåger	296955	6564072	granitic gneiss	Mylonite	70	70
Site 39	Arsvåger	297109	6564272	phyllite	MF	58	24
Site 39	Arsvåger	297109	6564272	phyllite	MF	49	47
Site 39	Arsvåger	297109	6564272	phyllite	MF	56	14
Site 39	Arsvåger	297109	6564272	phyllite	MF	63	17
Site 39	Arsvåger	297109	6564272	phyllite	MF	80	22
Site 39	Arsvåger	297109	6564272	phyllite	Shear band	100	40
Site 39	Arsvåger	297109	6564272	phyllite	Shear band	110	36
Site 39	Arsvåger	297109	6564272	phyllite	Shear band	103	43
Site 39	Arsvåger	297109	6564272	phyllite	Shear band	117	27

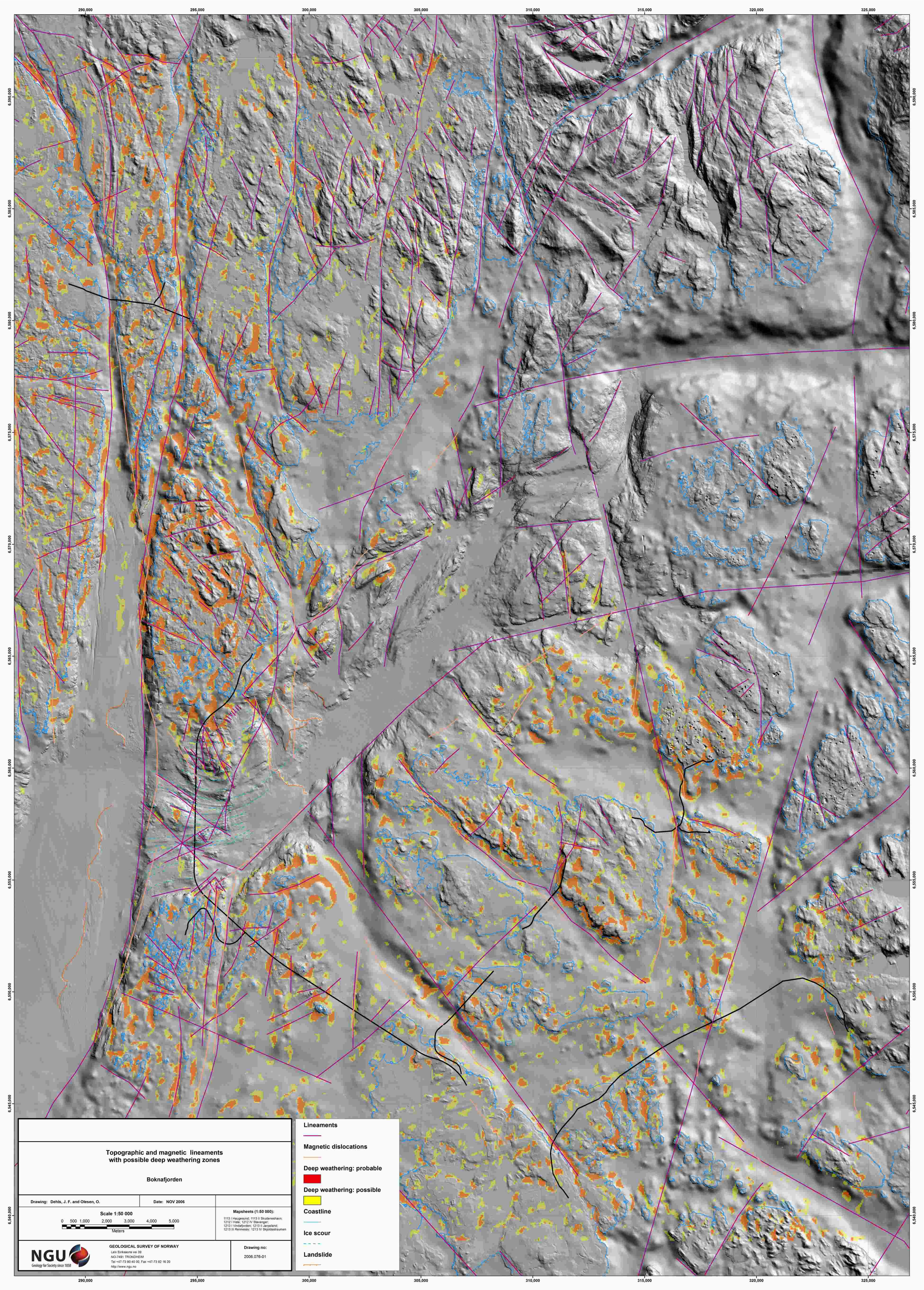


Site 40	Arsvåger	311168	6556475	layered gneiss		undulating foliation	
Site 40	Arsvåger	311168	6556475	layered gneiss	Calcite + pyrite JX	210	80
Site 40	Arsvåger	311168	6556475	layered gneiss	Calcite + pyrite JX	214	84



Field locations and structural data, observations. Keys for 'type structure' First index for faults: **F** / First index for striated faults is qualitative with **C**, certain; **P**, probable; **S**, supposed / Second index is the sense of shear with **R**, reverse; **N**, normal; **D**, right-lateral (dextral); **S**, left-lateral (sinistral) / \*\* as striated fault of unknown sense of shear/ **J**, joint, diacalse... / **JX**, mineral-filled fracture, tension gash / **JV**, dyke, vein / **MF**, metamorphic foliation / **ML**, metamorphic lineation

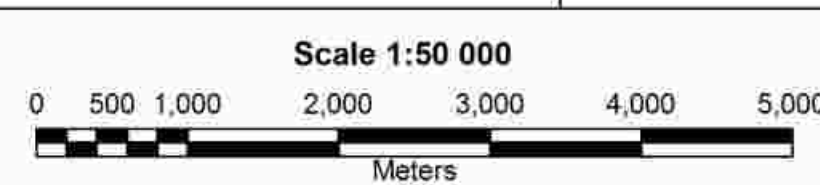




**Topographic and magnetic lineaments  
with possible deep weathering zones**

Boknafjorden

Drawing: Dehls, J.F. and Olesen, O. Date: NOV 2006



Mapsheets (1:50 000):  
1113 I Haugesund; 1113 II Skudeneshavn;  
1212 I Høy; 1212 IV Sjøanger;  
1213 I Vindafjord; 1213 II Jørund;  
1213 III Rennesøy; 1213 IV Sjødalstraumen

Drawing no:  
2006.076-01

**Lineaments**

- Lineaments
- Magnetic dislocations
- Deep weathering: probable
- Deep weathering: possible
- Coastline
- Ice scour
- Landslide



**GEOLOGICAL SURVEY OF NORWAY**  
Leiv Eirikssons vei 29  
NO-7491 TRONDHEIM  
Tel: +47 73 90 40 00 Fax: +47 73 92 16 20  
http://www.ngu.no